New Perspectives on Synaptic Development and the Tripartite Synapse

Christopher K. Salmon

Centre for Research in Neuroscience

Department of Neurology and Neurosurgery

Research Institute of the McGill University Health Centre

Integrated Program in Neuroscience McGill University, Montreal

December 2018

A thesis submitted to McGill University in partial fulfillment of the requirements of the degree of Philosophiae Doctor.

© Christopher K Salmon 2018

Abstract

Synapses are the means by which information, in the form of electrochemical impulses, is transmitted from neuron to neuron in the nervous system. Numbering many tens of trillions in the human brain, these micrometre-sized cellular compartments are the basic unit of neural computation and thus give rise to all that the brain and mind accomplishes. In this dissertation I present investigations of two classic problems in our understanding of synapses: how synapses are established in the correct numbers during development, and how they are supported by astrocytes, the partner cells of neurons in the central nervous system. Firstly, I have identified a novel role of immature GABAA transmission in glutamatergic synapse formation during development of mouse hippocampal circuitry. The findings from this study indicate that blocking GABA transmission during a brief window of development significantly enhances glutamatergic synapse formation through an activity-dependent mechanism. Importantly, this demonstrates a way in which different neurotransmitter systems cooperate to regulate neuronal connectivity during development. Secondly, I performed a three-dimensional ultrastructural analysis of the relationship between synapses and astrocytes in the mouse somatosensory cortex. This descriptive study focused on the distribution of mitochondria within astrocytes to examine potential relationships between synapses and local sites of astrocytic energy regulation and Ca²⁺ signalling. The results suggest that the location of astrocytic mitochondria, which provide energy and buffer Ca2+, is not dictated by the attributes of the surrounding synapses that are identifiable by electron microscopy, however, there does appear to be a non-random distribution of mitochondria relative to clusters of synapses. Finally, with the goal of enhancing our ability to probe synapse development and astrocyte-neuron interactions, I pioneered an approach for conditional gene expression in vivo that combines in utero electroporation with an inducible, transposable TetOn-based system. I showed that this approach offers reliable, specific, and controllable expression of genes of interest in neuronal populations across the lifespan of the mouse. Thus, the results presented

in this dissertation point to a new mechanism directing hippocampal synapse development, unveil a new level of detail in our understanding of astrocytic interactions with synapses, and provide a new approach with which to probe these and many other problems in cellular neurobiology.

Résumé

Les synapses sont le moyen par lequel l'information, sous forme d'impulsions électrochimiques, est transmise de neurone à neurone dans le système nerveux. Des dizaines de milliards de compartiments cellulaires mesurant des micromètres sont l'unité de base du calcul neuronal et sont ainsi à l'origine de tout ce que le cerveau et l'esprit accomplissent. L'objectif de cette thèse est de présenter mes recherches sur deux problèmes typiques liés aux synapses : la manière dont les synapses sont établies en nombre adéquats cours du développement et comment elles sont soutenues par les astrocytes, des cellules partenaires des neurones du système nerveux central. En premier lieu, j'ai identifié un nouveau rôle de la transmission immature de GABAA dans la formation de synapse glutamatergique au cours du développement de circuits de l'hippocampe de souris. Les résultats de cette étude indiquent que le blocage de la transmission du GABAA durant une brève période de développement améliore de manière significative la formation de synapses glutamatergiques par un mécanisme dépendant de l'activité neuronale. Il est important de noter que cela démontre une manière dont différents systèmes de neurotransmetteurs coopèrent pour réguler la connectivité neuronale au cours du développement. Deuxièmement, j'ai effectué une analyse ultrastructurale en trois dimensions de la relation entre les synapses et les astrocytes dans le cortex somatosensoriel de la souris. Cette étude descriptive est axée sur la distribution des mitochondries dans les astrocytes afin d'examiner les relations potentielles entre les synapses et les régions environnantes des astrocytes qui exigent d'énergie et l'homéostasie du Ca²⁺. Les résultats indiquent que l'emplacement des mitochondries astrocytaires n'est pas déterminé par les attributs des synapses environnantes identifiables par microscopie électronique. Cependant, il semble exister une distribution non-aléatoire des mitochondries par rapport aux groupes de synapses. Finalement, afin de mieux examiner le développement de la synapse et les interactions astrocyte-neurones, j'ai introduit une approche d'expression génique conditionnelle in vivo qui combine l'électroporation in utero avec un système inductible et transposable basé sur TetOn. J'ai démontré que cette approche permet une expression génétique fiable, précise et contrôlable dans des populations neuronales dans toute la durée de vie de la souris. Ainsi, les résultats présentés dans cette thèse suggèrent un nouveau mécanisme dirigeant le développement des synapses de l'hippocampe, dévoilent un nouveau niveau de détail dans notre compréhension des interactions astrocytaires avec les synapses et fournissent une nouvelle approche permettant la poursuite de ces problèmes et de nombreux autres en neurobiologie cellulaire.

To Mom and Dad, for getting me here, giving me the space to fail and succeed, and for unconditional support.

To Benjamin, Jonathan, Fraser and Jared for always reminding me who I truly am and where I am from.

To Christine, for all the reasons these words are inadequate.

Acknowledgements

I am first and foremost indebted to my supervisor Dr. Keith Murai for providing me the space to follow my interests, and for taking them on as his own with infectious enthusiasm. This came along with a great deal of trust and patience, for which I am grateful.

My advisory committee, Dr. Ed Ruthazer and Dr. David Stellwagen provided invaluable insight and critique, with a lighthearted approach that reminded me that doing science is supposed to be enjoyable. Both always made me feel like a colleague rather than a student, whether over the meeting table or outside the lab. I am also grateful to Dr. Don Van Meyel, who consistently acted as an unofficial advisor and provided a great deal of encouragement.

Over the years, I have worked in and with a number of laboratories that have been generous with their time and expertise. I am indebted to the principle investigators of these labs: Dr. Melanie Woodin, Dr. Charles Bourque, Dr. Anne McKinney, Dr. Samuel David, Dr. Yong Rao and again, Dr. David Stellwagen. Of course, most of all I must thank the trainees in these labs who performed experiments with or for me, Dr. Horia Pribiag, Dr. Eric Trudell, Dr. Scott Cameron, Dr. Andrew Greenhalgh and Mr. Andy Gao.

While I have learned something from everyone I have interacted with at the Centre for Research in Neuroscience, I owe the lions share of my technical knowledge to my teachers in the Murai lab: Dr. Emma Jones, Dr. Sabrina Chierzi, Dr. Todd Farmer, and Dr. Denise Cook. I have also been fortunate to share learning, particularly in the surgical and molecular biology realms, with Dr. Gaël Quesseveur and Dr. Ibrahim Kays. Finally, Mr. Benny Kacerovsky has been a constant and integral collaborator throughout the entirety of my doctorate, most significantly on the astrocytic ultrastructure project detailed here in Chapter 3.

Training, of course, extends far outside the technical realm, and while I am again indebted to everyone at the CRN for knowledge gleaned, I would like to thank Dr. Sejal Davla, Mr. Hunter Shaw, Dr. Ibrahim Kays, Ms. Renu Heir and Dr. Haider Altimimi for modelling many of the non-technical aspects of what it takes to do good science.

I have also been privileged to train a number of talented undergraduate students who all contributed in concrete ways to my work. To Ms. Anqi Zhang, Ms. Maria Zamfir, Mr. Gee Hung Leo Cheong, Mr. Michael Pratt, Ms. Nensi Alivodej, Mr. Michael Rosen and Ms. Miranda Green, thank for your hard work, engagement, and for teaching me about teaching.

I owe an outsized debt to Dr. Andrew Greenhalgh, Dr. Scott Cameron and Dr. Denise Cook, who during their tenures at the CRN provided me with templates of rigour and dedication to aspire to. If I have asked good questions and answered them well, you share in those small victories.

Finally, the CRN would not function without Ms. Yvonne Gardner who is always ready with a good tale, a wry smile, an open ear or a conciliatory and knowing sigh. Thank you for taking care of us all.

I would be remiss not to acknowledge that doctorates are accomplished with a great deal of support from outside the lab, before, during and after the degree.

To my parents, Ken and Sherry, my brothers, Benjamin, Jonathan, Fraser and Jared, and adopted sisters, Heather, Serena and Ashley: thank you for your love, support and patience, and for giving me places to come home to. You neither asked too much or too little and tolerated when my work got in the way.

I drew a great deal of support, solace, advice, encouragement and inspiration from Benjamin Tallon, Eric Brousseau, Matthew Parsons, Stephen Flood, Geoff McCausland, Margaret Pitts, Kevin McMullin, David Schecter, Chessi Miltner, Scott Baker, Hayley Lapalme, Matthew Woods, David Switchenko, Jean-Simon Fortin, Jeanne Portier, Alix Petter and Mark Dance. Thank you all.

I also owe a part of my work to my early mentors. To Ms. Debbie Garland, thank you for telling me that I would be a scientist some day, and to Dr. Mark Trifiro thank you for getting me started on the journey.

Support also often comes in the professional form. I owe my current mental health to three very talented therapists, Debbie, Emily and Marissa, without whom my degree very well may have had to be abandoned.

The last and undoubtedly most important acknowledgement goes to my partner, Christine Vidal, who deserves my gratitude for far more than can be listed here. Thank you for giving me a reason to get up in the morning, being my person, keeping me well, and for making and sharing a life with me through all of this. Any accomplishments I have made are yours as well.

Contributions of Authors

This thesis has been prepared in accordance with the guidelines of a Manuscript-Based thesis as laid out by the Faculty of Graduate and Postdoctoral Studies of McGill and is made up of three original manuscripts, one of which was under peer review at the time of the initial thesis submission. The citations from each manuscript have been inserted at the end of each chapter, while the citations pertaining to the rest of the dissertation are included at the end of the document.

Manuscript 1: Depolarizing but Inhibitory GABA_A Transmission Restrains Excitatory Synapse Formation in the Developing Hippocampus

Christopher K. Salmon, Horia Pribiag, W. Todd Farmer, Scott Cameron, Vivek Mahadevan, David Stellwagen, Melanie A. Woodin, and Keith K. Murai

CKS and KKM conceived of the project. CKS designed experiments with advice from KKM. CKS performed western blots, tissue culture, RNA extractions, and microscopy. MAW designed and performed patch recordings and CKS and MAW performed analysis. HP and DS designed and performed synaptic physiology, CKS and HP performed analysis. WTF performed qPCR. CKS wrote manuscript with editing from KKM.

Manuscript 2: Astrocytic Mitochondrial Location is not Associated with Ultrastructural Characteristics of Tripartite Synapses

Christopher K. Salmon, J. Benjamin Kacerovsky, Tabish Syed, Nensi Alivodej, Michael Pratt, Michael P. Rosen, Miranda Green, Kaleem Siddiqi, and Keith K. Murai

CKS, JBK and KKM designed project. JBK prepared tissue. Tissue was stained, embedded and imaged by the McGill Facility for Electron Microscope Research. CKS performed initial preparation of raw datasets. NA and MP performed the majority of segmentation with help

from CKS and JBK. CKS and JBK performed quality control and retouching of segmentation. CKS, MPR and MG performed postsynaptic density categorization. CKS and JBK coordinated and trained NA, MP, MPR and MG. TS and KS designed distance measurement methodology. TS performed advanced distance measurements, image rendering in Figure 2 and dominant set clustering. CKS designed and performed data analysis. HV and CAM provided valuable technical expertise and access to equipment. CKS wrote manuscript with editing from KKM.

Maniscipt 3: TetOn Inducible Gene Expression in the Mouse Brain Across the Lifespan

Christopher K. Salmon, Gael Quesseveur, J. Benjamin Kacerovsky, Gee Hung Leo Cheong, Michael P Rosen, Miranda Green, Andy Y.L. Gao, Hojatollah Vali, Craig A. Mandato, and Keith K. Murai

CKS and KKM conceived of the project. CKS established all *in utero* electroporation procedures and protocols in the lab. CKS, GQ and JBK designed experiments. CKS and GQ designed piggyBAC constructs. GQ cloned piggyBAC constructs. CKS designed and cloned all other constructs that were not acquired elsewhere. CKS performed heterologous cell culture/analysis, western blots and luciferase assays. CKS and AYLG prepared hippocampal cultures. CKS and GQ performed *in utero* electroporations. CKS, GQ and JBK collected brain tissue. CKS, GQ, GHLC, MPR and MG processed tissue. CKS, GHLC, MPR and MG performed microscopy and analysis. CKS coordinated and trained GHLC, MPR and MG. CKS wrote manuscript with editing from KKM.

List of Abbreviations

AP Action potential

ASD Autism spectrum disorder

BIC Bicuculline
BUME Bumetanide

EAAT Excitatory amino acid transporter

 E_{Cl} Chloride reversal potential E_{GABA} GABA reversal potential

E_{rev} Reversal or equilibrium potential
EPSP Excitatory post synaptic potential

FIBSEM Focussed ion beam serial electron microscopy/microscope

GABA γ-amino butyric acid

GABA_AR Ionotropic GABA receptor

GAT GABA transporter

GBZ Gabazine

IP₃ Inositol 1,4,5-triphosphate

IP₃R2 IP₃ receptor 2

IPSP Inhibitory post synaptic potential

IUE In utero electroporation

KCC2 Potassium-chloride cotransporter 2

Kir4.1 Inward rectifying potassium channel 4.1 NKCC1 Sodium-potassium-chloride cotransporter 2

MCT Monocarboxylate transporter

mEPSP Miniature EPSP mIPSP Miniature IPSP

MUS Muscimol

PAP Persynaptic astrocytic process

Shh Sonic hedgehog

SNAT Solute Neutral amino acid transporter

SSEM Serial section electro microscopy
TEM Transmission electron microscopy

tetO Tet Operator

tTA Tetracycline transactivator

rtTA Reverse tetracycline transactivator

Table of Contents

Abstract	1
Résumé	3
Acknowledgements	6
Contributions of Authors	9
List of Abbreviations	11
Introduction	16
Chapter 1 Literature Review	19
1.1 Depolarizing GABA Transmission In Synapse Formation And Neural Circuit Development	19
1.1.1 GABAergic Neurotransmission	19
1.1.2 The Developmental Depolarizing-to-Hyperpolarizing Shift in GABA _A Transmission	20
1.1.3 Depolarizing GABA _A Transmission as a Developmental Cue	21
1.1.4 Depolarizing GABA _A Transmission in Synapse Formation	24
1.1.5 Depolarizing GABA _A Transmission in Circuit Refinement	25
1.1.6 Depolarizing GABA Transmission in Primates	27
1.1.7 Depolarizing GABA Transmission in Neurodevelopmental Disorders	27
1.1.8 The Complexity of Understanding the Roles of Depolarizing GABA _A Transmission	29
1.2 Astrocytes at the Tripartite Synapse	30
1.2.1 Astrocytic Control of Synapse Formation	31
1.2.2 Roles of Astrocytes at the Mature Tripartite Synapse	31
1.2.3 Calcium Dynamics and Astrocyte Function	33
1.2.4 Ultrastructural Studies of the Tripartite Synapse	35
Chapter 2 Depolarizing but Shunting GABA _A Transmission Restrains Glutamatergic Synapse Formation	38

2.1 Preamble	38
2.2 Abstract	40
2.3 Significance Statement	41
2.4 Introduction	41
2.5 Materials and Methods	43
2.6 Results	47
2.7 Discussion	53
2.8 References	59
2.9 Figures	66
2.10 Figure Legends	74
Chapter 3 Astrocytic Mitochondrial Location is not Associated with	
Ultrastructural Characteristics of Tripartite Synapses	78
3.1 Preamble	78
3.2 Abstract	80
3.3 Introduction	81
3.4 Methods	84
3.5 Results	88
3.6 Discussion	94
3.7 References	99
3.8 Figures and Tables	104
3.9 Figure Legends	117
Chapter 4 TetOn Inducible Gene Expression in the Mouse Brain Acr	oss the
Lifespan	
4.1 Preamble	120
4.2 Abstract	122
4.3 Introduction	123
4.4 Materials and Methods	126
4.5. Regults	132

4.6 Discussion	140
4.7 References	146
4.8 Figures and Tables	151
4.9 Figure Legends	165
Chapter 5 Discussion and Future Directions	171
5.1 Discussion and Future Directions	171
5.2 Further Inquiry into Activity-Dependent Processes Driven by Inhibiting D but Shunting GABA _A Transmission	
5.3 Depolarizing GABA _A Transmission in Neurodevelopmental Disorders	172
5.4 New Tools for Blocking GABA _A Transmission	174
5.5 Next Steps in Examining Astrocytic Ultrastructure	175
5.6 The Possibility of Astrocytic Loops	176
5.7 Investigating Neuron-Astrocyte Shh Signalling with IUE of TetOn	177
5.8 Conclusion and Contribution to Knowledge	178
Bibliography	179

For the time being the nerve cell's zones of transfer appear histologically as mainly variable and variously constituted pathways between concrescing surfaces that I shall designate physiologically simply as zones for the transmission of stimuli.

– Hans Held, Beiträge zur Structur der Nervenzellen und ihrere Fortsätze

Introduction

A central pursuit in neuroscience is the understanding of how the brain wires itself into one of the most complex known biological systems. To achieve this goal, neurons must establish the correct number of synaptic connections with the correct partners in the appropriate brain regions. Although historically there has been some debate as to whether this intricate connectivity is established through an all-encompassing genetic program or through refinement of connections after initial, more random outgrowth and connection-making (Paul Weiss, 1947; Sperry, 1963), it is clear now that aspects of both of these processes participate in the development of mature neural circuits (Hensch, 2005; Akerman and Cline, 2007; Thomas C Sudhof, 2018). Growing axons are first guided to a particular brain area and to particular cells by a complex array of soluble and surface-tethered guidance cues (Berns et al., 2018). Initial formation of synaptic contacts then occurs, followed by the specification of synapse type and assembly of functional synaptic machinery (Chia et al., 2013). Finally, a refinement process ensues by which some connections are eliminated and some are strengthened (Kano and Hashimoto, 2009). A critical component in synapse and circuit development is the early action of GABA, the main inhibitory neurotransmitter in the mature brain. Paradoxically, GABA mediates depolarization in immature neurons. This depolarization is thought to promote synapse and circuit formation, and leads to aberrant circuitry and developmental disorders when it is misregulated. Chapter 2 of this dissertation presents a study that provides insight into a new mechanism for GABA in regulating synapse development, demonstrating that depolarizing GABA transmission is capable of restraining excitatory glutamatergic synapse development in the hippocampus.

An essential but sometimes overlooked fact of neurobiology is that almost all processes that occur in the central nervous system (CNS), including the steps of neural circuit development described above, require the actions of other cell types besides neurons. Glia, which outnumber neurons in the CNS, play many essential roles in controlling synaptic

transmission, protecting the brain from the external environment, clearing debris, providing energy for neuronal metabolism, and coordinating neural circuit development and function (Barres, 2008). In particular, protoplasmic astrocytes, intricate sponge-like glia that tile throughout the entirety of the cerebral cortices and many other regions, are intimately associated with synapses. Astrocytes coordinate synapse development (Allen and Eroglu, 2017), provide energy substrates to neurons to support synapse function (Magistretti and Allaman, 2015), and regulate synaptic transmission and plasticity by reuptake of neurotransmitters and by releasing gliotransmitters (Perea et al., 2009). The importance of astrocytes at synapses has led to the concept of the tripartite synapse, where perisynaptic astrocytic processes (PAPs) are an integral component of the synaptic apparatus along with neuronal pre- and post-synaptic terminals (Araque et al., 1999). The fine astrocytic filaments that compose PAPs are derived from thin, and often extremely small, astrocytic branches. Because of this, their specific properties have been a challenge to understand and scrutinize (Rusakov, 2015). However, new techniques are helping to demystify the organization and function of astrocytic filaments and the tripartite synapse. Chapter 3 details an investigation of the nanoscopic organization of the tripartite synapse and the mitochondria that are thought to play a role in supporting its function.

Progress in our understanding of the two scientific concepts above – and scientific progress in general – relies on technological advances. In neurobiology, progress has often been facilitated by approaches that increase resolution. Single and multiphoton confocal microscopy improved our ability to resolve fluorescently labelled structures in neural tissue, both spatially and temporally (Fine et al., 1988; Helmchen and Denk, 2005). The optogenetics and viral transduction revolutions have increased resolution by allowing selective manipulation and stimulation of not only small groups of neurons, but of genetically defined types of neurons (Kim et al., 2017). In Chapter 4, I present novel methodology designed to increase the temporal resolution with which genes of interest can be expressed *in vivo*, by

combining *in utero* electroporation and a transposable TetOn inducible gene expression system. We conceived of this technique to facilitate dissection of the rapid temporal sequence of events during early neural circuit formation, however, I also demonstrate that it can be used for studies in the adult, and for investigation of neuron-astrocyte interactions.

Chapter 1 Literature Review

1.1 Depolarizing GABA Transmission In Synapse Formation And Neural Circuit Development

1.1.1 GABAergic Neurotransmission

γ-Amino butyric acid (GABA) is the main inhibitory neurotransmitter in the developing brain, where it plays an essential role in controlling circuit activity by inhibiting runaway activity and contributing to information processing (Freund and Buzsáki, 1998; Douglas and Martin, 2009). Glycine is also a major inhibitory neurotransmitter, however its actions are mainly restricted to the brainstem and spinal cord, with some minor inhibitory roles in several brain areas (Gamlin et al., 2018). GABA was identified as an inhibitory neurotransmitter by Dr. Allan Elliot and colleagues running a project based at the Montreal Neurological Institute (Bazemore et al., 1956). While GABA and its synthesis pathway were observed in the brain in 1950, it was not until Elliot collaborated with Merck and Co. to process hundreds of pounds of cattle brains at a time that its identity as an inhibitory neurotransmitter was uncovered (Awapara et al., 1950; Roberts and Frankel, 1950; Jasper, 1984). GABA binds to heteropentameric iontropic GABA_A receptors (GABA_ARs) made up of different combinations of 19 subunits (Michels and Moss, 2007). When bound to GABA, GABA_ARs allow flux of chloride (Cl⁻), and to a lesser extent bicarbonate (HCO₃⁻), across the neuronal membrane. As the major anionic species in neurons, Cl- sets the GABA reversal potential (E_{GABA}), such that E_{GABA} is approximately equal to the Cl⁻ equilibrium (E_{Cl}). In the mature brain, where GABA is inhibitory, E_{GABA}, lies below the resting membrane potential, resulting in hyperpolarization of the postsynaptic cell when GABA_ARs open.

1.1.2 The Developmental Depolarizing-to-Hyperpolarizing Shift in GABA_A Transmission

It was noted that in certain contexts GABA mediated shunting inhibition rather than fully hyperpolarizing inhibition (Misgeld et al., 1986; Owens and Kriegstein, 2002). Shunting inhibition results from a current with an equilibrium potential (E_{rev}) lower than action potential (AP) threshold, which has the effect of holding membrane potential near its own E_{rev} by decreasing membrane resistance and thus the dendritic length and time constants (Staley and Mody, 1992). However, Ben-Ari and colleagues then showed conclusively that GABA was capable of depolarizing immature CA3 neurons of the hippocampus, in some cases past AP threshold, triggering firing in these cells (Ben-Ari et al., 1989). These findings have since been corroborated and further characterized by many groups with studies in tissues from numerous developing brains regions (Brickley et al., 1996; Chen et al., 1996; Owens et al., 1996, 1999; Dammerman et al., 2000; Gao and Pol, 2001; Wang et al., 2001). Following on this, it was observed in rodent brain slices that E_{GABA} gradually hyperpolarized from this depolarizing level early in development, reaching its mature hyperpolarized E_{rev} of approximately -70mV by the second postnatal week (Owens et al., 1996; Ben-Ari et al., 2007).

The gradual depolarizing-to-hyperpolarizing shift in GABA_A transmission is explained by gradual changes in the expression of cation-chloride transporters that determine E_{Cl}. The neuron-specific potassium-chloride cotransporter, KCC2, whose expression is upregulated from almost nil at birth to adult levels by the third postnatal week, transports Cl⁻ out of the cell (Clayton et al., 1998; Lu et al., 1999; Rivera et al., 1999; Vu et al., 2000). Over the same period, a simultaneous decrease in the expression of the Cl⁻-extruding neuronal sodium-potassium-chloride cotransporter-1, NKCC1, occurs (Spitzer and Rohrbough, 1996; Plotkin et al., 1997; Clayton et al., 1998; Fukuda et al., 1998; Li et al., 2002; Mikawa et al., 2002). The result of the reciprocal changes in the expression of these two transporters is a decrease in

intracellular chloride ([Cl_i]) to mature levels during the first weeks of postnatal development in rodents, and the ultimate establishment of mature, hyperpolarizing GABA_A transmission.

1.1.3 Depolarizing GABA_A Transmission as a Developmental Cue

A gradual, coordinated shift in gene expression such as that involved in the development of mature E_{GABA} is energetically and evolutionarily costly, suggesting that depolarizing GABA_A transmission likely plays an important role during development. Furthermore, the shift is highly conserved, having been reported in almost every model system studied, vertebrate and invertebrate alike (Ben-Ari, 2002; Ben-Ari et al., 2012). Indeed, early evidence suggested that GABA plays developmental roles in the superior cervical ganglion where its application was noted to cause synapse formation and alter the shape of the dendritic arbor (Wolff et al., 1978). By the late 1980s and early '90s, work in the cerebellum and spinal cord had led to the hypothesis that GABA was a general neurotrophic cue (Meier et al., 1991). In addition to these considerations, numerous reports demonstrated that depolarizing GABA_A transmission is sufficient to allow calcium entry into neurons via voltage gated calcium channels (Yuste and Katz, 1991; Lin et al., 1994; Leinekugel et al., 1995; LoTurco et al., 1995b; Owens et al., 1996). As calcium plays numerous important roles in many aspects of neurodevelopment (Michaelsen and Lohmann, 2010; Rosenberg and Spitzer, 2011; Toth et al., 2016; Kamijo et al., 2018), this work further bolstered the hypothesis that immature GABAergic depolarization is involved in coordinating development in the CNS. Evidence gathered in the last three decades demonstrates that this is indeed the case and implicates depolarizing GABA_A transmission as a key factor at numerous stages of neural development.

Before synaptic contacts are established, depolarizing GABA_A signalling plays paracrine roles in proliferation and differentiation of neural precursors. The earliest GABA responses are seen in neural precursors in the subventricular zone where GABA mediated depolarization inhibits both DNA synthesis and proliferation of glial fibrillary acidic protein (GFAP)-positive precursors (LoTurco et al., 1995a; Liu et al., 2005). Both effects are thought

to rely on depolarization-induced calcium influx. Depolarizing GABA_A transmission has also been demonstrated to play a key role in neuronal migration, providing a calcium-dependent stop signal when migrating neurons reach the cortical plate (Behar et al., 2000; Heck et al., 2007; Furukawa et al., 2014). Furthermore, following differentiation and migration, before they establish synapses, immature cortical pyramidal cells show GABA-mediated depolarization that leads to calcium influx (Demarque et al., 2002), a finding that has also been replicated *in vivo* in mice (Kirmse et al., 2015), as well as in immature neurons of developing zebrafish (Zhang et al., 2010; Bekri and Drapeau, 2018). Thus, early GABAergic depolarization may aid in initial calcium-dependent development of neurites and synapses (Demarque et al., 2002).

Once GABAergic synapses form, GABA remains depolarizing for the first one to two weeks of postnatal development. Importantly, GABAergic synapses form before excitatory glutamatergic synapses (Tyzio et al., 1999), which suggested that depolarizing GABA_A transmission, already known to cause calcium influx, may drive glutamatergic synapse unsilencing (Ben-ari et al., 1997; Hanse et al., 1997). This theory suggests that before any appreciable α -amino-3-hydroxy-5-methyl-4-isoxazolepropionic acid receptors (AMPARs) are present at glutamatergic synapses, depolarizing GABAA transmission relieves the magnesium blockade of N-methyl-D-aspartate receptors (NMDARs), allowing calcium influx during glutamatergic neurotransmission, which in turn drives trafficking of AMPARs to the synaptic membrane (Hanse et al., 2013; Vincent-Lamarre et al., 2018). It was further suggested that in the hippocampus, early network oscillations observed in acute brain slices, referred to as giant depolarizing potentials (GDPs), play a key role in driving rhythmic calcium influx and NMDAR unsilencing. Evidence from acute slices suggests that depolarizing GABAA transmission is necessary for the generation of GDPs (reviewed thoroughly in Ben-Ari et al., 2007). That being said, there are numerous examples of GABA_A blockade failing to silence GDPs; in some cases, GABA_A blockade increased activity by

eliciting interictal events or paroxysmal activity between the low frequency GDPs (Ben-Ari et al., 2007). These variable results may be explained by the fact that the system is dynamic and GABA becomes less and less depolarizing through postnatal development, suggesting that it will play a less important role in driving GDPs later in this period. One study in particular illustrates that this is likely the case by showing that (1) at postnatal day 3 (P3) in mouse, GABA_A blockade silences GDPs; then (2) at P6, GABA increases activity, causing interictal discharges between GDPs. This is then followed by the mature state where (3) at P9 GABA_A transmission is hyperpolarizing and its blockade results in epileptiform activity (Le Magueresse et al., 2006). This work suggests that there may be a definable transition phase prior to full maturation of E_{GABA} wherein GABA_A transmission has matured to the point of providing shunting inhibition and no longer contributes to driving GDPs.

Similar periodic correlated bursts of activity, referred to as spindle wave (SPW) bursts are also present in the developing rodent hippocampus *in vivo* and are contributed to by both GABA and glutamate (Leinekugel et al., 2002). This was originally taken to indicate that GABA_A transmission is also depolarizing and excitatory *in vivo*. However, recent work using *in vivo* patch clamping (Kirmse et al., 2015) and optogenetic stimulation of interneurons (Valeeva et al., 2016) has indicated that although GABA is depolarizing and can drive calcium influx in developing neurons, it is inhibitory as early as P3. Interestingly, a pair of studies in acute slices suggest a compromise between these positions. Firstly, depolarizing GABA_A transmission was shown to be capable of contributing to depolarization resulting in action potentials even when E_{GABA} was below AP threshold (Gulledge and Stuart, 2003). However, when coincident with glutamatergic transmission, somatic GABAergic inputs were inhibitory. More recently, it has been demonstrated that although GABA drives the initiation of GDPs, at their peak GABA is inhibitory and restricts their duration (Khalilov et al., 2015). Together, these studies provide evidence that even in acute slices where GABA has been

observed to be capable of driving APs and GDPs, GABA_A transmission can be both inhibitory and excitatory, even in the same circuit at the same developmental stage.

1.1.4 Depolarizing GABA_A Transmission in Synapse Formation

Despite the early hypothesis that depolarizing GABA_A transmission drives synaptic development (Ben-ari et al., 1997), evidence for this was lacking in vivo for close to a decade. However two studies emerged in the 2000's using in utero electroporation (IUE) to introduce genetic constructs to express KCC2 (Cancedda et al., 2007) or double-stranded RNA (dsRNA) to knock down NKCC1 (Wang and Kriegstein, 2008) in mouse cortex. These approaches prematurely rendered GABA hyperpolarizing in developing layer 2/3 cortical neurons. Both studies showed that loss of depolarizing GABA_A transmission causes abnormalities in dendrite growth; while Wang and Kriegstein (2008) showed that this causes a decrease in excitatory synapse maturation and dendritic spine density (Fiumelli et al., 2012). It is important to note that in utero electroporation relies on introduction of DNA to neural progenitors that line the subventricular zone. Therefore, when constitutively expressed plasmids are used, the electroporated cells express the genes of interest throughout their postmitotic lifespan. In other words, E_{GABA} was hyperpolarized in these cells as they exit the cell cycle, and differentiate and migrate into the cortex. These are all steps that depolarizing GABAA transmission is known to regulate (Owens and Kriegstein, 2002). Thus, in both these studies, GABA_A transmission was rendered prematurely hyperpolarizing over a period when this manipulation likely affects more than just dendrite and synapse development. More temporally precise work is therefore required to understand the role of depolarizing GABA_A transmission in synapse formation. Interestingly, further evidence supporting the findings was supplied by a study of long-range GABAergic projections from the zona incerta, a nucleus of the subthalamus, to the upper most apical branches of Layer 4 and 5 cortical neurons (Chen and Kriegstein, 2015). These GABAergic inputs are depolarizing during the first postnatal week in mice (Dammerman et al., 2000), and inactivating them during this time results in a local decrease in dendrite

branching and dendritic spine density in the region of the dendritic arbor that they target (Chen and Kriegstein, 2015).

Also in support of a role for depolarizing GABA_A transmission in promoting synapse formation are a number studies showing the roles of depolarizing GABA_A transmission in maturation of adult-born hippocampal dentate granule cells (DGCs) (Overstreet Wadiche et al., 2005; Tozuka et al., 2005; Ge et al., 2006; Waterhouse et al., 2012; Chancey et al., 2013). These studies indicate that GABA plays the same roles in the developmental sequence of adult-born DGCs as it does in neonatal neurons, and that these effects rely on depolarization and calcium influx. Furthermore, adult-born granule cells first receive tonic GABA input, and then sequentially develop synaptic GABA_A and glutamateric inputs, both of which are initially depolarizing (Ge et al., 2006). Significantly, when Ge and colleagues prematurely rendered GABA hyperpolarizing in these cells by knocking down NKCC1 expression, dendritic morphology and synapse density were disrupted. Again, however, the observed deficits in dendritic morphology may have preceded and/or led to decreased synapse densities. More temporally precise analysis is needed to determine the precise role of GABAergic depolarization in synapse formation in these cells as well.

1.1.5 Depolarizing GABAA Transmission in Circuit Refinement

Aside from its reported roles in the formation of synapses, depolarizing GABA_A transmission has been shown to direct synaptic maturation and the emergence of functional circuitry, events collectively referred to in the literature as circuit refinement (Akerman and Cline, 2007). When E_{GABA} was prematurely hyperpolarized by KCC2 overexpression in neurons in the developing optic tectum of *Xenopus laevis*, glutamatergic EPSCs developed to be weaker and less frequent, while GABAergic IPSC amplitude and frequency increased (Akerman and Cline, 2006). This raised the possibility that depolarizing GABA_A transmission is important for establishing proper excitatory/inhibitory (E/I) balance. Counterintuitively, silencing GABA_A transmission in the same system during development left EPSCs unaltered,

but did cause aberrant dendritic branching (Shen et al., 2009). Furthermore, development of GABAergic transmission was enhanced, resulting again in a disruption of E/I balance. Thus, the precise role of depolarizing GABA_A transmission in *Xenopus* optic tectum circuit development has yet to be fully elucidated. Interestingly, in rat visual cortex, prematurely hyperpolarizing E_{GABA} with systemic administration of the NKCC1-blocker, bumetanide (BUME), throughout the first postnatal week did not cause changes in synapse formation, dendritic branching or circuit function (Deidda et al., 2014). However, it was observed that the critical period for ocular dominance plasticity was extended by roughly 10 days. The systemic dosing of BUME in this study makes it hard to draw conclusions as to the role of depolarizing GABA_A transmission in any one particular cell type, circuit or brain area. Nevertheless, it is an important precedent suggesting that rendering GABA_A transmission prematurely hyperpolarizing specifically in the postnatal period does not alter synapse formation or circuit development in every system.

An intriguing new avenue by which immature GABA transmission is being shown to influence circuit development is through transient connections made by and onto interneurons during development. Somatostatin-positive interneurons in deep cortical layers have been observed to both receive and make transient connections during circuit wiring at developmental stages when GABA is known to be depolarizing (Marques-Smith et al., 2016; Tuncdemir et al., 2016). In both these cases, silencing somatostatin neurons caused local disruption of cortical circuitry. While these studies did not assess whether depolarizing GABA transmission is essential for the proper wiring of these circuits, it will be interesting to see if this is the case. Furthermore, these studies indicate that the development of local circuits can entail more elaborate processes than previously thought, a fact that will have to be taken into account when attempting to understand circuit development in general and the role that GABA_A transmission plays in this process.

1.1.6 Depolarizing GABA Transmission in Primates

Although depolarizing GABA_A transmission has been thoroughly studied in rodents and other vertebrate species, data has been difficult to obtain in humans and other primates for obvious reasons. However, seminal experiments performed in post mortem brain slices from gestational week 12 human fetuses demonstrates that GABA_A transmission depolarizes deep layer cortical neurons (Chen and Kriegstein, 2015). Puffing GABA onto neurons also elicited calcium transients in dendrites. This suggests that GABA is depolarizing early in gestation in humans. This is supported by the observation of progressive upregulation of KCC2 immunoreactivity in developing fetal tissue, with a large increase occurring between 24 postnatal weeks and birth, suggesting a prenatal depolarizing to hyperpolarizing shift in GABA_A in humans (Sedmak et al., 2015). GABA was also found to be inhibitory by the 3rd trimester in the macaque (Khazipov et al., 2001) indicating that GABA is indeed relatively mature at the time of birth in primates. However, some confusion does persist on this topic. Anticonvulsants tend to be ineffective in treating neonatal seizures, an issue that has been suggested to be attributable to depolarizing GABA_A transmission in neonates (Khanna et al., 2013). However, taking the above-mentioned data from macaque and human tissue into account, it seems likely that the inefficiency of anticonvulsants for treating neonatal seizure is likely caused by a still-underdeveloped GABAergic system that cannot overcome epileptic discharges in infants, rather than depolarizing GABAA transmission rendering the use of anticonvulsants ineffective.

1.1.7 Depolarizing GABA Transmission in Neurodevelopmental Disorders

Many neurodevelopmental disorders are associated with changes in synapse number and function. As a result, it has been hypothesized that disruption in depolarizing GABA_A transmission may be relevant in the etiology of these disorders. Indeed, a number of polymorphisms in KCC2 and GABA_A receptor subunits have been associated with austism spectrum disorders (ASD) (Cellot and Cherubini, 2014). In particular, polymorphisms in the

gene coding for the GABA_AR β 3 subunit have been well-characterized in this respect (Menold et al., 2001; Buxbaum et al., 2002; Cellot and Cherubini, 2014; Chen et al., 2014). The association of GABA_AR polymorphisms with ASD suggests that disrupting GABA_A transmission during development may play a role in the development of the disorder. Notably, in rats, β 3 subunit mRNA is most highly expressed early in development when GABA is depolarizing (Laurie et al., 1992). Thus, mutation of the β 3 subunit may be particularly influential during developmental steps that depend on depolarizing GABA_A transmission.

Disruptions in the progressive maturation of E_{GABA} are also associated with autism spectrum disorders (ASD). Maternal immune activation, a critical risk factor for ASD, has been observed to delay the development of mature GABA_A transmission (Corradini et al., 2017). Aberrant oxytocin signalling has also been connected to ASD and maturation of E_{GABA} . The oxytocin spike that occurs during parturition has been shown to cause brief hyperpolarization of E_{GABA} in the fetus during birth, and this hyperpolarization of E_{GABA} is lost in models of ASD (Ben-Ari et al., 2007; Tyzio et al., 2014). Furthermore, the loss of this transient hyperpolarization disrupts the usual maturation of the Cl⁻ gradient, leaving E_{GABA} depolarized in the hippocampus into adulthood (He et al., 2014; Tyzio et al., 2014). When BUME is administered in ASD models during birth to restore the transient oxytocin-dependent hyperpolarization, the developmental maturation of E_{GABA} is rescued and deficits linked with Fragile-X syndrome are ameliorated (Tyzio et al., 2014; He et al., 2018). This work has lead to successful stage 1 and 2 clinical trials in which BUME administration has emerged as a viable therapeutic approach for treating ASD in children and adolescents (Lemonnier et al., 2017; Hadjikhani et al., 2018). However, as E_{GABA} is likely mature in humans by birth, it is unlikely that BUME acts to correct synaptic deficits by restoring the proper developmental sequence in E_{GABA} maturation, and rather acts by enhancing the extent to which GABA_A transmission is hyperpolarizing, thereby readjusting E/I imbalance, a deficit thought to play a central role in the etiology of ASD (Lee et al., 2017).

Finally, environmental factors that cause neurodevelopmental disorders also disrupt depolarizing GABA_A transmission. A number of longitudinal studies in humans show that prenatal exposure to GABA-enhancing antiepileptic drugs can impair psychomotor development (Dean et al., 2002), suggesting that enhancing depolarizing GABA_A transmission during gestation may alter human neural circuit formation. In support of this possibility, perinatal administration of the anti-epileptic, Vigabatrin has been reported to disrupt expression of synaptic markers in rat hippocampus and has been associated with psychomotor deficits in human infants at birth and at 12 weeks (Levav et al., 2004, 2008). Furthermore, in some patient populations, up to 3% of pregnant mothers use benzodiazepines recreationally and studies suggest that this can result in delayed cognitive development and other neuropsychological deficits (Viggedal et al., 1993; Daw et al., 2012; El Marroun et al., 2014). These effects may be due to disruption of depolarizing GABA_A transmission, however, it is important to note that these deficits may be driven by alterations in any or all of the roles that depolarizing GABA_A transmission is thought to play throughout development, and that the timing of the administration or consumption of these drugs may alter outcomes.

1.1.8 The Complexity of Understanding the Roles of Depolarizing GABA_A Transmission

After nearly four decades of study, it is clear that depolarizing GABA_A transmission is a critical regulator of synapse and circuit development however the problem has become increasingly complex. To begin with, the many sequential roles of GABA in development require the use of techniques allowing for high temporal precision when manipulating E_{GABA} or GABA transmission. Furthermore, depolarizing GABA_A transmission plays variable roles in different cell types, circuits and brain areas, and thus experiments must also be spatially precise and should ideally target specific cell types. Finally, it appears that there may be small but critical differences when comparing E_{GABA} in acute slices versus *in vivo*, with recent work suggesting that depolarizing GABA is mainly inhibitory postnatally *in vivo* (Kirmse et al.,

2015; Che et al., 2018). Thus, new approaches are required to untangle the precise roles of GABA_A transmission at specific junctures of development. To begin to address this, in Chapter 2 of this thesis, I present a study employing a reductionist hippocampal slice culture approach that allowed for enhanced temporal resolution in studying the role of GABA_A transmission in hippocampal glutamatergic synapse development. The results of this study led to the unexpected conclusion that depolarizing GABA_A transmission can restrain glutamatergic synapse formation rather than promote it. Chapter 4 then presents a widely applicable inducible gene expression technique that can be used to investigate depolarizing GABA_A transmission *in vivo* with high temporal resolution. This is followed by a discussion of the path toward defining the precise role of GABA_A transmission in glutamatergic synapse formation in Chapter 5.

1.2 Astrocytes at the Tripartite Synapse

Once synapses and neural circuits have formed, they need to be supported and maintained. Although neurons themselves provide factors for this to some extent (Sudhof, 2018), other cell types are needed. Indeed, astrocytes play critical roles at synapses by making intimate contact with them and providing structural and functional support. This had led to the concept of the *tripartite synapse* where astrocytic processes, along with pre- and postsynaptic structures comprise the overall synaptic apparatus (Araque et al., 1999). While the essential roles of astrocytes in this tripartite arrangement are well established, the astrocytic extensions and branches that interact with neurons are exceedingly small and complex, and thus the structural relationship of astrocytes with synapses have been difficult to study. However, technical advances are beginning to provide the tools needed to examine these intriguing structures (Rusakov, 2015). In this section I give a brief introduction to the roles of astrocytes at the synapse and review the largescale ultrastructural investigations of the tripartite synapse undertaken to date.

1.2.1 Astrocytic Control of Synapse Formation

Astrocytes begin to play central roles at synapses by regulating synapse formation itself. Early evidence that the presence of astrocytes greatly enhanced viability of neurons in dissociated culture suggested astrocytes were important mediators of neural development (Banker, 1980). This was followed by the observation that the addition of astrocytes to neuronal cultures enhanced both synaptic number and strength (Pfrieger and Barres, 1997; Ullian et al., 2001), suggesting that astrocytes promote synapse formation and maturation through contact-dependent and independent cues. Since then, a number of astrocyte-derived signals, including thrombospondin, SPARC, glypicans, D-serine and TGF-β have been shown to regulate the formation and maturation glutamatergic, GABAergic and glycinergic synapses in a variety of neural circuits (Christopherson et al., 2005; Jones et al., 2011; Allen et al., 2012; Diniz et al., 2012, 2014; Allen and Eroglu, 2017; Van Horn et al., 2017). With the recent discoveries that astrocytic neuroligins and chordin-like 1 influence synaptogenesis and maturation respectively, the list of molecules through which astrocytes control synapse development continues to grow (Stogsdill et al., 2017; Blanco-Suarez et al., 2018).

1.2.2 Roles of Astrocytes at the Mature Tripartite Synapse

At mature synapses, astrocytes play key roles in clearing neurotransmitter, providing energy substrates, and secreting factors to modulate synaptic function (Araque et al., 1999; Perea et al., 2009; Magistretti and Allaman, 2015). Glutamate and GABA are the major synaptic neurotransmitters used by the mammalian brain, and once released during neurotransmission they must be cleared from the synaptic cleft. This generally rapid clearance serves to end neurotransmission and also avoid excessive spillover of neurotransmitter onto neighboring synapses (Rusakov and Kullmann, 1998). GABA released during inhibitory neurotransmission is mainly internalized by GABAergic interneurons, with only 10–20% of released GABA taken up by astrocytes (Bak et al., 2006). On the other hand, synaptically released glutamate is mainly internalized by astrocytes. Glutamate is then degraded to

glutamine and shuttled back to the neuron via a combination of astrocytic and neuronal solute neutral amino acid transporters (SNATs), and then converted back to glutamate to complete the cycle (Bak et al., 2006; Schousboe et al., 2013). Of the three glutamate transporters found in the brain, excitatory amino acid transporter 1 (EAAT1/GLAST/Slc1A3) and EAAT2/GLT-1/Slc1A2 are mainly expressed by astrocytes, while EAAT3/Slc1A1 is expressed only at low levels in neurons (Holmseth et al., 2012). Both motility of perisynaptic astrocytic processes (PAPs) and lateral diffusion of EAATs have been proposed to modulate the efficacy of glutamate removal from the synaptic cleft (Haber et al., 2006; Bernardinelli et al., 2014; Murphy-Royal et al., 2015), suggesting important roles for these processes in regulating neural circuit activity and synaptic plasticity. In addition to glutamate clearance, astrocytes have also been found to be capable of internalizing several neuromodulators as well (Weber and Barros, 2015).

Just as astrocytes deliver glutamine to neurons to replenish neuronal glutamate stores for neurotransmission, they also deliver energy substrates to neurons via the extracellular space. Astrocytes have historically been thought to mainly use glycolysis to produce energy substrates both for themselves and for neurons, and were thus not thought to perform mitochondrial oxidative phosphorylation (Magistretti and Allaman, 2015). Neurons, on the other hand, are thought to mainly derive energy from oxidative phosphorylation and to be incapable of metabolizing glucose. Thus, neurons rely on astrocytes to supply lactate as their main energy substrate. The process by which astrocytes uptake glucose, metabolize it to lactate and pass it to neurons is referred as the astrocyte-neuron lactate shuttle (ANLS), and relies on astrocytic and neuronal monocarboxylate transporters (MCTs) to pass lactate into and out of the extracellular space (Halestrap, 2011). More recent evidence suggests that neurons can perform glycolysis to some extent (Patel et al., 2014), and astrocytic mitochondria are capable of performing oxidative phosphorylation (discussed below). However the ANLS is still

thought to be a major way in which astrocytes support neural function (Magistretti and Allaman, 2015).

Aside from their functions to help maintain basic neuronal homeostasis and avoid extracellular neurotransmitter overload, astrocytes play active roles in regulating and modulating synaptic transmission and plasticity. One of the best-known examples of direct modulation of synaptic function by astrocytes is through the release of the gliotransmitter Dserine. D-Serine is a coagonist of NMDARs, and its release from astrocytes has been shown to be necessary for long term potentiation (LTP) (Henneberger et al., 2010) and to be associated with wakefulness (Papouin et al., 2012). ATP is also released from astrocytes as a gliotransmitter, and has the effect of enhancing synaptic transmission through adenosine receptors (Gordon et al., 2005). Both glutamate and norepinephrine released from neurons have been found to elicit astrocytic ATP release (Gordon et al., 2005; Panatier et al., 2011). Astrocytes also help maintain network homeostasis, coordinating both glutamatergic and GABAergic synaptic scaling in response to activity blockade by secreting tumor necrosis factor-α (TNFα) (Stellwagen and Malenka, 2006; Pribiag and Stellwagen, 2013). Notably, the scaling function of astrocytic TNF α has been implicated in circuit refinement in the visual cortex (Kaneko et al., 2008). Thus, through a variety of mechanisms, astrocytes maintain homeostasis and modulate neural function and plasticity at the tripartite synapse.

1.2.3 Calcium Dynamics and Astrocyte Function

To perform many of their functions at the tripartite synapse, astrocytes detect the state of the surrounding circuitry with a variety of cell surface receptors for neurotransmitters and neuromodulators that have been thoroughly characterized both electrophysiologically and with immunolabelling (Porter and McCarthy, 1997; Heller and Rusakov, 2015). A central way in which astrocytes respond to the detection of these signals is through complex patterns of internal calcium signalling (Perea et al., 2009; Bazargani and Attwell, 2016). A wealth of early work on astrocytic calcium signalling suggested that calcium transients, detected in the

astrocytic cell body, and which spread throughout astrocytic networks, were intimately involved with secretion of gliotransmitters that would in turn regulate neuronal function (Cornell-bell et al., 1990; Dani et al., 1992; Kang et al., 1998; Bazargani and Attwell, 2016). However, in the 2000s and early 2010s, the field became mired in controversy as evidence emerged refuting many previous studies (Bazargani and Attwell, 2016). For example, metabotropic glutamate receptors thought to be essential for initiating calcium waves in response to neuronal glutamate appeared not to be expressed in adult astrocytes (Sun et al., 2013). It was also argued that the kinetics of observable calcium dynamics were too slow to support their proposed role in the rapid vascular dilation evoked by neural activity (Fiacco et al., 2007; Schulz et al., 2012). Perhaps most problematic for the previous decades' worth of work were findings in mice lacking astrocytic endoplasmic reticulum (ER) calcium release. In astrocytes, inositol 1,4,5-triphosphate (IP₃)-dependent release of calcium from the ER relies on IP₃ receptor 2 (IP₃R2). Knocking out IP₃R2 eliminated almost all observable calcium signalling in astrocytes, but this did not alter neural excitability, synaptic transmission (Fiacco et al., 2007) or LTP (Agulhon et al., 2010), suggesting astrocytic calcium signalling was dispensable for these processes. However, the concerns surrounding calcium signalling raised by this line of evidence have largely been dispelled in recent years. Enhanced detection of calcium dynamics in astrocytes has been provided by membrane tethered genetically encoded calcium indicators (Shigetomi et al., 2010; Agarwal et al., 2017b), and it has become apparent that far more rapid and complex calcium signalling occurs in the thin protoplasmic astrocytic branches than was previously appreciated. Furthermore, while IP₃R2-dependent calcium release from the ER accounts for the majority of calcium signalling (~60%), mitochondria have also emerged as a major source of local calcium dynamics in astrocytes as well (Agarwal et al., 2017b). These fast, localized calcium signals, referred to as calcium microdomains, are now a major focus of study (Shigetomi et al., 2016; Agarwal et al., 2017a). Furthermore, while attempts to block calcium signalling by knocking out IP₃R2 were only partially effective,

possibly due to compensation by mitochondria, a recent gain-of-function study demonstrated that artificially augmenting calcium signalling in astrocytes with the designer receptor, hM3Dq, is sufficient for long-term potentiation in CA1 pyramidal cells of the hippocampus (Adamsky et al., 2018). Thus, astrocytic calcium signalling may yet prove to be necessary *in vivo* for the wide variety of neuronal processes it was originally shown to regulate. However, taking into account the speed, small size, and variable nature of calcium microdomains the picture is much more complex, and higher spatial and temporal resolution will likely still be required to truly understand how they regulate astrocytic and neuronal function (Wu et al., 2014).

1.2.4 Ultrastructural Studies of the Tripartite Synapse

The fine nanoscale structure of protoplasmic astrocytes has proven to be a limitation in understanding the architecture and function of these cells. However, building on early electron microscopy (EM) studies that identified the tripartite arrangement of astrocytes with synapses, largescale serial section electron microscopy (SSEM) has begun to provide insight into the organization of the smallest details of astrocytic morphology. Beginning in the 1950's, numerous studies observed that non-neuronal glial compartments were frequently found in close apposition with the synapse, and could be identified by the presence of dark staining glycogen granules, relatively clear cytoplasm, and bundles of intermediate filaments (Palay and Palade, 1955; Peters and Palay, 1965, 1996; Jones and Powell, 1970; Palay and Chan-Palay, 1974; Peters et al., 1976; Spacek, 1985). In 1985, a study that was pioneering at the time for its extensive three-dimensional reconstruction of synaptic components from short series of EM micrographs found that the extent to which synapses are ensheathed by astrocytes differs between brain regions (Spacek, 1985). Dendritic spines of pyramidal cells were observed to have only ~30% of their surface area covered by astrocytes, whereas ~75% of Purkinje cell spines were covered by Bergmann glial processes, suggesting differential regulation of these synapse types by their astrocytic partners. The observation that Purkinje

cell spines are almost totally ensheathed by Bergmann glia was confirmed 15 years later in a study that also noted the presence of morphological astrocytic microdomains, isolated from one another by thin connecting filaments, in the branches of Bergmann glia (Grosche et al., 1999). In the same year, a thorough geometrical investigation of tripartite spine synapses in the hippocampus revealed a number of interesting findings (Ventura and Harris, 1999). Firstly, only ~60% of synapses were contacted by astrocytic processes. However, over 80% of synapses that contained perforated post synaptic densities (PSDs), a hallmark of larger and thus stronger synapses with high proportions of docked vesicles, were associated with PAPs. These findings were also replicated in a later study that found newly formed spines were more thoroughly covered by PAPs (Witcher et al., 2007). More recent work on a single astrocytic volume derived from a larger SSEM dataset also showed that astrocytes are more closely associated with thin dendritic spines harboring smaller PSDs (Medvedev et al., 2014). These observations have sparked a debate as to whether astrocytes preferentially allow spillover form stronger synapses to promote heterosynaptic plasticity and local circuit synchronization, or whether this lack of coverage is simply due to spatial constraints. This debate has preoccupied a large portion of the literature on tripartite synapse ultrastructure, prompting a number of modelling studies and opinion pieces (Lehre and Rusakov, 2002; Lushnikova et al., 2009; Heller and Rusakov, 2015). Interestingly, it has been shown in acute hippocampal slices that LTP induces heightened PAP mobility and enhances coverage of synapses by PAPs (Bernardinelli et al., 2014). However, an as of yet unpublished study suggests that LTP decreases the volume fraction occupied by PAPs, and provides evidence that this results in reduced coverage of synapses using super resolution STED microscopy (Henneberger et al., 2018). On the other hand, a more recent study using SSEM reconstructions performed measurements of astrocytic volume fraction in the vicinity of the synapse and found that, based on modelling studies PAPs associated with spine synapses have equal capacity for glutamate uptake regardless of the size

of the synapse (Rusakov, 2001; Gavrilov et al., 2018). A clear answer on whether astrocytes preferentially allow spillover of glutamate under certain conditions is therefore still lacking.

Thus, SSEM investigations have begun to unveil the nanoscale organization of neuron-astrocyte interactions, however the field is still nascent and many questions remain. An important unaddressed question is how calcium sources are distributed in the convoluted network of astrocytic processes. One study examined this with indirect measurements of astrocytic volume fraction taken up by ER or mitochondria in the vicinity of synapses, with a main finding that astrocytic calcium sources are not present directly in PAPs (Patrushev et al., 2013). However, nothing is known about whether or not the distribution of astrocytic calcium sources is influenced by aspects of the local microcircuitry that astrocytes support and regulate. In Chapter 3, I present a study based on two large volumes of high resolution SSEM data, in which we reconstructed continuous portions of astrocytes that interact with hundreds of synapses. To begin to address the question of whether the distribution of astrocytic calcium stores is influenced by the surrounding microcircuitry that the astrocytes interact with, we assessed the spatial relationships of mitochondria with astrocyte-associated PSDs using an advanced computational technique to determine shortest paths and measure distances through convoluted astrocytic architecture.

Chapter 2 Depolarizing but Shunting GABA_A Transmission Restrains Glutamatergic Synapse Formation

2.1 Preamble

The work described in this section was born of a mistake made while attempting to test whether SPARC, an astrocyte secreted molecule studied in the lab, conferred neuroprotective properties when neurons were exposed to an epileptiform insult induced by blocking inhibitory neurotransmission. In a proof of concept experiment, we had verified that treating organotypic hippocampal slice cultures with the GABA_A antagonist, bicuculline (BIC) at 5 days *in vitro* (DIV) caused a loss of spines as described in the manuscript below (Figure 2), as would be expected following epileptiform activity (Zha et al., 2005)¹. However, in a follow up experiment to confirm that BIC did indeed decrease spine density, I added the drug at 3 DIV rather than 5 DIV. The result was the opposite; BIC applied to organotypic hippocampal slices for 48 hours starting at 3 DIV significantly increased spine density. This piece of data is the basis of the manuscript composing this chapter and forms the nucleus of the majority of my doctoral studies.

The following manuscript was submitted to the Journal of Neuroscience in November 2018 and was under review at the time this thesis was submitted.

¹ Incidentally, we found that BIC had the same effect in slices prepared from SPARC^{-/-} mice suggesting SPARC did not protect against epileptiform insult in this context. However, further work in the lab does suggest it is protective against oxygen glucose deprivation (Jones et al., 2018)

Depolarizing but Inhibitory GABA_A Transmission Restrains Excitatory Synapse Formation in the Developing Hippocampus

Running Title: GABA Restrains Excitatory Synapse Formation

Christopher K. Salmon¹, Horia Pribiag¹, W. Todd Farmer¹, Scott Cameron³, Vivek Mahadevan², David Stellwagen¹, Melanie A. Woodin², and Keith K. Murai^{1*}

¹Centre for Research in Neuroscience, Department of Neurology and Neurosurgery, The Research Institute of the McGill University Health Centre, Montreal General Hospital, Montreal, Quebec, H3G 1A4, Canada.

²Department of Cell & Systems Biology, University of Toronto, Toronto, Ontario, M5S 3G5, Canada.

Correspondence should be addressed to: Dr. Keith K. Murai Centre for Research in Neuroscience Montreal General Hospital 1650 Cedar Avenue L7-212 Montreal, QC, H3G 1A4 Canada Telephone: (514) 934-1934 x43477

Fax: (514) 934-8216 keith.murai@mcgill.ca

Number of figures: 8

Number of words: 8631 (Abstract 217; Intro 617; Discussion 1496)

Key Words: Dendrite, spine, synaptogenesis, chloride, neural circuit, NKCC1, KCC2.

Acknowledgements: The authors would like to acknowledge technical support and training from Dr. Emma Jones, and to thank Dr. Andrew Greenhalgh and Andy YL Gao for critical review of the manuscript. This work was supported by the Canadian Institutes of Health Research (M.A.W and K.K.M) and Natural Sciences and Engineering Research Council of Canada (K.K.M). C.K.S. was supported through a CGS-M from the CIHR and a Doctoral Award from the FRQS. The authors declare no competing financial interests.

³Center for Neuroscience, University of California Davis, Davis, California 95618, USA.

2.2 Abstract

GABA is the main inhibitory neurotransmitter in the mature brain but has the distinct property of depolarizing neurons in the immature brain. Importantly, depolarizing GABA_A transmission can either drive neural activity, or it can inhibit neural activity through shunting inhibition. When and where these different effects of depolarizing GABA_A transmission occur during development is unclear. While depolarizing GABAA transmission is implicated in many aspects of neural circuit development, its precise role in glutamatergic synapse formation has yet to be elucidated. Here we addressed the importance of depolarizing but inhibitory – or shunting – GABA_A transmission, for glutamatergic synapse development in hippocampal CA1 pyramidal neurons. Based on the expression profile of K⁺-Cl⁻ cotransporter 2 (KCC2), changes in the GABA reversal potential, and the inhibitory effect of GABA on spontaneous and evoked firing, we pinpointed the timing of the switch from depolarizing to hyperpolarizing GABA_A transmission in CA1 neurons in organotypic slice culture. Blocking depolarizing GABA_A transmission increased excitatory synapse number and function, and these changes were sustained more than a week later. The effects correlated with transcription of canonical activity-regulated genes but were independent of BDNF signalling. Together these findings point to the ability of immature GABAergic transmission to restrain glutamatergic synapse formation and suggest an unexpected role for depolarizing GABAA transmission in shaping excitatory connectivity during neural circuit development.

2.3 Significance Statement

GABA, the main inhibitory neurotransmitter in the mature brain, is paradoxically thought to promote neural excitation during development. GABAergic excitation is hypothesized to shape neural circuits in immature neurons. However, recent evidence suggests that GABA can be inhibitory during postnatal development in rodents. We present evidence that GABA is inhibitory during early hippocampal development, and that immature GABA neurotransmission restrains synapse formation during this time. Blocking GABA transmission for 2 days during development in cultured brain slices increases the number of excitatory synapses that form, and the number of synapses stay elevated for more than a week after GABA blockers are removed. These results suggest that disrupting GABA transmission during development can profoundly alter brain wiring in an unexpected way.

2.4 Introduction

γ-Aminobutyric acid (GABA) is the main inhibitory neurotransmitter in the mature brain. However, in rodents, during gestation and the first one to two weeks of postnatal development, GABA has been shown to be depolarizing. Many *in vitro* studies show that depolarizing GABA_A transmission provides excitatory drive in developing circuits, promoting early network oscillations referred to as giant depolarizing potentials (GDPs) (Ben-Ari et al., 2012), however, recent work suggests that despite providing local depolarization, immature GABA_A transmission has inhibitory effects *in vivo* (Kirmse et al., 2015; Oh et al., 2016; Valeeva et al., 2016). This ability of GABA to be simultaneously depolarizing and inhibitory relies on shunting inhibition, which results from a decrease in input resistance and membrane time constant when GABA_A receptors open (Staley and Mody, 1992). Importantly, shunting inhibition can occur in parallel with both hyperpolarizing and depolarizing GABA_A transmission. We therefore refer to depolarizing GABA_A transmission that results in shunting inhibition as depolarizing/inhibitory.

Depolarizing GABA_A transmission is implicated in numerous developmental processes including neural stem cell proliferation (Liu et al., 2005), cell migration (Behar et al., 2000), neurite outgrowth (Cancedda et al., 2007), and circuit refinement (Akerman and Cline, 2006; Cancedda et al., 2007; Wang and Kriegstein, 2008). Critically, circuit activity supported by depolarizing GABA_A transmission in vitro drives calcium influx thought to be important for glutamatergic synapse development and circuit refinement (Leinekugel et al., 1995; Ben-ari et al., 1997; Griguoli and Cherubini, 2017). Indeed, disrupting the depolarizing nature of GABA_A transmission by interfering with chloride homeostasis alters glutamatergic synapse formation and maturation (Akerman and Cline, 2006; Wang and Kriegstein, 2008). However, the effects of GABA_A transmission itself on glutamatergic synapse development and the timing of these effects remain poorly defined. This is due, in part, to the multiple roles of GABA during development and the difficultly in manipulating depolarizing GABAA transmission specifically during the period when glutamatergic synapses are forming. Several studies have prematurely hyperpolarized the reversal potential for chloride (E_{Cl}) by disrupting chloride homeostasis for more than a week during perinatal development, across a timespan in which the targeted neurons terminally divide, migrate, extend neurites and are incorporated into the surrounding circuitry (Cancedda et al., 2007; Wang and Kriegstein, 2008). This work suggests that disrupting E_{Cl} alters neurite and synapse maturation, however, additional studies with higher temporal resolution are needed. Understanding how GABAA transmission and its transition from a depolarizing to a hyperpolarizing state impacts glutamatergic synapse development is critical, as disruptions of GABA_A transmission during brain development are associated with intellectual disability (El Marroun et al., 2014; Tyzio et al., 2014).

Here we investigated the role of immature GABA_A transmission in glutamatergic synapse formation on CA1 hippocampal pyramidal cells. We took advantage of the properties of organotypic hippocampal slices, a preparation which preserves many anatomical features, and the developmental progression of the hippocampus, including the time course of

excitatory synapse formation (Buchs et al., 1993; Muller et al., 1993; De Simoni et al., 2003). This system enabled us to define a narrow time window during the first week of slice development in which GABA_A transmission shifts from immature, depolarizing/inhibitory transmission, to hyperpolarizing transmission in CA1 cells. Previous work suggests that blocking GABA_A transmission before it transitions to a hyperpolarizing current will remove excitatory drive and decrease excitatory synapse formation and maturation (Ben-Ari et al., 2007; Wang and Kriegstein, 2008). Contrary to these predictions, we show that transient blockade of immature, depolarizing but inhibitory GABA_A transmission increased glutamatergic synapse number and function on CA1 pyramidal cells. Changes in synapse numbers were stable for more than a week and were independent of BDNF signalling. Our results point to an important time window during hippocampal development when immature GABA_A transmission can control excitatory synapse development.

2.5 Materials and Methods

Animals

Experiments were approved by the Montreal General Hospital Facility Animal Care Committee and followed guidelines of the Canadian Council on Animal Care. Male and female C57BL6 mice kept on a 12:12 light-dark cycle were used to prepare organoptypic cultures.

Slice Preparation

Organotypic hippocampal slices were prepared as described previously (Haber et al., 2006). Briefly, hippocampi were extracted from postnatal day 5 mice and cut into 300µm slices with a McIllwain tissue chopper (Stoelting). Slices were cultured on semiporous tissue culture inserts (Millipore) that sat in culture medium composed of minimal essential medium (MEM) supplemented with Glutamax (Invitrogen, Cat. No. 42360032), 25% horse serum (Invitrogen, Cat. No. 26050088), 25% HBSS (Invitrogen, Cat. No. 14025092), 6.5 mg/mL D-glucose and

0.5% penicillin/streptomycin. Slices were cultured for 5-14 days with full medium changes every 2 days.

Labeling of CA1 Cells

Dendrites and spines of CA1 pyramidal cells were labelled using a Semliki Forest Virus (SFV)-mediated approach describe in detail elsewhere (Haber et al., 2006). Briefly, SFV driving expression of enhanced green fluorescent protein, targeted to the cell membrane through a farnesylation sequence (EGFPf), was injected into the stratum oriens via pulled glass pipette, broken to a diameter of approximately 50 to 100 μ m. Glass pipettes were attached to a Picospritzer III (Parker Hannifin) and SFV was delivered with 10ms pulses at 14 to 18 psi 18 to 20 hours before fixation in 4% formaldehyde/0.1 M PO₄ ²⁻ for 30 min.

Confocal Imaging and Spine Analysis

Imaging was performed using an Ultraview Spinning Disc confocal system (Perkin Elmer) attached to a Nikon TE-2000 microscope and a FV1000 laser scanning confocal microscope (Olympus). Z-stacks were acquired from approximately 100μm of CA1 primary apical dendrites, just above the primary dendrite bifurcation. This dendritic subfield is consistently identifiable, fully formed by the period of interest, harbors the highest density of asymmetric synapses, and retains its native connectivity in organotypic slices (Megias et al., 2001; Amaral and Lavenex, 2007). Ten to forty z-stacks were acquired per animal (4 to 8 slices per animal, 2-4 animals per experiment, minimum 3 experiments per dataset). Two-dimensional spine counts and geometric measurements of spines were quantified using Reconstruct (Fiala, 2005) and a custom ImageJ macro. 3D spine classification was performed with NeuronStudio (Rodriguez et al., 2008). All spine analysis was performed by an investigator blinded to the experimental condition.

Western Blot Analysis

For Western blots, 4-6 organotypic slices were lifted from nylon culture inserts with a No. 10 scalpel blade, rinsed in cold PBS and incubated on ice in 100µL of Triton lysis buffer (20 mM

Tris pH7.4, 137 mM NaCl, 2mM EDTA, 1% Triton X100, 0.1% SDS, 10% glycerol, with protease inhibitors and sodium orthovanadate) for 30 min. Lysates were centrifuged at high speed for 10 min and stored at -80°C in sample buffer. Supernatants were warmed to room temperature and run under standard SDS-PAGE conditions. Membranes were immunoblotted with anti-KCC2 1:1000 (N1/12, NeuroMab, CA) and GAPDH 1:300,000 (MAB374, Millipore). KCC2 blots were run immediately after developmental time courses ended to reduce experimentally-induced aggregation of KCC2 oligomers, which we observe to increase with time at -80°C.

Electrophysiology

Gramicidin perforated patch whole cell recordings were performed similar to previously described (Acton et al., 2012). Briefly, current-voltage (IV) curves were generated by step depolarizing the membrane potential in 10mV increments from ~-95 to -35mV (Fig. 1C) and during each increment GABAergic transmission was elicited via extracellular stimulation in the stratum radiatum. Pipettes had a resistance of 7–12 M Ω and were filled with an internal solution containing 150mM KCl, 10mM HEPES, and 50mM μ g/ml gramicidin (pH 7.4, 300 mOsm). We recorded E_{GABA} in current clamp mode. Glutamatergic transmission was inhibited with CNQX.

Miniature EPSCs (mEPSCs) were recorded using the whole-cell patch clamp configuration ($V_h = -70 \text{mV}$), at 30°C, in ACSF containing (in mM): 119 NaCl, 26.2 NaHCO₃, 11 D-glucose, 2.5 KCl, 1 NaH₂PO₄, 2.5 CaCl₂, 1.3 MgCl₂, 0.0002 TTX, 0.025 D-APV, 0.05 picrotoxin. Recording pipettes (2-5 M Ω) were filled with (in mM): 122 CsMeSO₄, 8 NaCl, 10 D-glucose, 1 CaCl₂, 10 EGTA, 10 HEPES, 0.3 Na₃GTP, 2 MgATP, pH 7.2. Signals were low-pass filtered at 2kHz, acquired at 10 kHz, and analyzed using Clampfit 10.3 (Molecular Devices).

For cell attached recordings, ACSF and pipette solutions were as described above for mEPSC recordings, but ACSF lacked TTX, D-APV and picrotoxin. Low resistance recording pipettes

(1-2 M Ω) were used to form loose patch seals (approximately 100-350 M Ω). Recordings were performed in I=0 mode. GABA was diluted in ACSF to 100 μ M and puffed in close proximity to the recorded cell using a glass pipette connected to a Picospritzer III (Parker Hannifin) delivering 10 ms duration air puffs at 14 psi. Electrically-evoked stimulations (1.3 V, 0.5 ms) were delivered by the recording amplifier via the recording pipette. Recorded signals were analyzed using threshold-based detection of spikes in Clampfit 10.3 (Molecular Devices).

Experiments comprised slices from at least 3 separate animals taken from at least 2 litters.

Pharmacology

Pharmacological agents (Tocris unless otherwise noted) were applied to the culture medium during a regular medium change. Gabazine (GBZ) (20 μ M), bicuculline-methiodide (20 μ M) and muscimol (10 μ M) were used to manipulate GABA_A transmission. GBZ was washed out by incubating slices in fresh medium for 30 minutes, then washing the top of the slices with equilibrated medium for 1-2 minutes before changing to fresh dishes and medium. Bumetanide (Bume, 10 μ M), TrkB-Fc bodies (5mg/mL, R&D Systems) and K252a (200 nM) were added to cultures 30 minutes before adding GBZ.

Quantitative Reverse Transcriptase PCR (qRT-PCR)

Six to eight organotypic slices per sample were lifted from nylon culture inserts with a No. 10 scalpel blade, washed briefly in ice cold PBS and flash frozen in microcentrifuge tubes in a 100% EtOH/dry ice slurry. Total RNA was extracted using the RNeasy Lipid Tissue Kit (Qiagen). cDNA libraries were created using QuantiTect Reverse Transcription Kit (Qiagen). Quantitative PCR was performed using Sybr Green Master Mix (Applied Biosystems Systems) on a StepOne Plus thermocycler (Applied Biosystems). Relative levels of mRNA were calculated using the ΔΔCT method with GAPDH as the internal control. Primer sequences were as follows: GAPDH forward TTG AAG TCG CAG GAG ACA ACC; GAPDH reverse ATG TGT CCG TCG TGG ATC; BDNF forward GTG ACA GTA TTA GCG AGT

GGG; BDNF reverse GGG ATT ACA CTT GGT CTC GTA G; Fos forward TCC CCA AAC TTC GAC CAT G; Fos reverse CAT GCT GGA GAA GGA GTC G.

Statistics

Data is presented as mean ± SEM. Student t-tests were used except where noted that Mann-Whitney tests were used with datasets with non-normal distribution. Post hoc pairwise comparisons following ANOVA were performed with Tukey's honestly significant difference (HSD) test. For mean comparisons: *p<0.05, **p<0.01, ***p<0.001. For Kolmogorov-Smirnov tests: ***p<0.0001.

2.6 Results

GABA_A transmission switches from depolarizing to hyperpolarizing in CA1 cells during the first week in hippocampal slice culture.

Depolarizing GABA_A transmission relies on relatively high [Cl⁻]_i. As neurons mature during the first weeks of postnatal CNS development, they downregulate Na⁺-K⁺-Cl⁻ cotransporter (NKCC1) and upregulate K⁺-Cl⁻ cotransporter 2 (KCC2), lowering [Cl⁻]_i (Rivera et al., 1999; Yamada et al., 2004). GABA_A receptors are largely permeable to Cl⁻, and to a lesser extent bicarbonate (HCO₃⁻) (Kaila, 1994; Staley and Proctor, 1999). When [Cl⁻]_i lowers to the point at which the reversal potential for GABA (E_{GABA}) hyperpolarizes below the resting membrane potential, GABA_A transmission switches from depolarizing to hyperpolarizing. To pinpoint when this switch from depolarization to hyperpolarization occurs in CA1 pyramidal cells in hippocampal organotypic slices, we first assessed the timing of KCC2 upregulation across the first two weeks *in vitro* and found expression of both KCC2 monomers (KCC2-M) and oligomers (KCC2-O) to be near maximal by 7 days *in vitro* (DIV) (Fig. 1B), with a large and graded increase between 3 and 7DIV (Fig. 1A,B). Using this timeframe as a guide, we performed gramicidin perforated patch recordings to determine the GABA_A reversal potential (E_{GABA}) in CA1 pyramidal cells, with exemplary traces and IV curves

shown in Figures 1C and D. At 3-4 DIV, E_{GABA} was depolarized with respect to resting membrane potential (RMP) (Fig. 1E-H). However, by 6-7 DIV E_{GABA} was hyperpolarized with respect to RMP, indicating a switch to hyperpolarizing GABA_A transmission by 6-7 DIV (Fig. 1C-H), a timeframe similar to that reported previously for CA1 pyramidal cells (Swann et al., 1989). E_{GABA} was more negative than action potential threshold at 3-4 DIV (Fig. 1E-F,H), suggesting GABA is depolarizing but not capable of depolarizing neurons past action potential (AP) threshold, and thus GABA potentially mediates shunting inhibition at this point (Fig. 1H). To test this possibility, we puffed GABA locally while recording spontaneous or electrically evoked firing. GABA inhibited both spontaneous (Fig. 1I,J) and evoked spiking (Fig. 1K-M), suggesting that although E_{GABA} is depolarized relative to RMP, it provides shunting inhibition during the 3-4 DIV timeframe.

Blocking depolarizing/inhibitory GABA_A transmission increases CA1 spine density.

Overexciting mature neurons by blocking hyperpolarizing GABA_A transmission is known to cause a collapse of dendritic spines in both *in vivo* models of epilepsy (Zeng et al., 2007) and pharmacologically induced overexcitation *in vitro* (Muller et al., 1993; Drakew et al., 1996; Jourdain et al., 2002; Zha et al., 2005). In particular, applying GABA_A antagonists to organotypic hippocampal cultures at 5 or 23 DIV over a period of 2 to 3 days causes a robust loss of spines (Drakew et al., 1996; Zha et al., 2005). Consistent with this, when we blocked GABA_A transmission with the GABA_AR antagonist, bicuculline (BIC) from 5-7 DIV (when GABA_A transmission is hyperpolarizing (Fig. 1C-H)), spine density decreased by 34% (Fig. 2). This suggests that by this stage, excitatory transmission causes overexcitation and spine loss in the absence of hyperpolarizing GABA_A transmission.

To assess the role of immature, depolarizing GABA_A transmission on dendritic spine development, we inhibited GABA_A transmission earlier, from 3–5 DIV (Fig. 3A). Previous work suggests that inhibiting depolarizing GABA_A transmission during development would decrease glutamatergic synapse formation and maturation (Ben-ari et al., 1997; Hanse et al.,

1997; Cancedda et al., 2007; Wang and Kriegstein, 2008). However, in contrast to these findings, BIC applied for 48 hours from 3 to 5 DIV significantly increased dendritic spine density (25% increase) (Fig. 3B-C). This effect was fully reproducible with the GABA_AR antagonist gabazine (GBZ) (31% increase), which is a more specific antagonist of GABAARs (Heaulme et al., 1986) and blocks inhibition more consistently in hippocampal neurons (Sokal et al., 2000). To assess whether the supernumerary spines induced by blocking depolarizing but inhibitory GABAA transmission showed structural differences, we analyzed spine morphology. GBZ treatment did not affect the proportions of mushroom, thin, and stubby spines (Fig. 3D), 2-dimensional head area (Control: 0.32±0.02 μm²; GBZ: 0.37±0.04 μm², p>0.10), head diameter (Control: $0.58\pm0.02 \,\mu\text{m}^2$; GBZ: $0.62\pm0.03 \,\mu\text{m}^2$, p>0.1), spine length (Control 1.66 \pm 0.09 μ m²; GBZ: 1.83 \pm 0.08 μ m², p>0.1) or dendrite diameter (Fig. 3E). We next asked whether the increased number of spines constituted an increase in bona fide glutamatergic synapses on CA1 cells by recording miniature EPSCs (mEPSC). Consistent with the increase in dendritic spine density, mEPSC analysis showed that GBZ treatment (3-5 DIV) increased mESPC frequency 3-fold (Fig. 3F,G). Miniature EPSC amplitude also increased, indicating enhanced synaptic strength (Fig. 3H,I). Together, these results suggest that depolarizing but inhibitory GABA_A transmission restrains glutamatergic synapse formation and maturation.

The narrow time window we examined raised the possibility that the spine-enhancing effect of GABA_A blockade is limited to a short period directly prior to the depolarizing to hyperpolarizing shift in GABA_A transmission. This would suggest that GABA_A transmission restrains glutamatergic synapse formation only during a very short transition state. To test whether this was the case, we prepared slices 3 days earlier (P2) and applied GBZ at 3DIV for 48h. We found that GABA_AR blockade in these younger slices also caused a significant increase in spines (Ctrl 0.22 ± 0.008 spines/ μ m, GBZ 0.28 ± 0.01 spines/ μ m, p<0.001, Mann

Whitney), suggesting that depolarizing GABA_A transmission is capable of restraining synapse formation for an appreciable period during postnatal development.

Driving depolarizing/inhibitory GABA_A transmission does not alter glutamatergic synapse number.

Next, we investigated if increasing GABA_A transmission over the 3-5 DIV period would reduce excitatory synapses. This hypothesis is supported by previous work demonstrating that propofol, a positive allosteric modulator of GABAARs, decreases spine density in developing layer 2/3 principal cells of the somatosensory cortex when administered to rat pups over a 6h period at postnatal day 10, when GABA is still depolarizing (Puskarjov et al., 2017). To test this in the CA1 pyramidal cells, we increased depolarizing GABA_A transmission by administering muscimol (MUS) or diazepam (DZP) from 3 to 5DIV. MUS treatment did not significantly decrease spine density (Fig. 4C). Furthermore, mEPSC frequency was unchanged, confirming MUS did not alter synapse numbers (Fig. 4D,E). MUS has varying effects on different GABA receptors and can cause GABAA receptor desensitization, making its effects difficult to interpret (Heck et al., 2007; Mortensen et al., 2010; Johnston, 2014). We therefore also tested whether enhancing GABA_A transmission with DZP could decrease glutamatergic synapses, but this also had no effect on spine density or mEPSCs (Fig 4 B-F). Based on these results, increasing GABA_A transmission was not sufficient to decrease glutamatergic synapse number or function, suggesting depolarizing GABAA transmission can only limit synapse formation up to a certain point at this stage of development. However, we cannot rule out the possibility that enhancing immature GABA_A transmission on different timescales or in other systems decreases glutamatergic synapse formation (Puskarjov et al., 2017).

BDNF is associated with, but not necessary for, the increase in glutamatergic synapses.

Blocking shunting GABA_A transmission likely increases activity in our preparation, suggesting that the increase in glutamatergic synapses may be driven by activity-dependent mechanisms (Balkowiec and Katz, 2002; Pérez-Gómez and Tasker, 2013). To address this hypothesis, we measured levels of *Bdnf* and *Fos* mRNA, two activity regulated genes associated with glutamatergic synapse formation (Vicario-Abejón et al., 1998, 2002; Tyler and Pozzo-Miller, 2003; Chapleau et al., 2009). Both transcripts were significantly upregulated following 48-hour blockade of depolarizing/inhibitory GABA_A transmission (*Bdnf*: 5-fold increase, *Fos*: 2.5-fold increase) (Fig. 5A). As BDNF is known to regulate activity-dependent synapse formation and plasticity (Park and Poo, 2013), we asked whether BDNF signaling was responsible for the increase in spines following blockade of depolarizing/inhibitory GABA_A transmission. We inhibited BDNF signalling using two approaches: with TrkB-Fc bodies or with the inhibitor K252a (Ji et al., 2010; Puskarjov et al., 2014). Neither treatment with TrkB-Fc nor K252a during 48-hour blockade of GABA_A transmission blocked the increase in spine density mediated by GBZ (Fig. 5B,C), suggesting that BDNF signalling is not necessary for the observed increase in spines.

Bumetanide treatment does not change spine numbers

Previous work suggests that GABA-mediated depolarization drives synapse formation and maturation. However, our data show that a loss of depolarizing GABAergic transmission increases spines and synapses. These contrasting results raise the question of whether the depolarizing nature of GABA_A is important for the normal development of glutamatergic synapses in our period of interest (3–5 DIV). To address this, we asked whether prematurely hyperpolarizing E_{GABA} could mimic the effect of GABA_A blockade. KCC2 overexpression (OE) can be used to lower E_{GABA} in immature neurons (Cancedda et al., 2007), but also enhances spine formation through KCC2's chloride transport-independent scaffolding role (Li et al., 2007; Fiumelli et al., 2012). Indeed, when we overexpressed KCC2 from 2–5 DIV

via biolistic transfection, preliminary data indicated that spine density trended toward an increase (Control plasmid: 0.43±0.06 spines/μm; KCC2 OE: 0.55±0.04 spines/μm, p=0.1). To avoid this confound, we treated slices with the NKCC1 antagonist, bumetanide, which is well established to lower E_{GABA} in immature neurons (Dzhala et al., 2005) and prematurely render GABA hyperpolarizing (Wang and Kriegstein, 2011). However, treatment with bumetanide did not alter spine density (Fig. 6A,B), indicating that the depolarizing nature of GABA is not important for restraining spine formation, and thus suggesting that the inhibition provided by shunting GABA_A transmission is likely the important factor for limiting spine density. However, bumetanide did abrogate the affect of GBZ on spine numbers (Fig. 6A,B). This may be explained by the expected decrease in RMP with bumetanide treatment (Sipilä et al., 2006), which would likely lower cell excitability, diminishing activity dependent synapse formation promoted by GABA_A blockade.

As mentioned, KCC2 overexpression can cause an increase in spines through its non-transport, scaffolding function (Li et al., 2007; Fiumelli et al., 2012). To address whether the increase in synapses following GBZ treatment from 3 to 5 DIV is mediated by an increase in KCC2 levels, we assessed KCC2 expression following GBZ treatment. GBZ did not significantly elevate expression of KCC2 oligomers or monomers (Fig. 6C-E).

Blocking depolarizing GABA_A transmission leads to a sustained increase in spine/synapse density.

The increase in spine density induced by blocking depolarizing/inhibitory GABA_A transmission may only lead to a transient alteration without a longer lasting effect on glutamatergic synapses. To determine whether blockade of GABA_A transmission caused a temporary or sustained increase in glutamatergic synapses, we treated slices with GBZ from 3–5 DIV and allowed them to recover for an additional 5–9 days in the absence of GBZ (Fig. 7A). This temporary GABA_A blockade resulted in a 37% increase in spine density after a 5–day recovery period (Fig. 7B, C). Furthermore, after this recovery period, CA1 cells had more

thin spines than mushroom spines, a difference not present in the control condition (Fig. 7D). No changes in dendrite diameter were observed (Fig. 7E). To determine if transient GBZ treatment led to long-term functional changes in glutamatergic synapses, we recorded mEPSC frequency and amplitude after 8-9 days of recovery. We found that mEPSC frequency was enhanced by 79%, while mEPSC amplitude was unchanged at this stage (Fig. 7F-H). Together these data suggest that inhibiting depolarizing GABA_A transmission during a narrow time window of 48 hrs can lead to persistent changes in glutamatergic synapse number in the hippocampus.

2.7 Discussion

Immature, depolarizing GABA_A transmission is believed to promote glutamatergic synapse formation and maturation (Ben-ari et al., 1997; Hanse et al., 1997; Wang and Kriegstein, 2009; Chancey et al., 2013). However, when and how GABA affects glutamatergic synapse formation remains to be fully understood. Indeed, several groups have noted that tools and approaches for manipulating depolarizing GABAA transmission with higher temporal and spatial precision are needed to resolve this (Akerman and Cline, 2007; Chancey et al., 2013; Kirmse et al., 2018). We therefore sought to address the role of GABA_A transmission in glutamatergic synapse formation by performing precisely timed pharmacological manipulations in hippocampal slice cultures. We first mapped the depolarizing to hyperpolarizing shift of GABA_A transmission in CA1 cells. This was followed by structural electrophysiological analysis which showed that blocking and immature, depolarizing/inhibitory GABA_A transmission enhanced glutamatergic synapse function and number. Interestingly, the enhanced synapse number was stable following a recovery period. These results suggest that immature GABA_A transmission restrains glutamatergic synapse formation during an early phase of hippocampal circuit development.

An unpredicted role for immature GABA_A transmission in restraining glutamatergic synapse formation

In the time window we examined, GABA_A transmission provides subthreshold depolarization and shunting inhibition, which when blocked alleviates a brake on glutamatergic synapse development. Taken in the context of previous work, our results suggest a couple of models for how immature GABA_A transmission affects hippocampal excitatory connectivity (Fig. 8). Firstly, the GABA-mediated restraint on glutamatergic synapse formation may be a short-lived feature of a shunting transition state that GABA passes through as E_{Cl} matures from depolarizing and excitatory to hyperpolarizing (Model 1, Fig. 8A-C). However, recent work suggests GABA may be inhibitory throughout most or all of postnatal development. Therefore, in a second model, depolarizing but inhibitory GABA_A transmission may inhibit circuit activity from birth onward (Model 2, Fig. 8B-C), thus restraining glutamatergic synapse formation across development.

Evidence from acute slices suggests that early GABA_A transmission is capable of driving excitation (Gulledge and Stuart, 2003) and that depolarizing GABA_A transmission drives GDPs, which promote glutamatergic synapse formation, unsilencing, and circuit refinement (Hanse et al., 1997; Ben-Ari, 2002; Wang and Kriegstein, 2009; Griguoli and Cherubini, 2017). Disrupting E_{Cl} or GABA_A transmission in this phase of development is hypothesized to interfere with synapse formation (Fig. 8A), and this has been borne out by experimentally lowering E_{Cl} across the postmitotic period in immature neurons (Ge et al., 2006; Cancedda et al., 2007; Wang and Kriegstein, 2008). Incorporating our results refines this model and accounts for the role of GABA_A transmission in circuit development as it transitions from a depolarizing and excitatory to a hyperpolarizing state. We posit that following the depolarizing and excitatory phase of GABA_A transmission, as E_{Cl} progressively matures, GABA_A transmission passes through a transient but developmentally relevant depolarizing but inhibitory phase (Fig. 8B). Such a transition phase is hinted at in the literature, as numerous

studies have shown that blocking depolarizing GABA_A transmission can either silence GDPs, or increase circuit activity by eliciting interictal discharges or paroxysmal activity (Le Magueresse et al., 2006; Ben-Ari et al., 2007). Our results suggest that during this transition phase, GABA_A transmission is inhibitory and restrains glutamatergic synapse formation. Blocking GABA_A transmission at this time alleviates the restraint, allowing for activity-dependent synapse formation (Fig. 8B). Following this transition phase, GABA_A transmission becomes fully hyperpolarizing as the glutamatergic system becomes capable of overexcitation. The result of GABA_A blockade at this stage is loss of spines (Fig. 2 and 8C) (Swann et al., 1989; Drakew et al., 1996; Zeng et al., 2007).

Alternatively, it is possible that GABA provides shunting inhibition throughout the postnatal period, thereby restraining synapse formation and circuit activity during development (Fig. 8B-C, green shaded area). Indeed, emerging evidence suggests that depolarizing GABA_A transmission exerts inhibitory effects on early network oscillations (ENOs) in vivo, from at least P3 onward (Kirmse et al., 2015; Valeeva et al., 2016; Che et al., 2018). Consistent with this, our results in slices cultured from younger mice suggest that GABA_A transmission restrains synapse formation over a period of up to 5 days of hippocampal circuit development. Although previous work has demonstrated that prematurely rendering GABA_A transmission hyperpolarizing in vivo decreases glutamatergic synapse formation (Ge et al., 2006; Cancedda et al., 2007; Wang and Kriegstein, 2008, 2011), it is noteworthy that these studies manipulated E_{Cl} over extended periods that spanned multiple phases of postmitotic neuronal development, including cell migration, axonal/dendritic growth, synapse formation and circuit refinement. Depolarizing GABA_A transmission is thought to play important roles in all of these processes (Owens and Kriegstein, 2002), and hence the observed effects of prematurely reducing E_{Cl} on synapses may be secondary to other alterations in neuronal and circuit development. Indeed, soma size and dendritic branching are altered when GABA is prematurely rendered hyperpolarizing over an extended time period

(Cancedda et al., 2007; Wang and Kriegstein, 2008). More temporally precise manipulations of GABA transmission and E_{Cl} are therefore essential for clarifying the role or roles of GABA during critical phases of synapse formation. It is also important to note that an overarching inhibitory effect of GABA_A transmission does not preclude a role for GABA in ENOs, as it has been demonstrated that depolarizing chloride currents are only involved in the initial generation of GDPs in acute slices, after which they inhibit the continuation of the same GDPs (Khalilov et al., 2015). Thus, depolarizing GABA may simultaneously generate ENOs, while also maintaining control of wider circuit activity, thereby limiting runaway glutamatergic synapse formation. Furthermore, despite evidence suggesting GABA is inhibitory throughout development, it has been shown that high frequency uncaging or stimulated release of GABA onto dendrites of layer 2/3 pyramidal cells in the neocortex can elicit formation of glutamatergic and GABAergic synapses during development in vivo (Oh et al., 2016). Although it remains to be seen whether endogenous patterns of GABA release can have similar effects, this study suggests a local trophic role for depolarizing GABAA transmission, which may promote synapse formation even as its circuit-wide inhibitory effects restrain the same process. More work is needed to dissect the possible roles of GABA in local synapse formation and more global circuit development, and to understand how the role of GABA changes across development.

GABA_A Transmission and Sustained Changes in Glutamatergic Synapses

Remarkably, transient blockade of depolarizing, inhibitory GABA_A transmission led to a sustained increase in both the number of glutamatergic synapses and the proportion of thin spines, indicating that transient manipulations of immature GABA_A transmission can profoundly alter hippocampal connectivity (Fig. 7). Using slice cultures allowed for more temporally precise manipulations that revealed this effect, though several limitations of this model system must be considered when interpreting our results. Exuberant glutamatergic

synapse formation has been observed in slice cultures, and has been attributed to increases in distal dendritic branching (De Simoni et al., 2003). We minimized this confound by focussing on primary apical dendrites, which are fully formed by the time of pharmacological treatment, but enhanced growth of distal dendrites and synapses may interfere with other developmental processes and alter circuit dynamics. Slice dissection is also followed by a decrease in synapses which offsets the development of normal synapse numbers by about a week (De Simoni et al., 2003). This raises the concern that the ontogeny of E_{Cl} and synapse formation may be offset from each other compared to *in vivo*, however we also observed a marked decrease in KCC2 expression between the day of culturing and 3DIV, suggesting that development of these two systems in organotypic slices may be equally delayed.

Taking these points into consideration, our work suggests that immature GABAA transmission is capable of restraining glutamatergic synapse formation. The finding that propofol administered to postnatal day 10 rats decreased spine number supports the notion that there is a developmental period in vivo during which immature GABAA transmission restrains glutamatergic synapse formation (Puskarjov et al., 2017). Further work is required to determine if and when disrupting GABA_A transmission in vivo also enhances glutamatergic synapse formation, and whether such changes are lasting. These questions are clinically relevant, as a role for GABA in restraining synapse formation may change how we understand and mitigate the effects of anticonvulsants, anaesthetics and drugs of abuse on neonatal, as well as fetal development, as GABA is believed to be depolarizing mainly in late gestation in humans (Vanhatalo et al., 2005; Sedmak et al., 2015). Both the increase in synapses and spines and the shift in spine morphologies we observed after recovery from transient GBZ treatment are reminiscent of "spinopathies" seen in intellectual disabilities including Fragile X syndrome and autism spectrum disorders (Lacey and Terplan, 1987; Irwin et al., 2000, 2001; Kaufmann and Moser, 2000; Fiala et al., 2002; Hutsler and Zhang, 2010). Further investigation is required to understand if impairments of inhibition provided by immature, depolarizing GABAA

transmission contribute to the lasting alterations of spines and synapses in these conditions. Furthermore, the possibility that GABA bidirectionally controls synapse formation may yield novel clinical approaches for correcting synaptic deficits in neurodevelopmental disorders.

2.8 References

- Acton BA, Mahadevan V, Mercado A, Uvarov P, Ding Y, Pressey J, Airaksinen MS, Mount DB, Woodin MA (2012) Hyperpolarizing GABAergic transmission requires the KCC2 C-terminal ISO domain. J Neurosci 32:8746–8751.
- Akerman CJ, Cline HT (2006) Depolarizing GABAergic conductances regulate the balance of excitation to inhibition in the developing retinotectal circuit in vivo. J Neurosci 26:5117–5130.
- Akerman CJ, Cline HT (2007) Refining the roles of GABAergic signaling during neural circuit formation. Trends Neurosci 30:382–389.
- Amaral D, Lavenex P (2007) The Hippocampus Book (Andersen P, Morris R, Amaral D, Bliss T, O'Keefe J, eds). Oxford: Oxford University Press.
- Balkowiec A, Katz DM (2002) Cellular mechanisms regulating activity-dependent release of native brain-derived neurotrophic factor from hippocampal neurons. J Neurosci 22:10399–10407.
- Behar TN, Schaffner AE, Scott CA, Greene CL, Barker JL (2000) GABA receptor antagonists modulate postmitotic cell migration in slice cultures of embryonic rat cortex. Cereb Cortex 10:899–909.
- Ben-Ari Y (2002) Excitatory actions of GABA during development: the nature of the nurture. Nat Rev Neurosci 3:728–739.
- Ben-Ari Y, Cherubini E, Corradetti R, Gaiarsa J (1989) Giant synaptic potentials in immature rat CA3 hippocampal neurones. J Physiol 416:303–325.
- Ben-Ari Y, Gaiarsa J-L, Tyzio R, Khazipov R (2007) GABA: a pioneer transmitter that excites immature neurons and generates primitive oscillations. Physiol Rev 87:1215–1284.
- Ben-ari Y, Khazipov R, Leinekugel X, Caillard O, Gaiarsa J (1997) GABAA, NMDA and AMPA receptors: a developmentally regulated 'ménage à trois.' Trends Neurosci 20:523–529.
- Ben-Ari Y, Woodin MA, Sernagor E, Cancedda L, Vinay L, Rivera C, Legendre P, Luhmann HJ, Bordey A, Wenner P, Fukuda A, van den Pol AN, Gaiarsa J-L, Cherubini E (2012) Refuting the challenges of the developmental shift of polarity of GABA actions: GABA more exciting than ever! Front Cell Neurosci 6:35.
- Buchs P-A, Stoppini L, Muller D (1993) Structural modifications associated with synaptic development in area CA1 of rat hippocampal organotypic cultures. Brain Res Dev Brain Res 71:81–91.
- Cancedda L, Fiumelli H, Chen K, Poo M (2007) Excitatory GABA action is essential for

- morphological maturation of cortical neurons in vivo. J Neurosci 27:5224-5235.
- Chancey JH, Adlaf EW, Sapp MC, Pugh PC, Wadiche JI, Overstreet-Wadiche LS (2013) GABA depolarization is required for experience-dependent synapse unsilencing in adult-born neurons. J Neurosci 33:6614–6622.
- Chapleau C a, Larimore JL, Theibert A, Pozzo-Miller L (2009) Modulation of dendritic spine development and plasticity by BDNF and vesicular trafficking: fundamental roles in neurodevelopmental disorders associated with mental retardation and autism. J Neurodev Disord 1:185–196.
- Che A, Babij R, Iannone AF, Liston C, Fishell G, De Marco Garcia N V (2018) Layer I Interneurons Sharpen Sensory Maps during Neonatal Development. Neuron 99:98–116.
- De Simoni A, Griesinger CB, Edwards FA (2003) Development of rat CA1 neurones in acute versus organotypic slices: role of experience in synaptic morphology and activity. J Physiol 550:135–147.
- Drakew A, Muller M, Gahwiler B, Thompson S, Frotscher M (1996) Spine Loss in Experimental Epilepsy: Quantitative Light and Electron Miscroscopic Analysis of Intracellularly Stained CA3 Pyramidal Cells in Hippocampal Slice Cultures. Neuroscience 70:31–45.
- Dzhala VI, Talos DM, Sdrulla DA, Brumback AC, Mathews GC, Benke TA, Delpire E, Jensen FE, Staley KJ (2005) NKCC1 transporter facilitates seizures in the developing brain. Nat Med 11:1205–1213.
- El Marroun H, White T, Verhulst FC, Tiemeier H (2014) Maternal use of antidepressant or anxiolytic medication during pregnancy and childhood neurodevelopmental outcomes: a systematic review. Eur Child Adolesc Psychiatry 23:973–992.
- Fiala JC (2005) Reconstruct: a free editor for serial section microscopy. J Microsc 218:52–61.
- Fiala JC, Spacek J, Harris KM (2002) Dendritic Spine Pathology: Cause or Consequence of Neurological Disorders? Brain Res Rev 39:29–54.
- Fiumelli H, Briner A, Puskarjov M, Blaesse P, Belem BJ, Dayer AG, Kaila K, Martin J-L, Vutskits L (2012) An Ion Transport-Independent Role for the Cation-Chloride Cotransporter KCC2 in Dendritic Spinogenesis In Vivo. Cereb Cortex.
- Garaschuk O, Hanse E, Konnerth A (1998) Developmental profile and synaptic origin of early network oscillations in the CA1 region of rat neonatal hippocampus. J Physiol 507 (Pt 1:219–236.
- Ge S, Goh ELK, Sailor K a, Kitabatake Y, Ming G, Song H (2006) GABA regulates synaptic integration of newly generated neurons in the adult brain. Nature 439:589–593.

- Griguoli M, Cherubini E (2017) Early Correlated Network Activity in the Hippocampus: Its Putative Role in Shaping Neuronal Circuits. Front Cell Neurosci 11:1–11.
- Gulledge AT, Stuart GJ (2003) Excitatory actions of GABA in the cortex. Neuron 37:299–309.
- Haber M, Zhou L, Murai KK (2006) Cooperative Astrocyte and Dendritic Spine Dynamics at Hippocampal Excitatory Synapses. 26:8881–8891.
- Hanse E, Durand GM, Garaschuk O, Konnerth A (1997) Activity-dependent wiring of the developing hippocampal neuronal circuit. Semin Cell Dev Biol 8:35–42.
- Heaulme M, Chambon JP, Leyris R, Molimard JC, Wermuth CG, Biziere K (1986) Biochemical characterization of the interaction of three pyridazinyl-GABA derivatives with the GABA_A receptor site. Brain Res 384:224–231.
- Heck N, Kilb W, Reiprich P, Kubota H, Furukawa T, Fukuda A, Luhmann HJ (2007) GABA-A receptors regulate neocortical neuronal migration in vitro and in vivo. Cereb Cortex 17:138–148.
- Hutsler JJ, Zhang H (2010) Increased dendritic spine densities on cortical projection neurons in autism spectrum disorders. Brain Res 1309:83–94.
- Irwin SA, Galvez R, William T (2000) Dendritic Spine Structural Anomalies in Fragile-X Mental Retardation Syndrome. :1038–1044.
- Irwin SA, Patel B, Idupulapati M, Harris JB, Crisostomo RA, Larsen BP, Kooy F, Willems PJ, Cras P, Kozlowski PB, Swain RA, Weiler IJ, Greenough WT (2001) Abnormal dendritic spine characteristics in the temporal and visual cortices of patients with fragile-X syndrome: a quantitative examination. Am J Med Genet 98:161–167.
- Ji Y, Lu Y, Yang F, Shen W, Tang TTT, Feng L, Duan S, Lu B (2010) Acute and gradual increases in BDNF concentration elicit distinct signaling and functions in neurons. Nat Neurosci 13:302–309.
- Johnston GAR (2014) Muscimol as an Ionotropic GABA Receptor Agonist. Neurochem Res 39:1942–1947.
- Jones E V., Bernardinelli Y, Zarruk JG, Chierzi S, Murai KK (2018) SPARC and GluA1–Containing AMPA Receptors Promote Neuronal Health Following CNS Injury. Front Cell Neurosci 12:1–13.
- Jourdain P, Nikonenko I, Alberi S, Muller D (2002) Remodeling of Hippocampal Synaptic Networks by a Brief Anoxia – Hypoglycemia. 22:3108–3116.
- Kaila K (1994) Ionic Basis of GABAA Receptor Channel Function in the Nervous System. Prog Neurobiol 42:489–437.
- Kaufmann WE, Moser HW (2000) Dendritic Anomalies in Disorders Associated with

- Mental Retardation. :981-991.
- Khalilov I, Dzhala V, Ben-Ari Y, Khazipov R (1999) Dual Role of GABA in the Neonatal Rat Hippocampus. Dev Neurosci 21:310–319.
- Khalilov I, Minlebaev M, Mukhtarov M, Khazipov R (2015) Dynamic Changes from Depolarizing to Hyperpolarizing GABAergic Actions during Giant Depolarizing Potentials in the Neonatal Rat Hippocampus. 35:12635–12642.
- Khazipov R, Leinekugel X, Khalilov I, Gaiarsa J, Ben-ari Y (1997) Synchronization of GABAergic interneuronal network in CA3 subfield of neonatal rat hippocampal slices. J Physiol 483:763–772.
- Kirmse K, Hübner CA, Isbrandt D, Witte OW (2018) GABAergic Transmission during Brain Development: Multiple Effects at Multiple Stages. Neurosci 24:36–53.
- Kirmse K, Kummer M, Kovalchuk Y, Witte OW, Garaschuk O, Holthoff K (2015) GABA depolarizes immature neurons and inhibits network activity in the neonatal neocortex in vivo. Nat Commun 6.
- Lacey DJ, Terplan K (1987) Abnormal Cerebral Cortical Neurons in a Child With Maternal PKU Syndrome. J Child Neurol 2:201–204.
- Lamsa KP, Palva JM, Ruusuvuori E, Kaila K, Taira T (2000) Synaptic GABA A Activation Inhibits AMPA-Kainate Receptor Mediated Bursting in the Newborn (P0 P2) Rat Hippocampus. J Neurophysiol 83:359–366.
- Le Magueresse C, Safiulina V, Changeux J-P, Cherubini E (2006) Nicotinic modulation of network and synaptic transmission in the immature hippocampus investigated with genetically modified mice. J Physiol 576:533–546.
- Leinekugel X, Tseeb V, Ben-ari Y, Bregestovski P (1995) Synaptic GABAA activation induces Ca2+ rise in pyramidal cells and interneurons from rat neonatal hippocampal slices. J Physiol 487:319–329.
- Li H, Khirug S, Cai C, Ludwig A, Blaesse P, Kolikova J, Afzalov R, Coleman SK, Lauri S, Airaksinen MS, Keinänen K, Khiroug L, Saarma M, Kaila K, Rivera C (2007) KCC2 interacts with the dendritic cytoskeleton to promote spine development. Neuron 56:1019–1033.
- Liu X, Wang Q, Haydar TF, Bordey A (2005) Nonsynaptic GABA signaling in postnatal subventricular zone controls proliferation of GFAP-expressing progenitors. Nat Neurosci 8:1179–1187.
- Megias M, Emri Z, Gulyas A, Freund T (2001) Total number and distribution of inhibitory and excitatory synapses on hippocampal CA1 pyramidal cells. Neuroscience 102:527–540.

- Mohajerani MH, Cherubini E (2005) Spontaneous recurrent network activity in organotypic rat hippocampal slices. Eur J Neurosci 22:107–118.
- Mortensen M, Ebert B, Wafford K, Smart TG (2010) Distinct activities of GABA agonists at synaptic- and extrasynaptic-type GABAA receptors. J Physiol 588:1251–1268.
- Muller D, Buchs P-A, Stoppini L (1993) Time course of synaptic development in hippocampal organotypic cultures. Brain Res Dev Brain Res 71:93–100.
- Oh WC, Lutzu S, Castillo PE, Kwon HB (2016) De novo synaptogenesis induced by GABA in the developing mouse cortex. Science (80-) 353.
- Owens DF, Kriegstein AR (2002) Is there more to GABA than synaptic inhibition? Nat Rev Neurosci 3:715–727.
- Park H, Poo MM (2013) Neurotrophin regulation of neural circuit development and function. Nat Rev Neurosci 14:7–23.
- Pérez-Gómez A, Tasker RA (2013) Transient domoic acid excitotoxicity increases BDNF expression and activates both MEK- and PKA-dependent neurogenesis in organotypic hippocampal slices. BMC Neurosci 14:72.
- Pfeffer CK, Stein V, Keating DJ, Maier H, Rinke I, Rudhard Y, Hentschke M, Rune GM, Jentsch TJ, Hübner C a (2009) NKCC1-dependent GABAergic excitation drives synaptic network maturation during early hippocampal development. J Neurosci 29:3419–3430.
- Puskarjov M, Ahmad F, Khirug S, Sivakumaran S, Kaila K, Blaesse P (2014) BDNF is required for seizure-induced but not developmental up-regulation of KCC2 in the neonatal hippocampus. Neuropharmacology 88:1–7.
- Puskarjov M, Fiumelli H, Briner A, Bodogan T, Demeter K, Lacoh C, Mavrovic M, Blaesse P, Kaila K, Vutskits L (2017) K-Cl Cotransporter 2-mediated Cl- extrusion determine developmental stage-dependent impact of propofol mediated anesthesia on dendritic spines. Anesthesiology 126:1–13.
- Rivera C, Voipio J, Payne JA (1999) The K+/Cl- co-transporter KCC2 renders GABA hyperpolarizing during neuronal maturation. Nature 397:251–255.
- Rodriguez A, Ehlenberger DB, Dickstein DL, Hof PR, Wearne SL (2008) Automated threedimensional detection and shape classification of dendritic spines from fluorescence microscopy images. PLoS One 3.
- Sedmak G, Jovanov-Milošević N, Puskarjov M, Ulamec M, Krušlin B, Kaila K, Judaš M (2015) Developmental Expression Patterns of KCC2 and Functionally Associated Molecules in the Human Brain. Cereb Cortex:1–16.
- Shen W, Da Silva JS, He H, Cline HT (2009) Type A GABA-receptor-dependent synaptic

- transmission sculpts dendritic arbor structure in Xenopus tadpoles in vivo. J Neurosci 29:5032–5043.
- Sipilä ST, Schuchmann S, Voipio J, Yamada J, Kaila K (2006) The cation-chloride cotransporter NKCC1 promotes sharp waves in the neonatal rat hippocampus. J Physiol 573:765–773.
- Sokal DM, Mason R, Parker TL (2000) Multi-neuronal recordings reveal a differential effect of thapsigargin on bicuculline- or gabazine-induced epileptiform excitability in rat hippocampal neuronal networks. Neuropharmacology 39:2408–2417.
- Staley KJ, Mody I (1992) Shunting of excitatory input to dentate gyrus granule cells by a depolarizing GABAA receptor-mediated postsynaptic conductance. J Neurophysiol 68:197–212.
- Staley KJ, Proctor WR (1999) Modulation of mammalian dendritic GABAA receptor function by the kinetics of Cl- and HCO3- transport. J Physiol 519:693–712.
- Swann JW, Brady RJ, Martin DL (1989) Postnatal development of GABA-mediated synaptic inhibition in rat hippocampus. Neuroscience 28:551–561.
- Tyler WJ, Pozzo-Miller L (2003) Miniature synaptic transmission and BDNF modulate dendritic spine growth and form in rat CA1 neurones. J Physiol 553:497–509.
- Tyzio R, Nardou R, Ferrari DC, Tsintsadze T, Shahrokhi A, Eftekhari S, Khalilov I, Tsintsadze V, Brouchoud C, Chazal G, Lemonnier E, Lozovaya N, Burnashev N, Ben-Ari Y (2014) Oxytocin-Mediated GABA Inhibition During Delivery Attenuates Autism Pathogenesis in Rodent Offspring. Science (80-) 343:675–680.
- Valeeva G, Tressard T, Mukhtarov M, Baude A, Khazipov R (2016) An Optogenetic Approach for Investigation of Excitatory and Inhibitory Network GABA Actions in Mice Expressing Channelrhodopsin-2 in GABAergic Neurons. J Neurosci 36:5961–5973.
- Vanhatalo S, Palva JM, Andersson S, Rivera C, Voipio J, Kaila K (2005) Slow endogenous activity transients and developmental expression of K+-Cl- cotransporter 2 in the immature human cortex. Eur J Neurosci 22:2799–2804.
- Vicario-Abejón C, Collin C, McKay RD, Segal M (1998) Neurotrophins induce formation of functional excitatory and inhibitory synapses between cultured hippocampal neurons. J Neurosci 18:7256–7271.
- Vicario-Abejón C, Owens D, McKay R, Segal M (2002) Role of neurotrophins in central synapse formation and stabilization. Nat Rev Neurosci 3:965–974.
- Wang DD, Kriegstein AR (2008) GABA regulates excitatory synapse formation in the neocortex via NMDA receptor activation. J Neurosci 28:5547–5558.

- Wang DD, Kriegstein AR (2009) Defining the role of GABA in cortical development. J Physiol 587:1873–1879.
- Wang DD, Kriegstein AR (2011) Blocking early GABA depolarization with bumetanide results in permanent alterations in cortical circuits and sensorimotor gating deficits. Cereb Cortex 21:574–587.
- Wells JE, Porter JT, Agmon A, Virginia W (2000) GABAergic Inhibition Suppresses Paroxysmal Network Activity in the Neonatal Rodent Hippocampus and Neocortex. J Neurosci 20:8822–8830.
- Yamada J, Okabe A, Toyoda H, Kilb W, Luhmann HJ, Fukuda A (2004) Cl- uptake promoting depolarizing GABA actions in immature rat neocortical neurones is mediated by NKCC1. J Physiol 557:829–841.
- Zeng L, Xu L, Rensing NR, Sinatra PM, Rothman SM, Wong M (2007) Kainate Seizures Cause Acute Dendritic Injury and Actin Depolymerization In Vivo. J Neurosci 27:11604–11613.
- Zha X-M, Green SH, Dailey ME (2005) Regulation of hippocampal synapse remodeling by epileptiform activity. Mol Cell Neurosci 29:494–506.

2.9 Figures

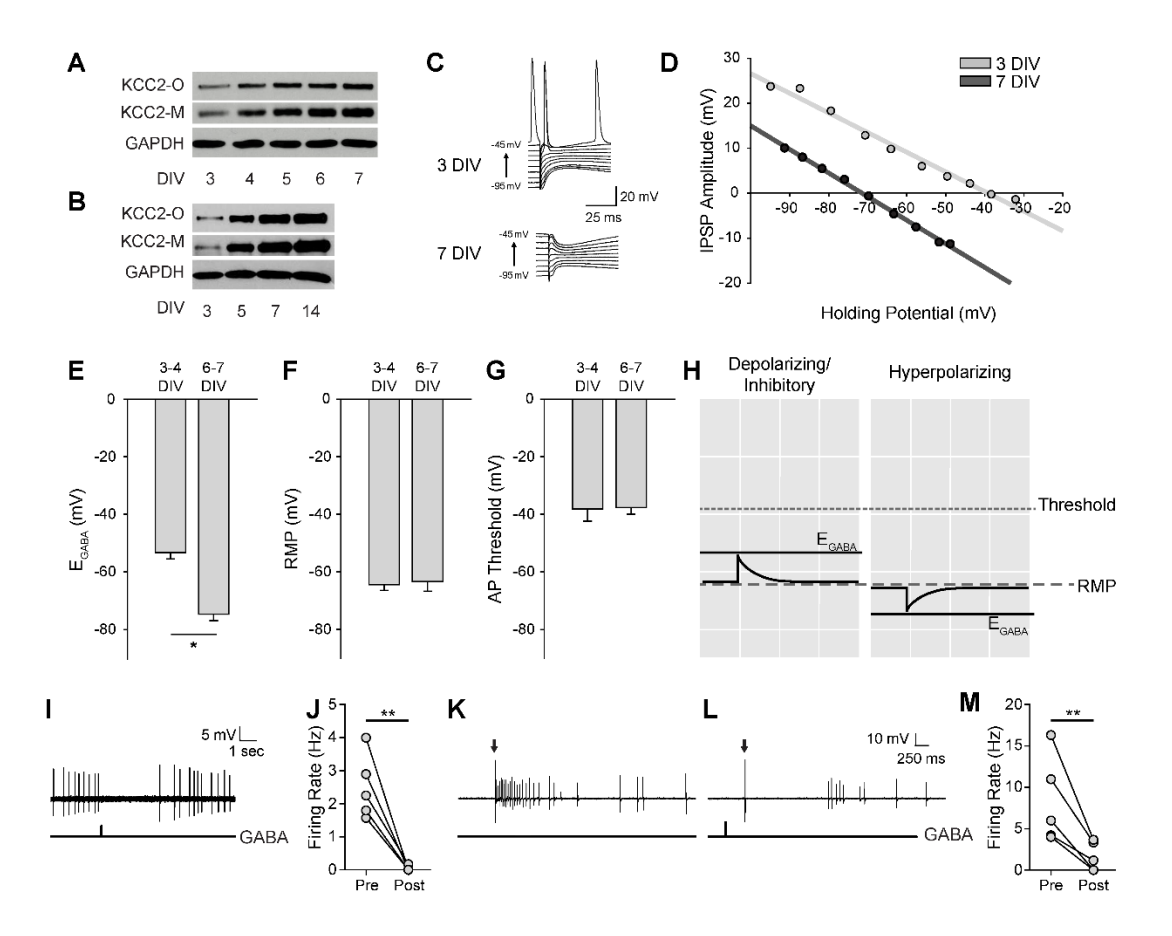


Figure 1

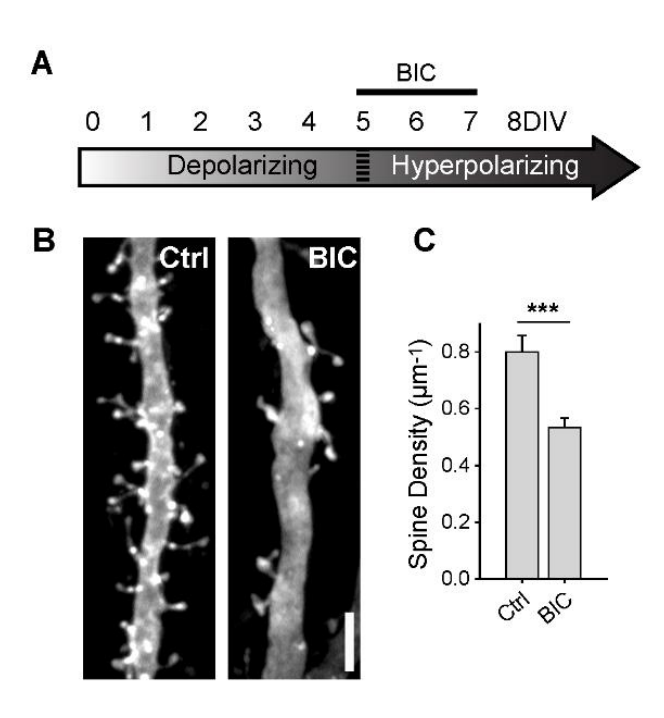


Figure 2

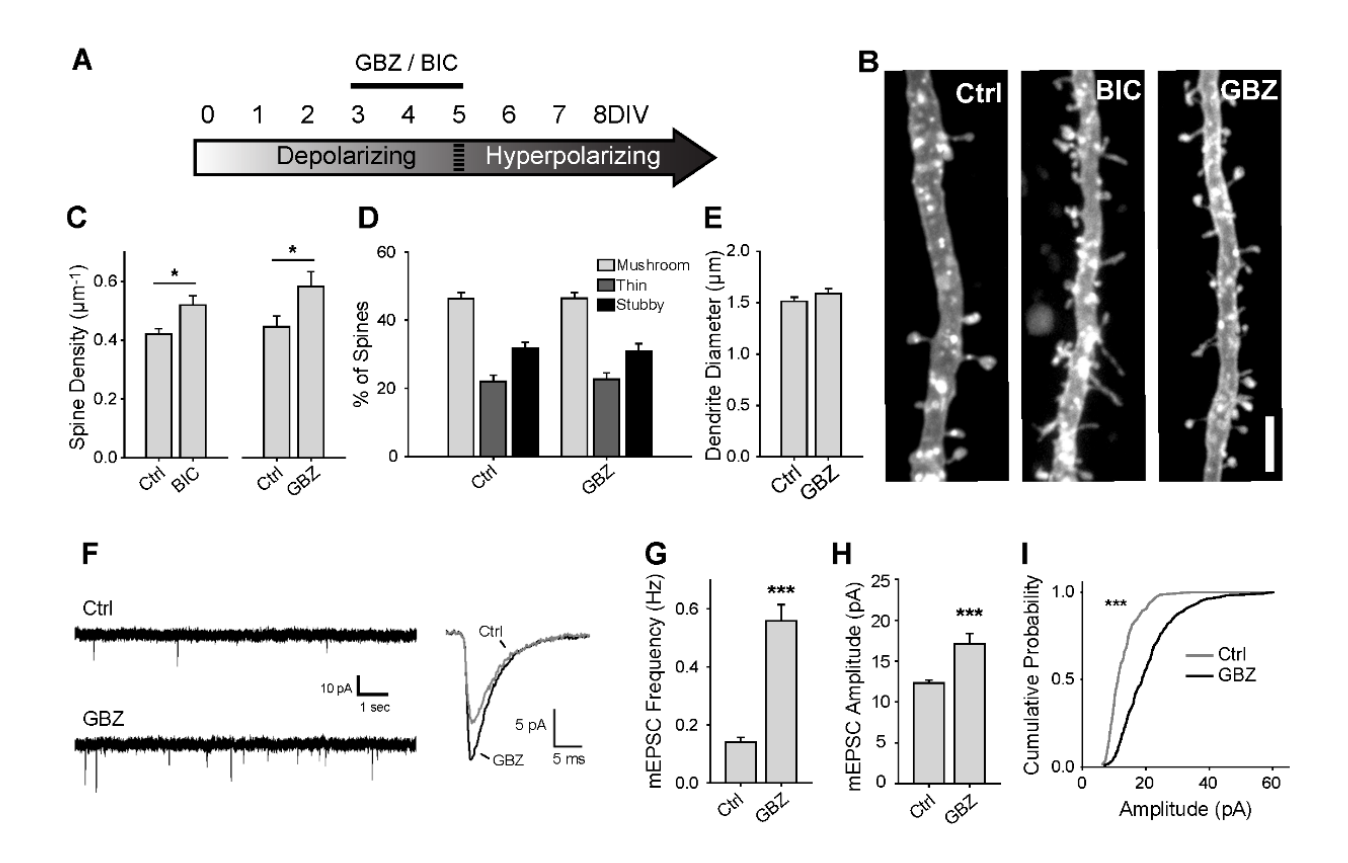


Figure 3

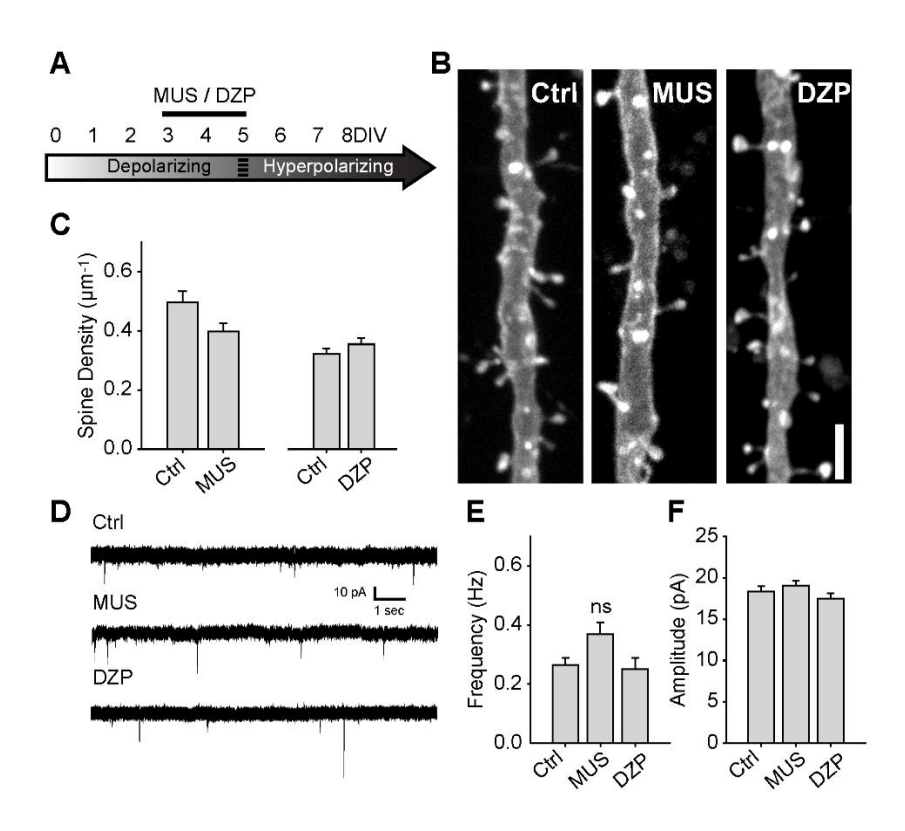


Figure 4

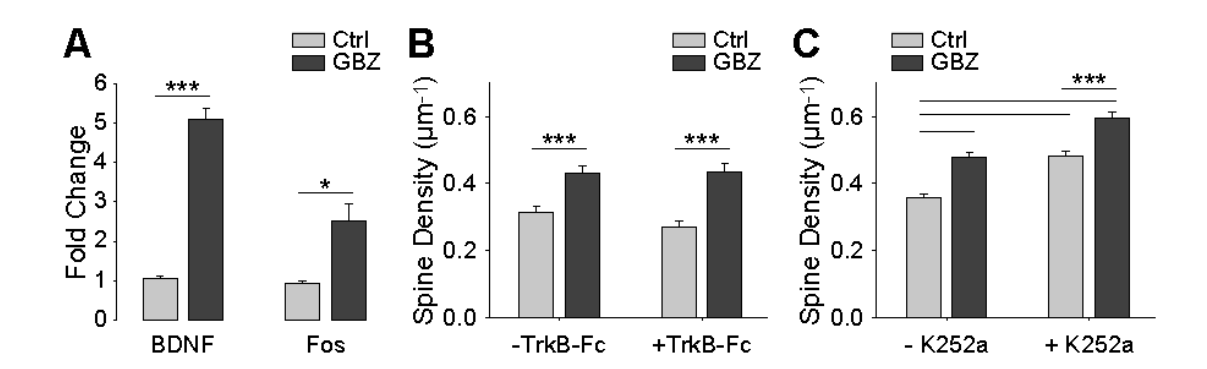


Figure 5

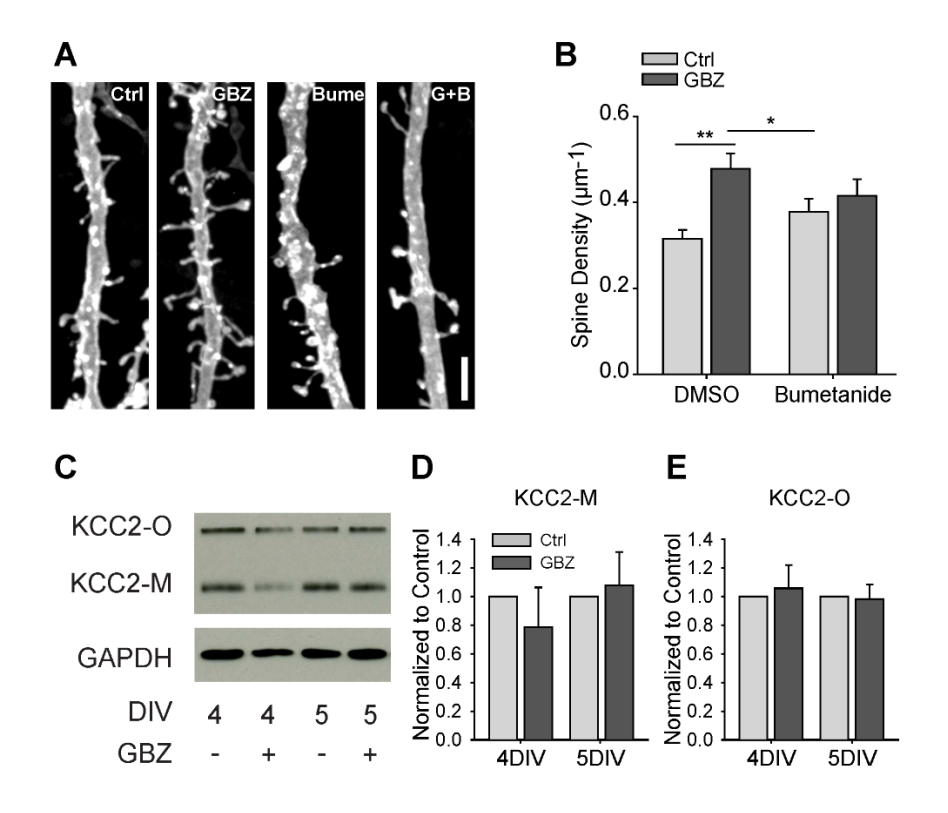


Figure 6

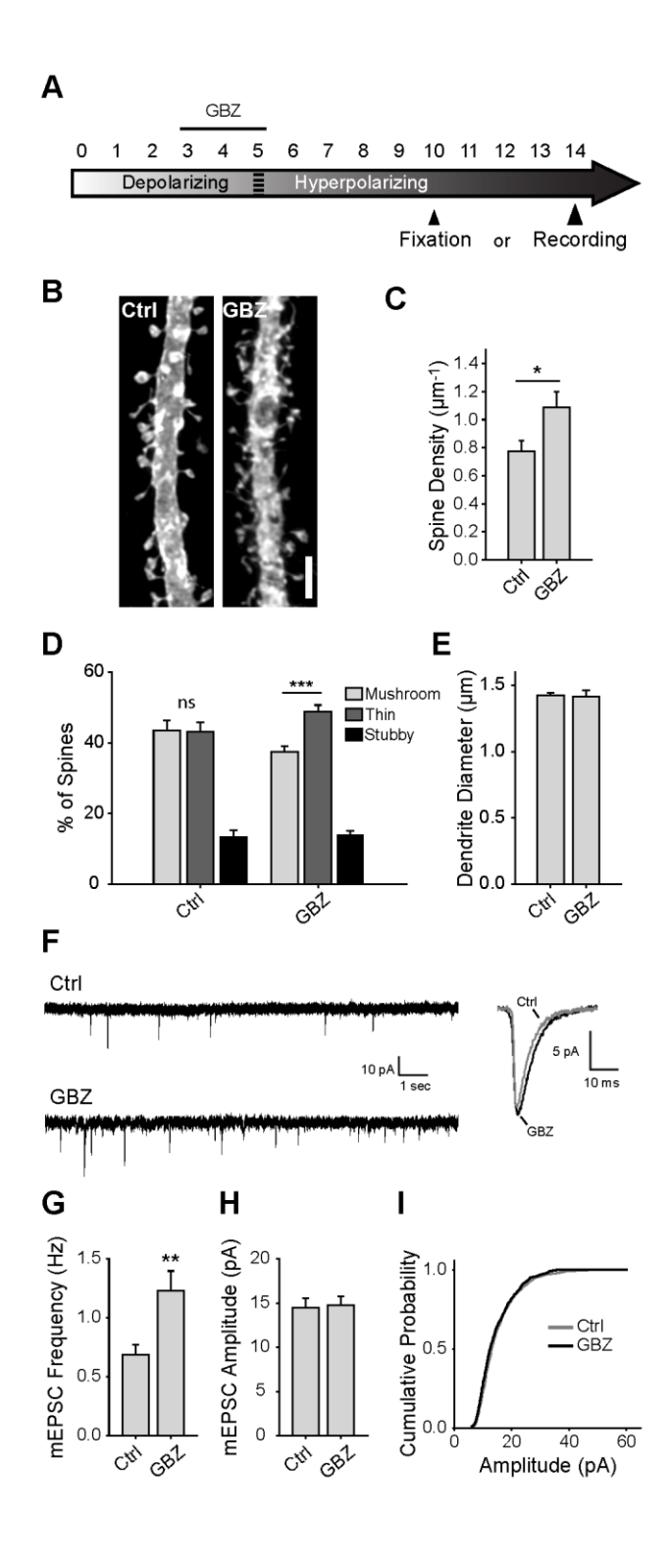


Figure 7

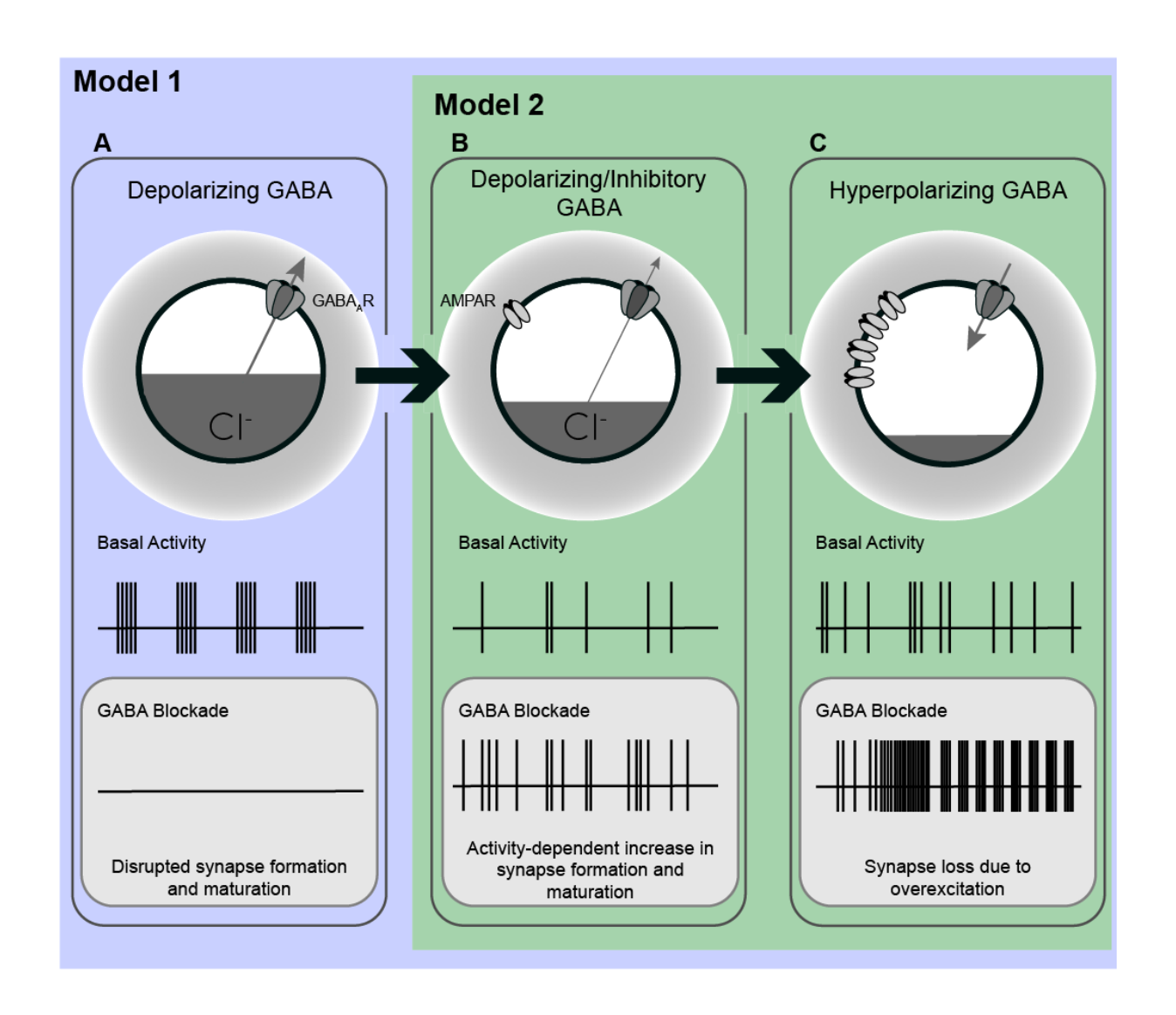


Figure 8

2.10 Figure Legends

Figure 1. GABA reversal potential (E_{GABA}) shifts from depolarizing to hyperpolarizing between 3 and 7 DIV. A-B, Western blots showing increasing expression of KCC2 monomers (KCC2-M) and oligomers (KCC2-O). C-D, Representative traces and representative IV curves from GABAergic responses at 3DIV and 7DIV. E, E_{GABA} summary plots (3/4 DIV: -53.3±6.1mV, n=5; 6/7 DIV: -74.7± 6.4mV, n=5, p=0.04). F, Resting membrane potential summary plots (3/4 DIV: -64.5±2.3mV, n=5; 6/7 DIV: -63.4 ± 3.8mV, n=5). G, Action potential threshold summary plot (3/4 DIV: -38.2 ± 4.2mV, n=5; 6/7 DIV-37.7 ± 2.3mV, n=5). H, Schematic demonstrating the likely shunting and hence inhibitory nature of GABA_A transmission due to the relative values of AP Threshold>E_{GABA}>RMP. The scale in H aligns with that of E, F and G such that the threshold, RMP and E_{GABA} values are represented accurately relative to each other. I, Sample trace of spontaneous activity inhibited by puffing on GABA. The line trace below indicates time of GABA puff. J. Summary plots of spontaneous activity pre- and post-GABA puff. K,L, Sample traces from the same cell demonstrating that activity could be evoked electrically (K) and that puffed GABA inhibited electrically evoked activity (L) The arrow above the traces denotes the timing of electrical stimulation. M, Summary plots of electrically evoked activity in the absence and presence of puffed GABA.

Figure 2. Blocking hyperpolarizing GABA transmission decreases dendritic spine density. *A*, Time course of bicuculline (BIC) treatment. *B-C*, Spine density after 5-7 DIV BIC treatment (Control: 0.80±0.06 spines/um; BIC: 0.53±0.03; p<0.001, Mann-Whitney).

Figure 3. Blocking depolarizing GABA_A transmission increases excitatory synapse number. **A**, Time course of pharmacological treatments. **B**,**C**, Spine density after 3-5 DIV GBZ (Control: 0.44±0.12 spines/um; GBZ: 0.58±0.17; p=0.04) and BIC treatment (Control: 0.42±0.02 spines/um; BIC: 0.52±0.03 spines/um; P=0.027, Mann-Whitney). **D**,**E**, 3D spine morphology and dendrite diameter after GBZ. **F**, Representative traces of mEPSCs. **G**, mEPSC frequency summary plot (Control: 0.14±0.02 Hz, GBZ: 0.56±0.06 Hz, p<0.001, Mann-Whitney). *H*, mEPSC amplitude summary plot (Control: 12.32±0.37 pA, n=8, GBZ: 17.12±1.27 pA, n=10, p<0.001, Mann-Whitney). *I*, Cumulative distributions of amplitudes (p<0.0001, Kolmogorov-Smirnov test). Scale bars 3μm.

Figure 4. Driving depolarizing GABA_A transmission does not decrease glutamatergic synapse numbers. *A*, Time course of MUS and DZP treatment. *B*, *C*, Spine density after 3–5 DIV MUS treatment (Ctrl: 0.50 ± 0.04; MUS: 0.40 ± 0.03; p = 0.07) and DZP treatment (Ctrl: 0.321 ± 0.02; DZP: 0.36 ± 0.02; p = 0.11, Mann–Whitney). *D*, Representative traces of mEPSCs following 3–5DIV treatment with MUS or DZP. *E*, mEPSC frequency summary plot (Ctrl: 0.27 ± 0.02 Hz, n=9; MUS: 0.37 ± 0.04 Hz, n=8; DZP: 0.25 ± 0.04 Hz, n=8; One way ANOVA p=0.046; Ctrl vs MUS, p=0.09; Ctrl vs DZP, p=0.9). *F*, mEPSC amplitude summary plot (Ctrl: 18.3 ± 0.7 pA, n=9; MUS: 19.0 ± 0.6 pA, n=8; DZP: 17.5 ± 0.6 pA, n=8; One Way ANOVA, p=0.263)

Figure 5. BDNF signalling is not necessary for increase in spine density. *A*, BDNF and Fos transcript levels following GBZ from 3–5DIV (BDNF: Ctrl 1.07±0.04, GBZ 5.08±0.3 p<0.001; Fos: Ctrl 0.94±0.04, GBZ 2.52±0.4, p=0.02). *B*, Change in spine density following GBZ and/or TrkB-Fc treatment (Ctrl 0.31±0.02, GBZ 0.42±0.02, TrkB-Fc 0.27±0.02, TrkB-Fc+GBZ 0.43±0.02, 2 Way ANOVA, no interaction, Tukey post test). *C*, Change in spine density following GBZ and/or K252a treatment (Ctrl 0.35±0.01, GBZ 0.49±0.03, K252a 0.47±0.02, K252a+GBZ: 0.58±0.04; all significant differences <0.001, 2 Way ANOVA, no interaction, Tukey post test).

Figure 6. GBZ-induced increase in spines is not reproduced by bumetanide and is not associated with changes in KCC2 expression. *A,B*, Bumetanide does not increase spine density above control levels, (B, Control: 0.31±0.02 um⁻¹; GBZ: 0.47±0.04 um⁻¹; BUME: 0.37±0.02 um⁻¹; BUME+GBZ: 0.39±0.03 um⁻¹. Two-way ANOVA indicates significant interaction

between GBZ and BUME treatment (p=0.009). Tukey HSD post test indicates significant differences between Ctrl and GBZ (p=0.0002) and GBZ and BUME (p=0.03)). *C-E*, Western blot (C) showing no changes in monomeric (D) or oligomeric (E) KCC2 expression following GBZ from 3-4DIV (p=0.52 and 0.77, respectively, One Sample t-Test, n=3) and 3-5 DIV (p=0.76 and 0.87, respectively, One Sample t-Test, n=3). Scale bar 3μm.

Figure 7. Transient blockade of depolarizing GABA_A transmission causes a lasting increase in excitatory synapses and alters spine morphology. *A*, Schematic time course of GBZ treatment and experimental endpoints. *B*,*C*, Spine density after 3–5 DIV GBZ treatment and 5 days of recovery (Control: 0.78±0.08 spines/μm; GBZ washout: 1.07±0.07 spines/μm; p=0.024,). *D*, 3D spine morphology after 5 days of recovery (***p<0.001, critical level 0.05, Two Way ANOVA with Holm Sidak Post Test). *E*, Dendrite diameter after recovery (p=0.86). *F*, Representative mEPSC traces from slices after 8–9 days recovery. *G*, mEPSC frequency summary plot (Control: 0.70±0.08 Hz, n=10 GBZ: 1.23±0.17 Hz, n=10, p=0.009). *H*, mEPSC amplitude summary plot (Control: 14.50±1.07 pA, n=10, GBZ: 14.80±1.00 pA, n=10, p=0.84). *I*, Cumulative mEPSC distributions (p=0.58, Kolmogorov-Smirnov test). Scale bar 3μm.

Figure 8. A model of the possible roles of GABA_A transmission in glutamatergic synapse formation as chloride homeostasis matures. *A*, Work performed in acute slices suggests that depolarizing GABA_A transmission provides the initial excitatory drive required for activity- and calcium-dependent formation and maturation of glutamatergic synapses. Blocking GABA_A transmission at this stage eliminated GDPs. For the sake of simplicity we have depicted that GABA_A blockade would eliminate GDPs and silence network activity at this stage, however it should be noted that in acute slices, blocking GABA_A transmission at this point has been shown to decrease circuit activity in immature acute hippocampal slices as depicted (Ben-Ari et al., 1989; Garaschuk et al., 1998; Mohajerani and Cherubini, 2005), but has also been shown to induce interictal discharges (Khazipov et al., 1997; Khalilov et al., 1999; Lamsa et al., 2000) or paroxysmal activity (Wells et al., 2000). These latter effects may be due

to an overarching inhibitory role for GABA during development. B, Our work suggests a possible transition state wherein blocking GABA_A transmission alleviates a depolarizing but inhibitory restraint on circuit activity, allowing for activity dependant formation of glutamatergic synapses. Such a transition state would likely rely on a still underdeveloped glutamatergic system that is not yet capable of pathological levels of overexcitation. Importantly, recent *in vivo* work suggests that GABA may be inhibit circuit activity throughout postnatal development, indicating that blocking GABA_A transmission might enhance glutamatergic synapse formation from birth until GABA becomes fully hyperpolarizing. C, When E_{Cl} and the glutamatergic system are mature, blocking hyperpolarizing GABA_A transmission causes overexcitation and loss of glutamatergic synapses.

Chapter 3 Astrocytic Mitochondrial Location is not Associated with Ultrastructural Characteristics of Tripartite Synapses

3.1 Preamble

While investigating glutamatergic synapse formation in the organotypic hippocampal slice, I performed a short trial to test the utility of using transmission electron microscopy (TEM) to assess the number of synapses developing under the different conditions outlined in the last chapter. Although I ultimately did not pursue this approach, our collaborators at the McGill Facility for Electron Microscopy Research invited us to test a newly acquired focus ion beam scanning electron microscope (FIB-SEM) on the organotypic hippocampal slice culture tissue I had prepared. We found that the resulting data presented an exciting opportunity to pursue another topic of interest in the lab: neuron-astrocyte interactions. FIB-SEM allowed for a rarely seen level of detail in the investigation of the three-dimensional organization of fine astrocytic processes and tripartite synapses. The following chapter presents a detailed description of these structures and how they are arranged relative to mitochondria in astrocytes of the mouse barrel cortex.

Astrocytic Mitochondrial Location is not Associated with Ultrastructural Characteristics of Tripartite Synapses.

Christopher K. Salmon¹, J. Benjamin Kacerovsky¹, Tabish Syed², Nensi Alivodej¹, Michael Pratt¹, Michael P. Rosen¹, Miranda Green¹, Hojatollah Vali³, Craig A. Mandato³ Kaleem Siddiqi^{2*}, Keith K. Murai^{1*}

¹Centre for Research in Neuroscience, Department of Neurology and Neurosurgery, Brain Repair and Integrative Neuroscience Program, The Research Institute of the McGill University Health Centre, Montreal General Hospital, Montreal, QC, H3G 1A4, Canada. ²School of Computer Science and Centre for Intelligent Machines, McGill University, Montreal, QC, H3A 2A7, Canada

³Department of Anatomy and Cell Biology, McGill University, Montreal, QC Canada.

The authors declare no financial conflict of interest.

*Correspondence should be addressed to:

Dr. Keith K Murai Centre for Research in Neuroscience Montreal General Hospital 1650 Cedar Avenue L7-212 Montreal, QC, H3G 1A4 Canada Telephone: (514) 934-1934 x43477

Fax: (514) 934-8216 keith.murai@mcgill.ca

Dr. Kaleem Siddiqi
School of Computer Science and Centre for Intelligent Machines
McGill University
Montreal, QC, H3A 2A7, Canada
siddiqi@cim.mcgill.ca

Number of Figures: 5 Number of Tables: 8 Number of Words: 6735

Key Words: FIBSEM, ultrastructure, astrocyte, calcium dynamics, calcium microdomains, mitochondria, tripartite synapse, wavefront propagation

Acknowledgments: The authors are indebted to Jeannie Mui, Lee Ann Monaghan, Weawkamol Leelapornpisit and Dr. Kelly Sears of the McGill Facility for Electron Microscope Research for superb technical assistance

3.2 Abstract

Astrocytes are the non-neuronal support cells of the brain and play active roles in regulating central nervous system function. To support neuronal functions, astrocytes form close associations with synapses, where they regulate neurotransmission, provide energy substrates to neurons, and modulate synaptic function and plasticity. The fine presynaptic astrocytic processes that contact synapses, and indeed a large portion of the astrocytic branches, are difficult to resolve with traditional microscopy techniques, and thus their architecture, as it relates to the surrounding microcircuitry and to the rest of the convoluted network of astrocytic branches, has not been fully described. To address this, we acquire two large serial section electron microscopy datasets in the mouse barrel cortex using focussed ion beam scanning electron microscopy. We segmented extensive, continuous volumes of astrocyte, as well as the mitochondria contained in the astrocytic branches and all synapses contacted by the segmented portions of astrocytes. Three-dimensional reconstructions showed that perisynaptic astrocytic processes are often separated from the main network of branches by thin filaments and tend to associate with clusters of synapses. To determine the spatial relationships between mitochondria and synapses contacted by the astrocyte, we employed eikonal equation-based wave-front propagation to measure shortest paths through the complex astrocytic branches, and found that mitochondria do not tend to localize more closely to certain types of synapses, or to clusters containing certain types of synapses. Mitochondria did however lie closer to some clusters of synapses than others, suggesting the existence of a higher order organization in the distribution of astrocyte mitochondria that is determined by parameters that were not unveiled simply by assessing the surrounding microcircuitry.

3.3 Introduction

Astrocytes are non-neuronal cells of the central nervous system (CNS) that play vital roles in sustaining and modulating neuronal function (Barres, 2008). It has been appreciated for over four decades that astrocytes are involved in maintaining neuronal health (Banker, 1980), and through the years it has become clear that astrocytes have diverse functions in regulating neural blood flow, neuronal energy supply, extracellular ion and neurotransmitter homeostasis, as well as synapse development, transmission and plasticity (Barres, 2008; Perea et al., 2009). To accomplish these wide-ranging functions, astrocytes express numerous receptors to monitor the state of the surrounding CNS microenvironment and secrete a variety of factors and gliotransmitters to regulate neural function.

Astrocytes are not passive cells, rather they respond actively to a variety of stimuli with elevations in intracellular calcium. Astrocytic calcium signalling is fundamental for many functions carried out by these cells (reviewed in Guerra-Gomes et al. 2018). Early work on astrocytic calcium signalling observed two types of calcium events: large, full-cell calcium transients and also smaller, more localized calcium events in subcellular compartments of astrocytes (Grosche et al., 1999). In recent years, the smaller, faster events, termed calcium microdomains, have emerged to be most relevant to astrocytic functions (Bazargani and Attwell, 2016). Although calcium microdomains were initially difficult to monitor, with the advent of relatively fast, high affinity, and membrane-tethered genetically encoded calcium indicators specifically expressed in astrocytes, calcium microdomains can now be more easily monitored and studied (Shigetomi et al., 2010, 2013, 2016; Di Castro et al., 2011; Panatier et al., 2011; Kanemaru et al., 2014; Paukert et al., 2014; Agarwal et al., 2017).

A major constraint in studying astrocytic calcium signalling is understanding how it relates to the complex cellular architecture of these cells. When imaged with light microscopy, membrane labelled protoplasmic astrocytes resemble bushy oblong volumes. Generally, only a few central astrocytic branches are large enough to be discerned from the haze of spongelike processes and fine filaments that make up the majority of the astrocytic arborization (Kacerovsky and Murai, 2016). These fine filaments can be as thin as 30 nm, falling below the diffraction limit for conventional live imaging needed to observe calcium dynamics (Ventura and Harris, 1999; Witcher et al., 2010; Rusakov, 2015). As a result, calcium imaging of discrete subcellular compartments within astrocytes has been challenging. Furthermore, due to the sometimes nanoscopic size of astrocytic filaments, it has been difficult to relate astrocytic architecture to the organization of surrounding synapses and neural circuits. Fine astrocytic compartments referred to as perisynaptic astrocytic processes (PAPs) make intimate contact with synapses, forming the tripartite synapse (Spacek, 1985a). This tripartite arrangement has generally been studied from the perspective of individual dendritic spines, and it is not well understood how astrocytes or their internal calcium stores relate to relate to individual synapses or groups of synapses (Ventura and Harris, 1999; Witcher et al., 2007).

Recently it has been demonstrated that mitochondria are major contributors to calcium microdomains in astrocytes (Agarwal et al., 2017). Mitochondria can be actively trafficked within astrocytes and mitochondrial movement has been shown to be dictated by neuronal activity and astrocytic neurotransmitter detection (Jackson et al., 2014; Stephen et al., 2015). In neurons, mitochondria are trafficked to areas of higher metabolic demand, such as synapses, where they provide energy and calcium buffering capacity (Misgeld et al., 2007; MacAskill et al., 2010). This has led to the prediction that astrocytic mitochondria localize to regions in the astrocyte associated with higher levels of neuronal activity, where they can better support neurons with calcium signalling and by supplying energy substrates (Jackson and Robinson, 2018). Interestingly, astrocytic mitochondria show low baseline trafficking *in vivo* slices, with only ~10% showing motility (Jackson and Robinson, 2018). This combination of active trafficking in response to neuronal signals, and an overarching static positioning suggests an organized distribution of mitochondria in astrocytic processes at or near locations of higher metabolic demand (i.e. areas of high synaptic activity).

To better understand the ultrastructural features of astrocytes at tripartite synapses and the positioning of mitochondria with respect to those synapses, we utilized focused ion beam scanning electron microscopy (FIB-SEM) to examine astrocytic ultrastructure. We hypothesized that mitochondrial position in astrocytes would be determined by the organization and properties of nearby synapses. To address this, we acquired two large, high spatial resolution serial section electron microscopy volumes of mouse barrel cortex, and segmented extensive, continuous portions of the processes and mitochondria of astrocytes in these volumes along with their associated post synaptic densities (PSDs). To accurately determine the spatial relationships between these structures, we developed new approaches to quantitatively measure the three-dimensional properties of astrocytes, synapses, and mitochondria using eikonal equation wavefront propagation-based shortest path measurements. We observed that synapses tend to cluster around astrocytic branches that are separated from the rest of the astrocytic volume by thin constrictions. However, we found that mitochondrial localization in astrocytes does not correspond with the location of synapses with specific attributes - such as PSD volume and synapse type. Spatial clustering of particular types of synapses contacted by astrocyte processes also did not predict the location of astrocytic mitochondria. However, clusters of synapses did differ in their proximity to mitochondria, suggesting that mitochondria are not randomly distributed. These results suggest that mitochondrial location in astrocytes is not simply related to specific synapse types or synaptic organization, but rather relies on a more complex set of properties (possibly structural and/or cell signaling) that dictate mitochondria positioning in astrocytes.

3.4 Methods

Tissue preparation

Postnatal day 35 C57BL/6 male mice were transcardially perfused with a 10mL PBS wash followed by 250mL of 2% formaldehyde/ 2.5% glutaraldehyde in 0.1M phosphate buffer. Brains were extracted, post-fixed in the same solution at 4°C for 12 hours and cut into 300µm vibratome sections. Approximately 1mm x 4mm blocks of somatosensory cortex (S1BF) were manually dissected and prepared with a protocol similar to that used previously (Knott et al., 2011; Korogod et al., 2015). Following postfixation, the tissue was washed 3 times in 0.1M sodium cocodylate buffer and stained with 1.5% potassium ferrocyanide and 1% osmium tetroxide/0.1M cocodylate for 30min. Tissue was then washed in ddH₂0 twice for 5 min, and block stained in 1% uranyl acetate in ddH₂0 for 30 min and washed twice with ddH₂0. Tissue was passed through an acetone/ddH₂0 dehydration series of 30%, 50%, 70%, 80%, 90% and 3x100% acetone for 2 min at each step. This was followed by an epon infiltration series of 1:1, 2:1 and 3:1 epon:acetone for 30 min at each step. Tissue was left in 100% epon for 6 hours before being allowed to harden at the point of a conical mold at 65°C for 24 hours. Thin sections were prepared and stained with toluidine blue to select the area for imaging. Ultrathin sections were examined by transmission electron microscopy on a Tecnai 12 BioTwin 120kV TEM equipped with an AMT XR80C CCD Camera (FEI, OR) to assess tissue and staining quality.

Focussed Ion Beam Scanning Electron Microscopy (FIB-SEM)

FIBSEM imaging was performed as described previously (Morita et al., 2017). Epon blocks containing tissue were trimmed with a razor blade to expose the region of interest, then mounted on a 45° pre-titled SEM stub and coated with a 4-nm layer of platinum to enhance electrical conductivity. Gallium ion beam milling of serial sections and block face imaging

after each mill were carried out on a Helios Nanolab 660 DualBeam system using Auto Slice & View G3 ver 1.5.3 software (FEI).

The sample block was first imaged to determine the orientation of the block face and ion and electron beams. A protective platinum layer 80 μm long, 19 μm wide and 2 μm thick was deposited on the surface orthoganol to the block, where the ion beam is first incident, to protect the sample from ion beam damage and to correct for stage and/or specimen drift. Trenches were milled on both sides of the region of interest to minimize re-deposition of milled material during automated milling and imaging. Fiducial markers were generated for both ion and electron beam imaging and were used to dynamically correct for drift in the xand y-directions during data collection by applying appropriate scanning EM beam shifts. Milling was carried out at 30 kV with an ion beam current of 9.3 nA, stage tilt of 6.5°, and working distance of 4 mm. At each step, an 8 nm slice of the block face was removed by the ion beam. This mill depth was chosen to ensure resolution of the smallest astrocytic processes while still collecting images of an appreciable volume. Each newly milled block face was imaged simultaneously with the Through the Lens Detector (TLD) for backscattered electrons and In-Column Detector (ICD) at an accelerating voltage of 2 kV, beam current of 0.4 nA, stage tilt of 44.5°, and working distance of 3 mm. The pixel resolution was 4.13 nm with a dwell time of 30 µs per pixel. Pixel dimensions of the recorded image were 3072 x 2048 pixels. The FIBSEM was allowed to mill and image for ~48 hours, resulting in stacks of 12.7 X 8.5 X 4.4 µm for Astrocyte 1 (551 images) and 12.7 X 8.5 X 5.1 µm for Astrocyte 2 (635 images).

FIBSEM block preparation and imaging setup was performed by Weawkamol Leelapornpisit at the McGill Facility for Electron Microscopy Research and coordinated by Dr. Kelly Sears.

Segmentation and PSD Categorization

Segmentation was performed manually and with a fast-marching tool in the TrakEM2 plugin for ImageJ. Astrocytes were identified by clear cytoplasm devoid of visibly oriented microtubules, the presence of dark staining glycogen granules, and the absence of synaptic contacts (Spacek, 1985a and personal communication with Dr. Spacek). We also noted that in our preparations, astrocytic mitochondria stained more lightly than neuronal mitochondria (Fig. 1 B). As mentioned, astrocytic filaments can be extremely thin. The reduced resolution provided by backscattered electrons meant that the interstitial space and occasionally the band of cytoplasm in protoplasmic filaments could not be distinguished. In these cases, when it was unclear whether there was an obvious continuation of cytoplasm on either side of the restriction, the connection was not traced. Thus, we likely underestimated the extent of continuous astrocyte in the volumes considered.

PSDs were considered to be associated with the astrocyte if the perisynaptic astrocytic process (PAP) made contact anywhere on the synaptic unit (defined as spine head, spine neck and axonal bouton). Only PSDs that had clear symmetric or asymmetric dark staining and had at least one docked vesicle were segmented. Nearly all PSDs were associated with many docked and undocked vesicles.

PSDs were categorized by 1) their location (spine, dendritic shaft, cell body); 2) their type (asymmetric or symmetric); 3) the presence or absence of a spine apparatus (SA); 4) whether they were macular or perforated; 5) whether they were associated with endoplasmic reticulum (ER) at the PSD, spine base or in the spine neck; 6) whether they were associated with a mitochondrion that directly overlapped with the PSD or the spine base; and 7) whether the synapse-associated ER made a contact point (mitochondria-associated membrane; MAM) with a mitochondrion somewhere in the postsynaptic neuron. Obtaining direct measurements of the distance of mitochondria or MAMs from the synapse would have required a great deal

more segmentation, and they were thus estimated. It is important to note that mitochondrial and MAM distance categories are further complicated by the fact that we considered only very small proportions of total astrocytes, and the astrocytes in question thus extend outside the volumes we imaged, meaning that mitochondria or MAMs could occur just out of frame. This was mitigated in two ways: PSDs that were close to the edge of the block were not categorized for their association with mitochondria or MAMs, and only a minority of synapses where on dendrites that completely lacked mitochondria or MAMs (Table 1). Three-dimensional models were generated with Blender.

Measurement of shortest paths

We used fast marching to solve the eikonal equation inside and outside segmented astrocytes to compute distance from mitochondria to PSDs. The segmented mitochondrial surfaces were used as the initial wave-front inside the astrocytic volume, and the astrocytic surface was used as the initial wave-front outside the astrocytic volume. We used fast marching to evolve the initial surfaces to compute distance at every point inside the astrocyte volume. We assumed a constant isotropic metric everywhere inside and outside the astrocytic surface. The total distance to each PSD is the sum of the distance from PSD to astrocyte surface and the distance from mitochondria to the surface. To compute shortest paths, we use gradient descent on the computed distance map.

Statistics

Dominant set clustering of PSDs was performed using a similarity score based on geodesic distances between PSDs along the surface of Astrocytes. We associated each PSD to the closest point on the astrocyte surface. Geodesic distance was then computed between points on astrocyte surface closest to each PSD using fast marching. To compute pairwise distance from each PSD surface point to every other PSD surface point on the astrocyte, we repeated the process with every PSD as the starting point. Dominant set clustering was done on the

Adjacency matrix generated from negative exponential of distance as the similarity weight between PSD pairs.

Both PSD volumes and the distances measured were distributed non-normally, and thus the non-parametric, Mann-Whitney t-tests and Kruskal-Wallace ANOVAs were performed to assess differences using Sigmaplot software.

Significance: *p<0.05, **p<0.01, ***p<0.001

3.5 Results

Three-Dimensional Reconstruction of Astrocyte Anatomy Using FIB-SEM

To investigate the fine structural properties of astrocytes, we performed serial electron microscopy using FIB-SEM. Image stacks were acquired from mouse barrel cortex (S1BF) resulting in tissue volumes of 475 µm³ (Astrocyte 1) and 550.5 µm³ (Astrocyte 2)(Fig. 1A). The astrocytic cytoplasm was identified by the relative clarity of the cytoplasm of astrocytic processes and the presence of electron dense glycogen granules (Fig. 1B). Asymmetric and symmetric synapses whose pre- and postsynaptic compartments were contacted by the astrocytes were identified by clear pre- and postsynaptic terminals and the presence or absence of a postsynaptic density (Fig. 1C-E) (Ventura and Harris, 1999). To produce three dimensional reconstructions of astrocytes, we pre-screened the volumes for major astrocytic branches giving rise to filaments that filled the block extensively and segmented the entire astrocytic compartment connected to a main starting point. The final volumes for each segmented astrocyte were 5.56µm³ and 15.63 µm³, respectively. These volumes were consistent with the fact that neuropil-associated astrocytic processes largely consist of small calibre branches and branchlets, and thus make up only a small fraction of the total volume. Astrocytes displayed highly convoluted morphology consistent with previous EM reconstructions (Grosche et al., 1999; Mishchenko et al., 2010; Patrushev et al., 2013; Kasthuri

et al., 2015) (Fig. 1F,G). The two astrocyte's volumes shared characteristics including having neuropil-associated portions with numerous peripheral astrocyte processes (PAPs) that wrap synapses. However, the two astrocytes differed with respect to other anatomical features of the samples. For example, Astrocyte 1 abutted a cell body that occupied a portion of the imaged volume (Fig. 1A and F), while Astrocyte 2 had a large perivascular region with endfeet connected to the main astrocytic volume by thin bridges (Fig. 1 G).

To map synapses associated with each astrocyte, we segmented PSDs of all synapses contacted by the astrocytes (seafoam green, Fig. 1C-J). Large numbers of PSDs were associated with PAPs (174, Astrocyte 1; 360, Astrocyte 2)(Fig. 1H,I), some of which were quite complex and in contact with many synapses (Fig. 1J). The segmented PSDs fell into well-described categories (Spacek, 1985b, 1985a; Mishchenko et al., 2010) (Fig. 2 and Table 1) with dendritic spines and asymmetric synapses accounting for the vast majority of synapses (Fig. 2A and Table 1). A subset of spines contained a spine apparatus, the important calciummodulating extension of smooth ER into spines (Breit et al., 2018). A mostly overlapping but distinct subset of spines also possessed a perforated PSD, which have been seen to increase in number following stimuli inducing synaptic potentiation (Sorra et al., 1998; Nikonenko et al., 2002) (Fig 2A). Both spine apparatuses and perforations have been shown to be a hallmark of larger spines with larger PSDs, observations that we confirmed in both datasets (Spacek and Harris, 1997; Yuste and Bonhoeffer, 2001) (Fig 2B and C). Volumes of all spine PSDs also fell into the expected right-skewed Rayleigh distribution as observed previously (Bartol et al., 2015). Combined, these measurements suggest that the astrocytes in the present study contact pools of synapses that distribute as expected.

Mitochondria (purple) were also segmented and found to be distributed within the astrocytic volumes (Fig. 1 B-G, H,J). In some instances, astrocytic mitochondria were positioned very close to synapses (Fig. 1 Ei, ii, iii), in contrast to previous reports that calcium sources do not appear in PAPs (Patrushev et al., 2013; Rusakov, 2015). We also noted the

proportions of PSDs associated with endoplasmic reticulum (ER) and ER contacts with mitochondria (mitochondria-associated membranes; MAMs). ER was present underneath nearly all PSDs or spine necks, but more variability was observed in the proximity of PSDs to dendritic mitochondria and MAMs to synapses (Figure 2A and Table 1).

Measuring Shortest Paths Through Convoluted Astrocytic Processes Using Wavefront Propagation

To investigate if mitochondrial distribution in astrocytes is related to specific synapse types and their organization, we measured distances between PSDs and their nearest astrocytic mitochondrion. Such shortest path measurements between multiple possible objects can be performed manually or by applying Dijkstra's algorithm. However given the convoluted nature of the astrocytic volumes and the resulting complexity of shortest paths between PSDs and mitochondria, this was not an option. Similarly, the complexity of the intracellular space complicated potential adaptations of existing methods such as measuring paths along the surface mesh or centreline tracing, the latter of which works well for more uniform dendritic structures in neuronal arbors (Jorstad et al., 2014, 2018).

Given these challenges, we implemented a novel approach for 3D astrocytic distance measurements in reconstructions by using an eikonal equation fast-marching wave-front propagation algorithm to measure shortest paths. This approach can be visualized by propagating an outwardly evolving surface from the initial surface of the mitochondria (Fig. 3A). As this wave-front spreads, it fills the astrocytic volume and encounters the boundaries of the astrocytic volume. The iteration at which the wave-front encounters each point on the boundary can then be used to retrogradely trace the shortest path back to mitochondria from that point. This provides shortest paths between any point on the surface to any point on the mitochondria, bounded by the complex geometry of the astrocyte. Similarly, a wave-front can be propagated from the astrocytic surface (Fig. 3B) until it encounters each PSD, and

shortest paths back to the astrocyte can then be calculated. To obtain the overall distances between PSDs and mitochondria, we measured the shortest paths from each PSD to the astrocytic surface. This defined a specific landing point on the astrocyte via which shortest distance from the mitochondria to each PSD landing point was then calculated (Figs. 3C and D). We reasoned that the most meaningful measure of how closely astrocytic mitochondria associate with PSDs is based on the distance between mitochondria and the astrocytic surface, as this is the site that will be interacting directly with the extracellular space from which factors release by neurons are detected. We refer to this measurement as PSD-mitochondrial distance, and the entire distance from PSD surface to landing point on the astrocyte to the mitochondrion as PSD-Astro-Mito distance. By mapping the magnitude of PSD-mitochondrial distances onto three dimensional models of PSD surfaces, we were able to visualize the relative proximity of each PSD to their nearest mitochondrion (blue-closer; red-further; Fig. 3Eii and Eiii). While there was variability apparent in the PSD-mitochondrial distances, no overarching pattern emerged on visual inspection.

Spatial Relationships Between Astrocytic Mitochondria and PSD Subcategories

If astrocytic mitochondria are preferentially trafficked to and localized at regions of high synaptic activity and/or neuronal metabolic need, larger, and hence stronger and more active synapses (Matsuzaki et al., 2001, 2004) may be closer to astrocytic mitochondria. We therefore asked whether any particular category of synapses tends to be located closer to or further away from astrocyte mitochondria, and found that this was not the case for the synaptic characteristics examined (Fig. 4A, B and Table 2) or for total PSD-Astro-Mito distance (Table 3). Furthermore, PSD volume did not covary with PSD to mitochondria distance (Fig. 4C, D). In Astrocyte 2 a significant correlation was observed (dashed grey line; r = 0.13, p = 0.014, Pearson), however, when three outlying PSDs apparent in Fig. 4D were removed, this correlation was lost (solid black line; r = 0.05, p= 0.40, Pearson). These results suggest that

qualitative identities of individual PSDs, in particular hallmarks of stronger synapses including PSD volume, are not specifically related to the positioning of astrocytic mitochondria.

We also assessed whether the direct distance from PSD to PAP membrane was influenced by PSD category and found no significant relationship (Table 4). This was unexpected since multiple lines of evidence suggest that larger synapses are less well covered by astrocytes, either due to spatial constraints or to allow for neurotransmitter spillover and heterosynaptic plasticity (Rusakov and Kullmann, 1998; Ventura and Harris, 1999; Witcher et al., 2007; Bernardinelli et al., 2014; Medvedev et al., 2014). However, these results most likely indicate that direct distance measurements are simply a poor estimate of astrocytic coverage of individual synapses. Interestingly, it has also been previously observed that mitochondria were excluded from PAPs, with a minimal distance of ~0.5µm between PSD and any astrocytic calcium source (ie mitochondrion or ER) (Patrushev et al., 2013; Rusakov, 2015). However, we found that in mouse barrel cortex there is an appreciable portion of synapses within less than 0.5µm of mitochondria when considering PSD-Astro-Mito distance (11.5% of PSDs in Astrocyte 1; 14.2% Astrocyte 2; also apparent in Fig. 4C and D). Thus, mitochondria are not fully excluded from PAPs as previously thought. However, the PSDs that are closer to mitochondria do not appear to be of any particular type.

Spatial relationships between clusters of PSDs and astrocytic mitochondria

Given that the numbers of both mitochondria and the calcium microdomains with which they colocalize are lower than the number of synapses contacted by an astrocyte (5 mitochondria Astrocyte 1; 12, Astrocyte 2)(Agarwal et al., 2017), we hypothesized that mitochondria might be preferentially localized near clusters of PSDs enriched for synapses of particular types. Rather than focusing directly on PSD location in space, we examined clusters of PSD landing sites on the astrocytic surface. To define spatial clusters of PSDs based on these sites in an unsupervised manner, we performed dominant set clustering (Pavan et al., 2003),

which identified 13 clusters of PSDs in Astrocyte 1, and 24 clusters in Astrocyte 2 (Fig. 5, Table 5). These clusters were clearly apparent as distinct groups in correlation matrices comparing the pairwise distances between all PSD landing sites along the astrocytic surface (Fig. 5A). Interestingly, the mean volume of PSDs contained in each cluster was not found to vary significantly between clusters (Fig. 5C, D), which indicates that there is no higher order organization of synapses of a particular size, and thus likely strength, at different regions of the astrocyte. Contrary to this, we did find that there were significant differences in the mean PSD to mitochondria distance between clusters (Fig 5E, F), suggesting that there is likely a larger organizing principle to the distribution of mitochondria relative to clusters of synapses (p values of pairwise comparisons in Tables 7 and 8).

Although there is significant variation in the mean PSD to mitochondria distances in clusters of PSDs, this variability was not consistently associated with any particular category of PSD. We tested this by asking whether mean PSD to mitochondria distance of each cluster covaried with the proportion of PSDs of a particular category that made up each cluster (Table 6). In Astrocyte 2, a higher proportion of spines making up a cluster correlated significantly with greater mean distance to the nearest mitochondria for the PSDs in that cluster (r= 0.432, p = 0.035). The opposite was true for shaft synapses (r = -0.432, p = 0.035). Shaft synapses are often inhibitory, and spine synapses generally excitatory, and hence symmetric and asymmetric, respectively. However, the proportion of asymmetric and symmetric synapses in PSD clusters did not covary with mean PSD to mitochondria distance, and so whether clusters contained inhibitory synapses or excitatory synapses does not seem to explain the significant results for spines and shaft synapses. Furthermore, the fact that this was only seen in one of the datasets makes it hard to interpret.

3.6 Discussion

Astrocytes are made up of a convoluted network of thin, irregular processes, that lack a readily apparent pattern or organization. These thin processes make intimate contacts with neurons to form the tripartite synapse, where they play key roles in regulating neural function (Perea et al., 2009). To complement the intricacy of their structure, astrocytes also display complex internal calcium dynamics. Despite the seeming randomness of their structure and calcium dynamics, calcium transients and microdomains can be influenced by neural activity and neuromodulators (Paukert et al., 2014; Shigetomi et al., 2016), and are thought to be important in metabolic support of neural activity and synaptic transmission (Jackson and Robinson, 2018). In light of the lack of evidence for higher order principles directing astrocytic structure and calcium signals relative to the microcircuitry with which astrocytes interact, we asked whether we could define rules by which astrocytes and astrocytic mitochondria are organized with respect to neighboring synapses. Due to the extraordinarily small size of protoplasmic astrocytic filaments, we took an ultrastructural approach to answer this question, in which we segmented portions of astrocytes and categorized all synapses that they contacted. Due to the complex nature of the astrocytic volumes, we applied advanced spatial analysis techniques to map distances through the astrocytic cytoplasm.

Geometry of astrocyte-neuron interactions at the tripartite synapse

We observed that within the portions of astrocytes we reconstructed, individual processes tended to form small or complex varicosities that interact with multiple synapses, and that these are often separated from adjacent astrocytic compartments by thin connecting filaments (Fig. 1H-J). In accordance with this, we found that synapses segregated into clusters based on the distance between points on the astrocyte surface with which their PSDs most closely associated. These clusters varied in size from 2 to 30 synapses (Table 5). The qualitative and quantitative presence of clusters of synapses associating with small astrocytic domains suggests there may be some kind of segregation of synapses into different groups, however

there were no significant differences between mean volumes of the PSDs across clusters. This suggested that different "types" of clusters, based on synaptic strength (which can be approximated from PSD volume), do not exist. However, other attributes of synapses that cannot be assessed through their ultrastructure, such as how often they fire, their probability of release, or the circuitry they belong to, may be more represented in some clusters than in others and drive differences between the clusters.

Astrocytic Mitochondria and Calcium Microdomains

Calcium dynamics play essential roles in the ability of astrocytes to support and regulate neuronal function (Bazargani and Attwell, 2016). Initially, astrocyte calcium was thought to originate solely from the extracellular space and endoplasmic reticulum (Petravicz et al., 2008), however subsequent work has shown that mitochondria are a major source of calcium in astrocytes (Jackson and Robinson, 2018). Furthermore, mitochondria are closely associated with, and are responsible for generating a significant portion of astrocytic calcium microdomains (Agarwal et al., 2017). Exactly what roles calcium microdomains play in astrocyte-neuron interactions, and how their locations are determined, is unclear. With these points in mind, we asked whether astrocytic mitochondria preferentially localized near certain types or clusters of synapses, where they would be better positioned to support and regulate those synapses. Interestingly, we found no relationships between the locations of astrocytic mitochondria and features of individual synapses that are readily distinguishable in ultrastructural datasets. Furthermore, although synapses clustered around distinct areas of the astrocytic surface varied significantly in their properties, no higher-order spatial relationships were observed between astrocytic mitochondria and the categories of synapses making up these clusters.

What drives mitochondrial localization in astrocytes?

Our hypothesis that mitochondria may be situated closer to clusters of synapses containing more synapses of a particular category was predicated on the notion that calcium microdomains may be integrating signals from multiple synapses and responding to them as a group. This assumes higher order organization in the structure of astrocytes. However, the gross architecture of astrocytes may simply be dictated by the interstitial space they fill, a notion that is supported by the fact that astrocytes migrate and ramify in the neuropil only after large swathes of neuronal architecture have been established (Rowitch and Kriegstein, 2010). Furthermore, astrocytes recapitulate almost none of their in situ complexity when grown in vitro in a monolayer (McCarthy and Vellis, 1980; Foo et al., 2011; Rusakov, 2015; Sun et al., 2017), whereas neurons that have been cultured develop a stereotypical branching dendritic pattern (Banker and Cowan, 1977). Thus, although astrocytes do appear to have some local ability to establish PAPs associating with larger, and thus stronger and likely more active synapses (Ventura and Harris, 1999; Witcher et al., 2007; Bernardinelli et al., 2014), on a larger scale, astrocyte morphology may not inherently produce any higher order organization of its branching structure. One potential way in which astrocyte function can potentially be tuned to overcome this lack of structural organization is through active positioning and activation of calcium sources to areas of higher need. Interestingly our data suggest that synapses with particular attributes, including hallmarks of stronger synapses, do not recruit mitochondria either individually or as groups. Importantly, calcium microdomains do respond to neurotransmitters and increases in neuronal activity (Agarwal et al., 2017). However, a number of factors need to be considered here. Firstly, mitochondria are not the only calcium source contributing to microdomains. In fact, when IP₃R2 is knocked out, abrogating the bulk of calcium release from astrocytic ER and whole-cell calcium transients (Petravicz et al., 2008; Okubo et al., 2018), the number of active microdomains decrease by 65%. Blocking calcium release by mitochondria only partially disrupts calcium microdomains,

decreasing their number by 35%, frequency by 42% and amplitude by 14% (Agarwal et al., 2017). To take this into account and assess the relative locations of all intracellular calcium sources, the entire ER network in the astrocyte will need to be considered as well. Importantly, this also raises questions about what roles specific calcium sources play in contributing to calcium signalling in different contexts, complicating the matter. Secondly, whether or not microdomains are actually discrete, reappearing entities is not clear. In their pioneering work exposing mitochondria as a source of calcium microdomains, Agarwal and colleagues have used a machine learning approach to define ROIs representing recurring microdomains across time points (Agarwal et al., 2017). However, we and others have observed that subcellular calcium transients in astrocytes are spatially very dynamic, and that the concept of an entity such as a reproducible microdomain may be overly simplistic (Wu et al., 2014, and unpublished observations). Thus, reframing the question from what structures are likely to constitute localized microdomains, to what conditions are likely to promote calcium transients from which types of sources, will allow for a more nuanced approach to disentangling how subcellular calcium dynamics regulate astrocyte and neuronal function. This will likely involve taking into account functional characteristics of the neuronal circuitry that astrocytes respond to. While synaptic strength and stability can be estimated from PSD size (Matsuzaki et al., 2004), other aspects of synaptic physiology, such as the rate or pattern of EPSCs, or the extent to which EPSCs at synapses in a cluster are synchronized, cannot. Thus, correlated functional and ultrastructural studies, which have been successful in probing neural circuit function (Bock et al., 2011; Briggman et al., 2011), should be implemented. Importantly, other determined from ultrastructure or correlated anatomical features that can be fluorescence/ultrastructure studies, such as the identity of the pre- and postsynaptic neurons, and the dendritic subregion(s) that astrocytes are monitoring, may influence mitochondrial positioning. Therefore, moving forward, studies of astrocytic calcium sources and neuronastrocyte interaction should be harmonized with largescale functional and anatomical

ultrastructure projects currently underway (Schmidt et al., 2017; Zheng et al., 2018). The resulting data sets will allow for greater understanding of what drives astrocyte morphology in the vicinity of synapses and will aid in determining whether there are higher order organizing principles dictating the distribution of astrocytic calcium sources.

3.7 References

Agarwal A, Wu P, Hughes EG, Langseth AJ, Wirtz D, Bergles DE, Agarwal A, Wu P, Hughes EG, Fukaya M, Tischfield MA, Langseth AJ (2017) Transient Opening of the Mitochondrial Permeability Transition Pore Induces Microdomain Calcium Transients in Astrocyte Processes. Neuron 93:587–605.e7.

Banker GA (1980) Trophic interactions between astroglial cells and hippocampal neurons in culture. Science (80-) 209:809–810.

Banker GA, Cowan WM (1977) Rat hippocampal neurons in dispersed cell culture. Brain Res 126:397–425.

Barres BA (2008) The Mystery and Magic of Glia: A Perspective on Their Roles in Health and Disease. Neuron 60:430–440.

Bartol TM, Bromer C, Kinney J, Chirillo MA, Bourne JN, Harris KM, Sejnowski TJ (2015) Nanoconnectomic upper bound on the variability of synaptic plasticity. Elife 4:1–18.

Bazargani N, Attwell D (2016) Astrocyte calcium signaling: The third wave. Nat Neurosci 19:182–189.

Bernardinelli Y, Muller D, Nikonenko I (2014) Astrocyte-Synapse Structural Plasticity. Neural Plasticity 2014.

Bock DD, Lee W-CA, Kerlin AM, Andermann ML, Hood G, Wetzel AW, Yurgenson S, Soucy ER, Kim HS, Reid RC (2011) Network anatomy and in vivo physiology of visual cortical neurons. Nature 471:177–182.

Breit M, Kessler M, Stepniewski M, Vlachos A, Queisser G (2018) Spine-to-Dendrite Calcium Modeling Discloses Relevance for Precise Positioning of Ryanodine Receptor-Containing Spine Endoplasmic Reticulum. Sci Rep:1–17.

Briggman KL, Helmstaedter M, Denk W (2011) Wiring specificity in the direction-selectivity circuit of the retina. Nature 471:183–188.

Di Castro MA, Chuquet J, Liaudet N, Bhaukaurally K, Santello M, Bouvier D, Tiret P, Volterra A (2011) Local Ca2+detection and modulation of synaptic release by astrocytes. Nat Neurosci 14:1276–1284.

Foo LC, Allen NJ, Bushong EA, Ventura PB, Chung WS, Zhou L, Cahoy JD, Daneman R, Zong H, Ellisman MH, Barres BA (2011) Development of a method for the purification and culture of rodent astrocytes. Neuron 71:799–811.

Grosche J, Matyash V, Möller T, Verkhratsky A, Reichenbach A, Kettenmann H (1999) Microdomains for neuron-glia interaction: Parallel fiber signaling to Bergmann glial cells. Nat Neurosci 2:139–143.

Jackson JG, O'Donnell JC, Takano H, Coulter D a, Robinson MB (2014) Neuronal activity and glutamate uptake decrease mitochondrial mobility in astrocytes and position mitochondria near glutamate transporters. J Neurosci 34:1613–1624.

Jackson JG, Robinson MB (2018) Regulation of mitochondrial dynamics in astrocytes: Mechanisms, consequences, and unknowns. Glia 66:1213–1234.

Jorstad A, Blanc J, Knott G (2018) NeuroMorph: A Software Toolset for 3D Analysis of Neurite Morphology and Connectivity. Frontiers in Neuroanatomy 12:1–12.

Jorstad A, Nigro B, Cali C, Wawrzyniak M, Fua P, Knott G (2014) NeuroMorph: A Toolset for the Morphometric Analysis and Visualization of 3D Models Derived from Electron Microscopy Image Stacks. Neuroinformatics 13:83–92.

Kacerovsky JB, Murai KK (2016) Stargazing: Monitoring Subcellular Dynamic of Brain Astrocytes. Neuroscience 323:84–95.

Kanemaru K, Sekiya H, Xu M, Satoh K, Kitajima N, Yoshida K, Okubo Y, Sasaki T, Moritoh S, Hasuwa H, Mimura M, Horikawa K, Matsui K, Nagai T, Iino M, Tanaka KF (2014) In Vivo visualization of subtle, transient, and local activity of astrocytes using an ultrasensitive Ca2+indicator. Cell Rep 8:311–318.

Kasthuri N et al. (2015) Saturated Reconstruction of a Volume of Neocortex. Cell 162:648–661.

Knott G, Rosset S, Cantoni M (2011) Focussed ion beam milling and scanning electron microscopy of brain tissue. J Vis Exp:e2588.

Korogod N, Petersen CCH, Knott GW (2015) Ultrastructural analysis of adult mouse neocortex comparing aldehyde perfusion with cryo fixation. Elife 4:1–17.

MacAskill AF, Atkin TA, Kittler JT (2010) Mitochondrial tracking and the provision of energy and calcium buffering at excitatory synapses. Eur J Neurosci 32:231–240.

Matsuzaki M, Ellis-Davies GC, Nemoto T, Miyashita Y, Iino M, Kasai H (2001) Dendritic spine geometry is critical for AMPA receptor expression in hippocampal CA1 pyramidal neurons. Nat Neurosci 4:1086–1092.

Matsuzaki M, Honkura N, Ellis-Davies GCR, Kasai H (2004) Structural basis of long-term potentiation in single dendritic spines. Nature 429:761–766.

McCarthy KD, Vellis J de (1980) Preparation of separate astroglial and oligodendroglial cell cultures from rat cerebral tissue. J Cell Biol 85:890–902.

Medvedev N, Popov V, Henneberger C, Kraev I, Rusakov DA, Stewart MG (2014) Glia selectively approach synapses on thin dendritic spines. Philos Trans R Soc B Biol Sci 369:1–6.

Misgeld T, Kerschensteiner M, Bareyre FM, Burgess RW, Lichtman JW (2007) Imaging axonal transport of mitochondria in vivo. Nat Methods 4:559–561.

Mishchenko Y, Hu T, Spacek J, Mendenhall J, Harris KM, Chklovskii DB (2010) Ultrastructural analysis of hippocampal neuropil from the connectomics perspective. Neuron 67:1009–1020.

Morita M, Prudent J, Basu K, Goyon V, Katsumura S, Hulea L, Pearl D, Siddiqui N, Strack S, McGuirk S, St-Pierre J, Larsson O, Topisirovic I, Vali H, McBride HM, Bergeron JJ, Sonenberg N (2017) mTOR Controls Mitochondrial Dynamics and Cell Survival via MTFP1. Mol Cell 67:922–935.e5.

Nikonenko I, Jourdain P, Alberi S, Toni N, Muller D (2002) Activity-induced changes of spine morphology. Hippocampus 12:585–591.

Okubo Y, Kanemaru K, Suzuki J, Kobayashi K, Hirose K (2018) IP 3 R2-independent Ca 2 + release from the endoplasmic reticulum in astrocytes. Glia:1–12.

Panatier A, Vallée J, Haber M, Murai KK, Lacaille JC, Robitaille R (2011) Astrocytes are endogenous regulators of basal transmission at central synapses. Cell 146:785–798.

Patrushev I, Gavrilov N, Turlapov V, Semyanov A (2013) Subcellular location of astrocytic calcium stores favors extrasynaptic neuron-astrocyte communication. Cell Calcium 54:343–349.

Paukert M, Agarwal A, Cha J, Doze VA, Kang JU, Bergles DE (2014) Norepinephrine Controls Astroglial Responsiveness to Local Circuit Activity. Neuron 82:1263–1270.

Pavan M, Pelillo M, Informatica D, Torino V, Mestre V (2003) Dominant sets and hierarchical clustering. Proc Ninth IEEE Int Conf Comput Vis:362–369 vol.1.

Perea G, Navarrete M, Araque A (2009) Tripartite synapses: astrocytes process and control synaptic information. Trends Neurosci 32:421–431.

Petravicz J, Fiacco TA, McCarthy KD (2008) Loss of IP3 Receptor-Dependent Ca2+ Increases in Hippocampal Astrocytes Does Not Affect Baseline CA1 Pyramidal Neuron Synaptic Activity. J Neurosci 28:4967–4973.

Rowitch DH, Kriegstein AR (2010) Developmental genetics of vertebrate glial-cell specification. Nature 468:214–222.

Rusakov DA (2015) Disentangling calcium-driven astrocyte physiology. Nat Rev Neurosci 16:226–233.

Rusakov DA, Kullmann DM (1998) Extrasynaptic Glutamate Diffusion in the Hippocampus: Ultrastructural Constraints, Uptake, and Receptor Activation. J Neurosci 18:3158–3170.

Schmidt H, Gour A, Straehle J, Boergens KM, Brecht M, Helmstaedter M (2017) Axonal synapse sorting in medial entorhinal cortex. Nature 549:469–475.

Shigetomi E, Bushong EA, Haustein MD, Tong X, Jackson-Weaver O, Kracun S, Xu J, Sofroniew M V., Ellisman MH, Khakh BS (2013) Imaging calcium microdomains within entire astrocyte territories and endfeet with GCaMPs expressed using adeno-associated viruses. J Gen Physiol 141:633–647.

Shigetomi E, Kracun S, Khakh BS (2010) Monitoring astrocyte calcium microdomains with improved membrane targeted GCaMP reporters. Neuron Glia Biol 6:183–191.

Shigetomi E, Patel S, Khakh BS (2016) Probing the Complexities of Astrocyte Calcium Signaling. Trends Cell Biol 26:300–312.

Sorra KE, Fiala JC, Harris KM (1998) Critical Assessment of the Involvement of Perforations, Spinules, and Spine Branching in Hippocampal Synapse. J Comp Neur 240:225–240.

Spacek J (1985a) Three-dimensional analysis of dendritic spines III. Glial sheath. Anat Embryol (Berl) 171:245–252.

Spacek J (1985b) Three-dimensional analysis of dendritic spines; II. Spine appartus and other cytoplasmic components. Anat Embryol (Berl) 171:235–243.

Spacek J, Harris KM (1997) Three-Dimensional Organization of Smooth Endoplasmic Reticulum in Hippocampal CA1 Dendrites and Dendritic Spines of the Immature and Mature Rat. J Neurosci 17:190–203.

Stephen T-L, Higgs NF, Sheehan DF, Al Awabdh S, López-Doménech G, Arancibia-Carcamo IL, Kittler JT (2015) Miro1 Regulates Activity-Driven Positioning of Mitochondria within Astrocytic Processes Apposed to Synapses to Regulate Intracellular Calcium Signaling. J Neurosci 35:15996–16011.

Sun X, Hu X, Wang D, Yuan Y, Qin S, Tan Z, Gu Y, Huang X, He C, Su Z (2017) Establishment and characterization of primary astrocyte culture from adult mouse brain. Brain Res Bull 132:10–19.

Ventura R, Harris KM (1999) Three-dimensional relationships between hippocampal synapses and astrocytes. J Neurosci 19:6897–6906.

Witcher MR, Kirov SA, Harris KM (2007) Plasticity of Perisynaptic Astroglia During Synaptogenesis in the Mature Rat Hippocampus. Glia 55:13–23.

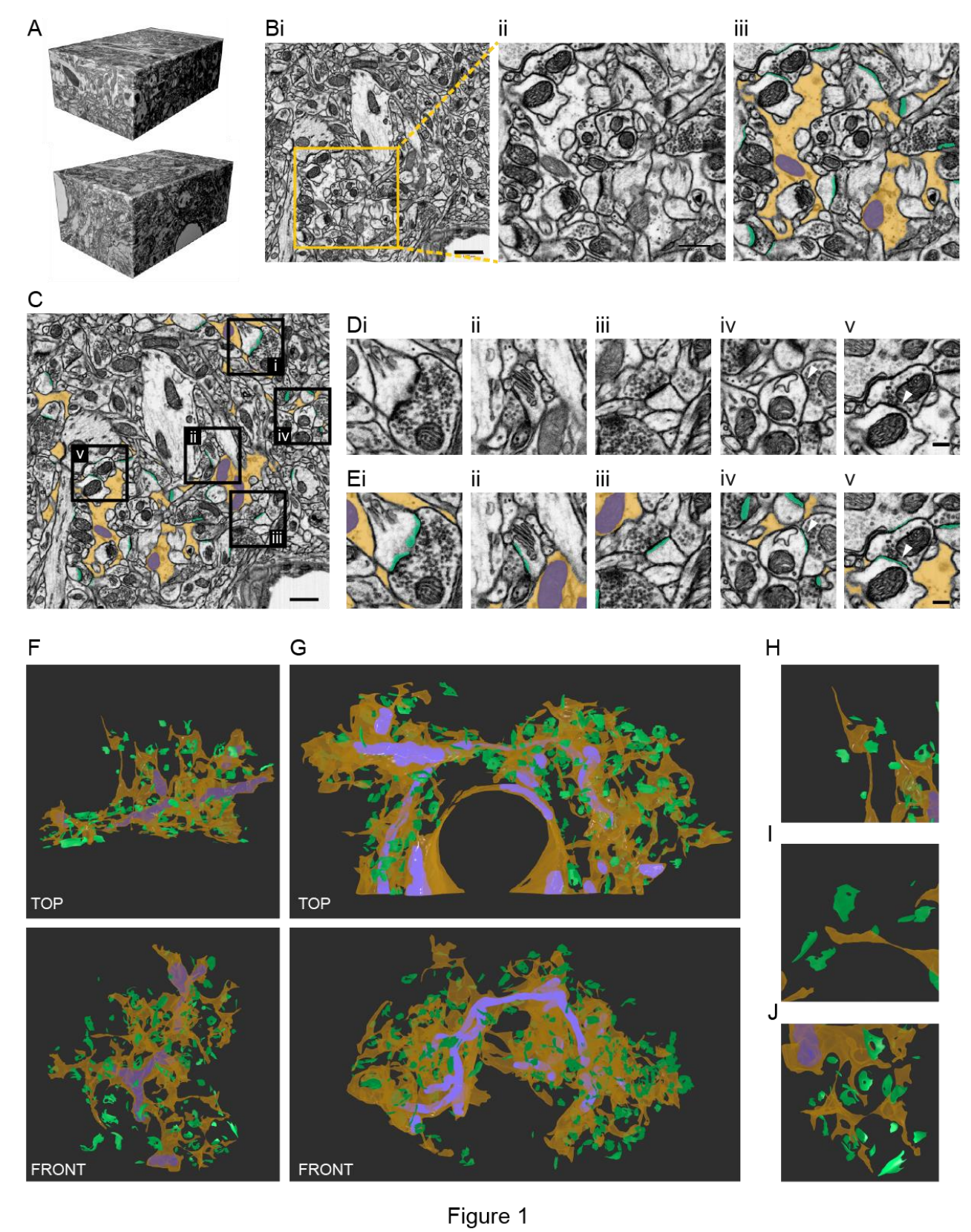
Witcher MR, Park YD, Lee MR, Sharma S, Harris KM, Kirov SA (2010) Three-dimensional relationships between perisynaptic astroglia and human hippocampal synapses. Glia 58:572–587.

Wu YW, Tang X, Arizono M, Bannai H, Shih PY, Dembitskaya Y, Kazantsev V, Tanaka M, Itohara S, Mikoshiba K, Semyanov A (2014) Spatiotemporal calcium dynamics in single astrocytes and its modulation by neuronal activity. Cell Calcium 55:119–129.

Yuste R, Bonhoeffer T (2001) Morphological Changes in Dendritic Spines Associated with Long-Term Synaptic Plasticity. Annu Rev Neurosci 24:1071–1089.

Zheng Z et al. (2018) A Complete Electron Microscopy Volume of the Brain of Adult Drosophila melanogaster. Cell 174:730–743.e22.

3.8 Figures and Tables



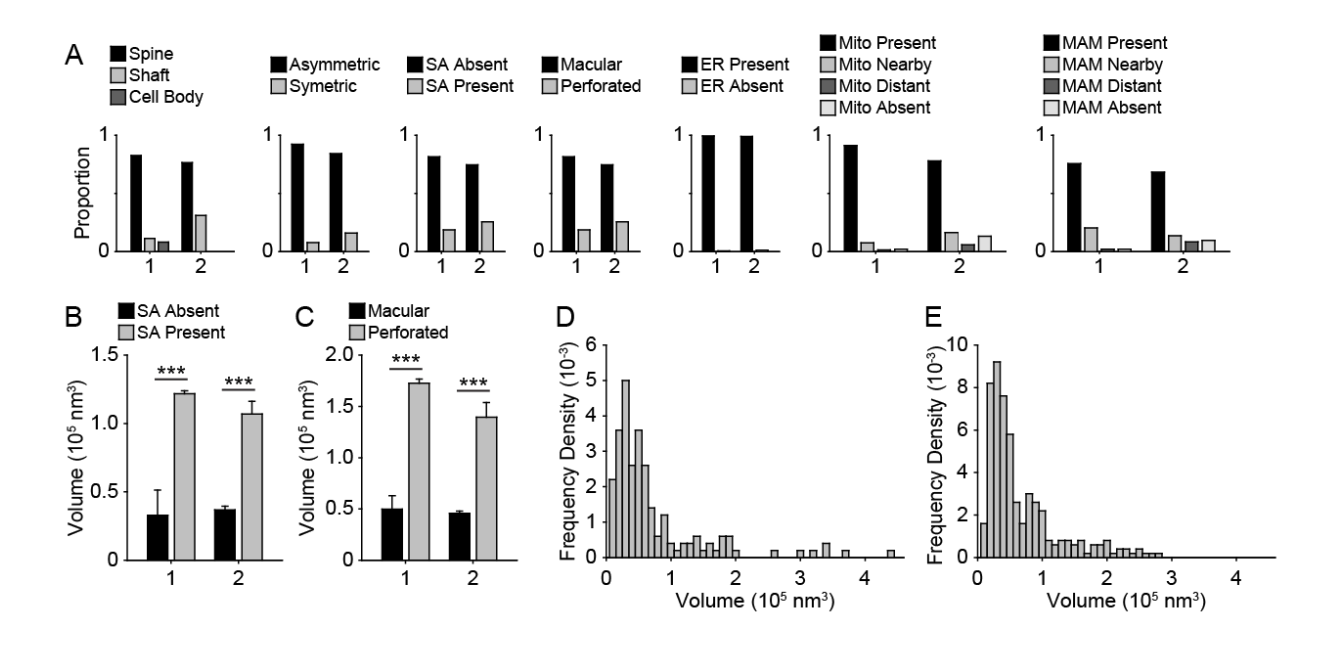


Figure 2

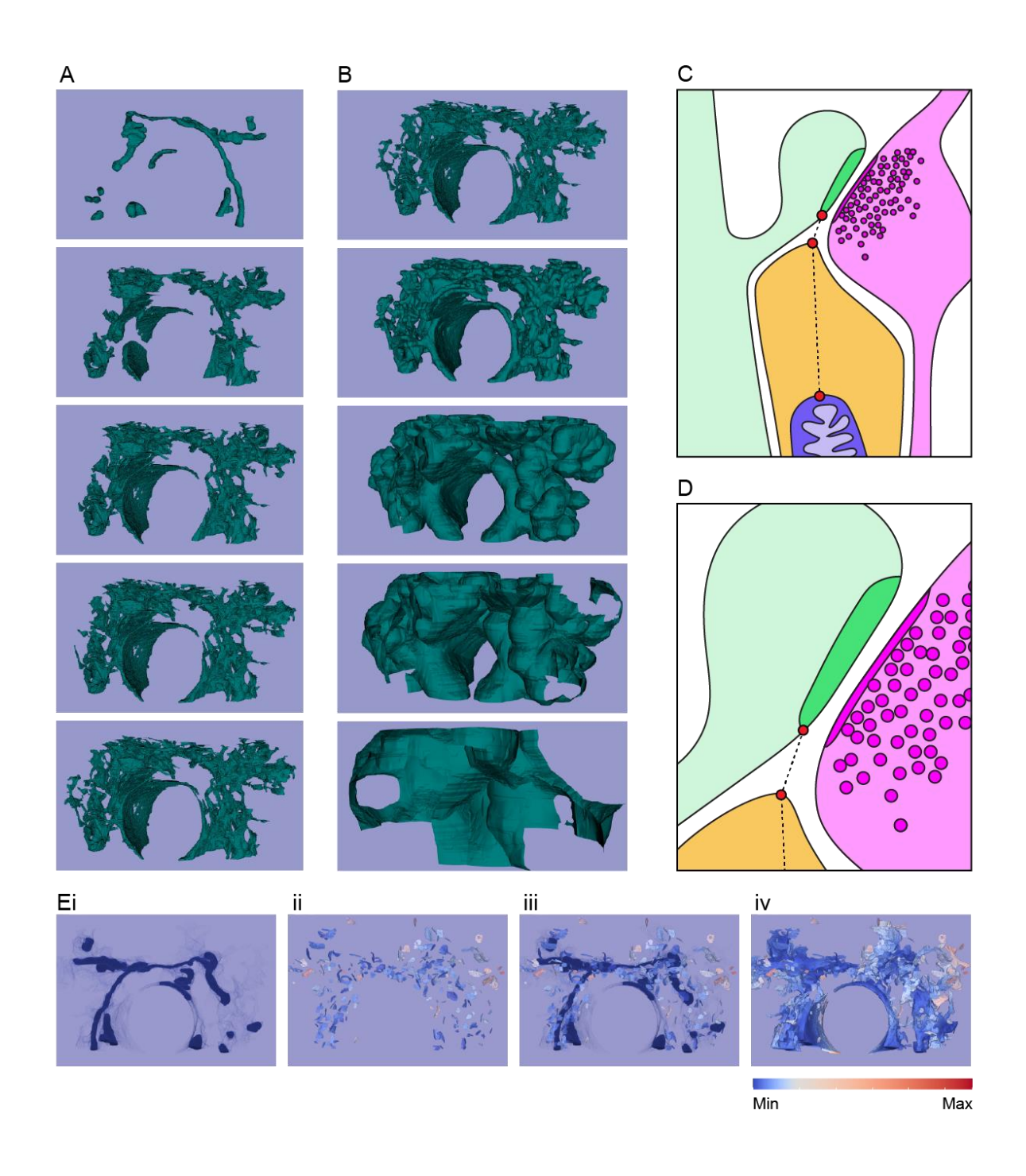


Figure 3

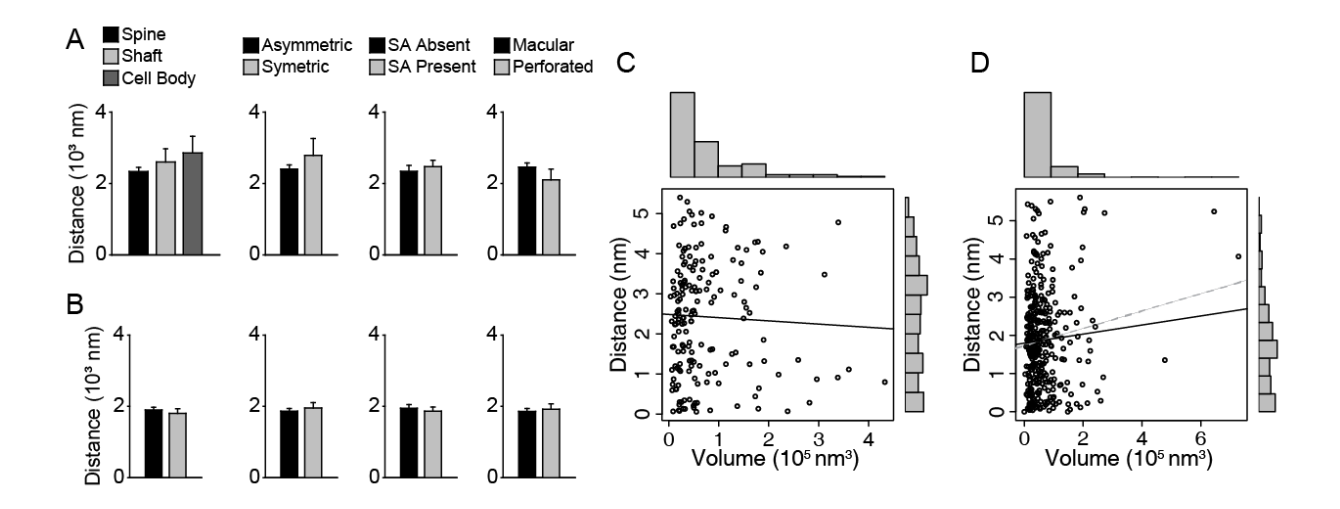


Figure 4

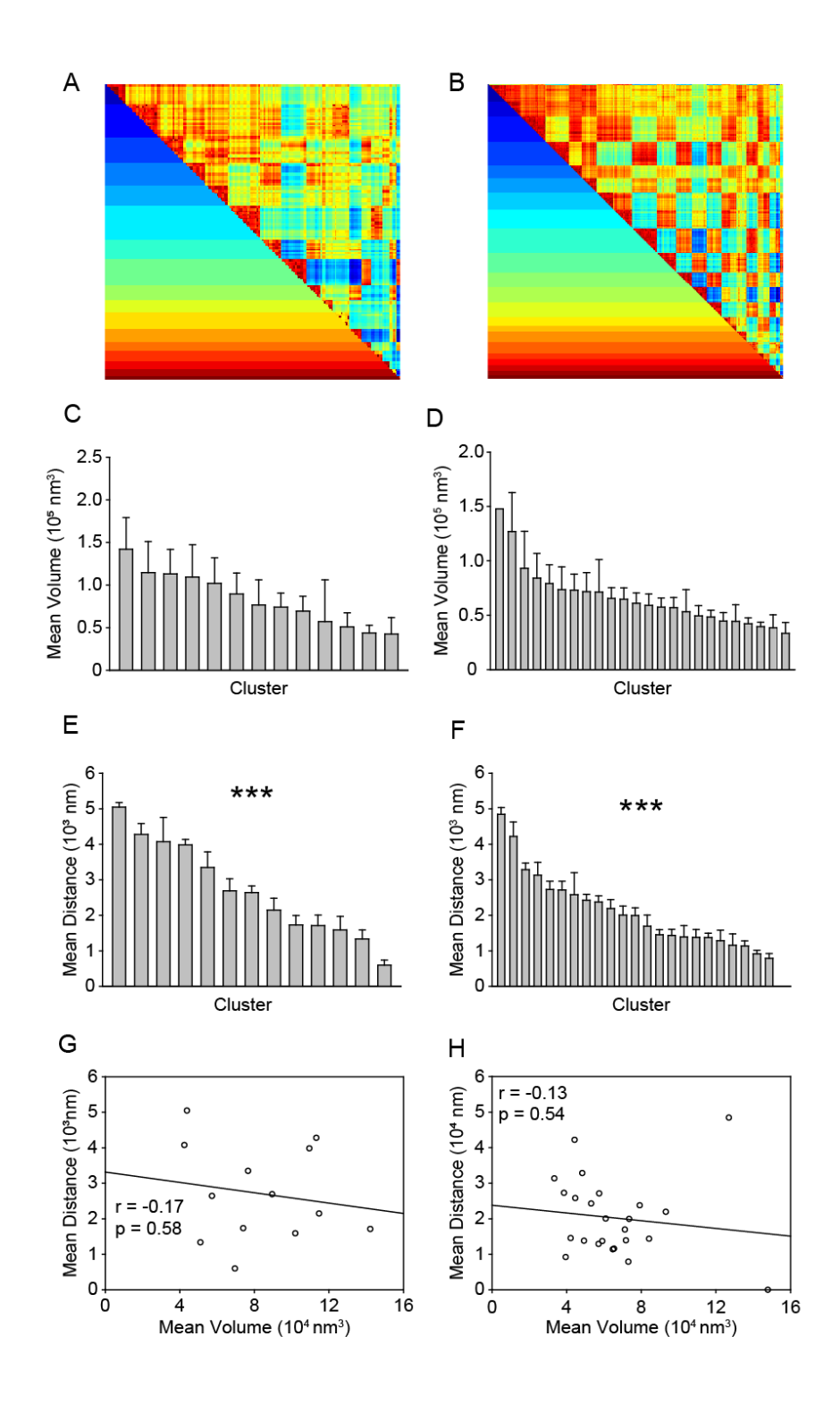


Figure 5

Table 1. PSD Category Counts and Volumes

	Astrocyte 1						Astrocyte 2						
	Count	Proportion	Volume (nm³)	SEM	Significance	p value	Count	Proportion	n Volume (nm³)	SEM	Significance	p value	
Synapse Location													
Spine	143	0.82	67201.44	6427.21			0	0.00					
Shaft	17	0.10	71359.75	16518.81	ANOVA ***	<0.001 ‡	85	0.24	55321.71	3634.72	ns	0.183	
Cell Body	15	0.09	147221.14	18596.31			274	0.76	67303.97	4935.46	115	0.103	
Synapse Type													
Asym	143	0.92	69987.49	6468.60		0.477	300	0.84	68219.20	4522.72	*	0.043	
Sym	13	0.08	71733.67	18398.43	ns	0.477	57	0.16	44067.27	3946.62		0.043	
Spine Apparatus (SA)													
Absent	80	0.58	32976.00	2193.18		*** <0.001		149	0.54	36716.87	2761.36	***	
Present	57	0.42	121682.14	13005.22	***	<0.001	125	0.46	106865.36	9337.46	***	<0.001	
Perforation													
Macular	126	0.82	49788.64	4065.86	***	<0.001	279	0.79	45661.73	2189.73	***	<0.001	
Perforated	27	0.18	172597.54	21677.60		<0.001	72	0.21	139406.03	14359.64		<0.001	
ER at Synapse													
Yes	148	0.99					328	0.99					
No	1	0.01					4	0.01					
Synaptic Mitocondria													
At	133	0.88	80457.61	7323.88			226	0.68	67047.16	5302.37			
Near	12	0.08	54304.36	8918.55	ANOVA ns	0.247	48	0.15	64277.53	8404.42	ANOVA ns	0.614	
Distant	3	0.02	34024.00	10880.00	ANOVATIS	0.247	18	0.05	53777.65	10465.46	ANOVATIS	0.014	
Absent	3	0.02	14862.00	5018.00			39	0.12	50351.05	6734.48			
MAM by Synaptic ER													
At	109	0.75	82407.26	8555.50			219	0.67	66776.18	5337.40			
Near	30	0.21	68440.55	9914.15	ANOVA ==	0.25	45	0.14	67695.82	9256.27	ANOVA ==	0.389	
Distant	4	0.03	37998.67	7433.45	ANOVA ns	U.25	29	0.09	58868.14	10995.85	ANOVA ns	0.389	
Absent	3	0.02	14862.00	5018.00			32	0.10	48881.03	7755.74			

[‡] Dunn's pairwise comparision for Astrocyte 1 Syapse location, Spine vs Shaft p>0.05, Spine vs Cell Body p<0.05, Shaft vs Cel body p<0.05

Table 1

Table 2. PSD to Mitochondria Distance

		Astroc	yte 1		Astrocyte 2			
	Distance (nm)	SEM	Significance	p value	Distance (nm)	SEM	Significance	p value
Synapse Location								
Spine Shaft Cell Body	2335.212 2603.7 2857.835	116.887 370.568 466.512	ns	0.351	1896.364 1800.686	78.834 130.313	ns	0.586
Synapse Type								
Asym Sym	2402.326 2787.838	120.389 471.709	ns	0.452	1866.348 1955.827	74.991 152.574	ns	0.348
Spine Apparatus (SA)								
Absent Present	2342.302 2471.811	161.171 179.752	ns	0.499	1946.422 1863.182	106.369 116.562	ns	0.52
Perforation								
Macular Perforated	2456.456 2104.12	121.463 297.544	ns	0.269	1860.26 1918.768	77.488 150.134	ns	0.556
Synaptic Mitocondria								
At Near Distant Absent	2497.536 3115.162 1134.564 2865.698	124.11 341.423 64.56 269.682	ns	0.327	1919.518 2150.647 1470.997 1715.448	87.258 202.609 229.891 192.643	ns	0.268
MAM by Synaptic ER								
At Near Distant Absent	2396.438 3178.363 1270.304 2865.698	139.015 223.425 140.765 269.682	ANOVA * No pairwise differences	0.031	1920.05 2200.99 1440.943 1705.731	86.795 209.707 196.1 229.816	ns	0.088

Table 2

Table 3. PSD-Astrocyte-Mitochondria Distance

		Astroc	yte 1	Astrocyte 2				
	Distance (nm)	SEM	Significance	p value	Distance (nm)	SEM	Significance	p value
Synapse Location								
Spine	2428.597	118.669						
Shaft	2762.559	358.074	ns	0.233	1992.105	79.907	ns	0.759
Cell Body	3080.417	474.084			1919.266	129.736	113	0.700
Synapse Type								
Asymmetric	2493.376	122.431		0.054	1964.933	75.727		0.277
Symmetric	2963.426	474.239	ns	0.351	2072.934	153.802	ns	0.211
Spine Apparatus (SA)								
Absent	2440.579	163.644		0.499	2045.643	106.881		0.462
Present	2559.997	183.103	ns	0.499	1958.174	119.107	ns	
Perforation								
Macular	2571.117	122.635		0.204	1961.714	78.213		0.604
Perforated	2160.298	299.349	ns	0.204	2013.462	152.389	ns	0.004
Synaptic Mitocondria								
At	2608.232	123.834			2031.178	88.079		
Near	3253.139	363.611	ns	0.294	2233.134	202.707		0.247
Distant	1232.602	68.862	115	0.294	1575.103	245.021	ns	0.247
Absent	3004.768	172.22			1806.859	195.214		
MAM by Synaptic ER								
At	2510.578	138.286			2029.265	87.893		
Near	3303.281	229.775	ANOVA * No pairwise	0.021	2312.971	208.991	ne	0.063
Distant	1351.429	125.302	differences	0.021	1537.166	204.877	ns	0.003
Absent	3004.768	172.22	311101011003		1790.152	227.668		

Table 3

Table 4. PSD to Astrocytic Membrane Distance

	Astrocyte 1				Astrocyte 2			
	Distance (nm)	SEM	Significance	p value	Distance (nm)	SEM	Significance	p value
Synapse Location								
Spine	93.385	11.344			95.741	7.284		
Shaft	158.857	32.907	ANOVA ***	<0.001	118.579	15.038	ns	0.389
Cell Body	222.582	32.31						
Synapse Type								
Asym	91.05	10.925		0.02	98.586	7.27		0.010
Sym	175.587	47.97		0.02	117.106	16.304	ns	0.218
Spine Apparatus (SA)								
Absent	98.276	17.423		0.005	99.221	9.73		0.709
Present	88.187	14.543	ns	0.995	94.992	11.34	ns	0.709
Perforation								
Macular	114.661	13.335	(+)	0.059	101.453	7.293		0.835
Perforated	56.181	12.05	ns (‡)	0.059	94.694	16.27	ns	0.835
Synaptic Mitocondria								
At	110.697	10.601			111.66	9.092		
Near	137.979	53.173	ANOVA ns	0.858	82.487	14.865	ANOVA ns	0 794
Distant	98.038	4.302	ANOVATIS	0.000	104.107	29.78	ANOVATIS	0.734
Absent	139.068	97.461			91.411	18.14		
MAM by Synaptic ER								
At	114.14	12.049			109.214	8.696		
Near	124.92	25.692	ANOVA ns	0.887	111.981	26.078	ANOVA ns	0.923
Distant	81.125	17.094	ANOVATIS	0.007	96.225	19.177	ANOVATIS	0.020
Absent	139.068	97.461			84.422	14.146		

Table 4

Table 5. PSD Cluster Summary Statistics

	Astrocyte 1					Astrocyte 2					
	PSD Count	Mean PSD V (nm3)	SEM	Mean PSD-Mito Distance (nm)	SEM	PSD Count	Mean PSD V (nm3)	SEM	Mean PSD-Mito Distance (nm)	SEM	
Cluster											
0	13	51022.46	16496.29	1334.57	253.51	1	147848.00		0.00		
1	16	73981.75	16584.63	1733.21	264.47	21	73044.57	14601.54	789.40	135.32	
2	15	89510.13	24529.99	2690.16	337.41	30	42126.00	5502.05	1453.23	142.26	
3	11	114672.00	36432.66	2148.63	332.02	28	64725.71	10304.07	1139.08	143.47	
4	8	69528.50	17283.50	598.82	138.26	16	79158.75	17269.98	2377.21	172.92	
5	8	142141.50	36972.90	1710.29	296.42	17	59052.00	10371.17	1371.32	124.79	
6	11	101916.36	30068.55	1590.06	383.91	17	49290.35	9446.00	1378.50	224.84	
7	5	76601.60	29590.57	3347.35	438.38	21	57396.76	8426.30	2711.83	245.63	
8	7	109442.29	37902.67	3981.54	158.85	22	93130.91	34075.96	2193.66	249.06	
9	3	57230.67	48889.94	2641.12	187.60	30	39448.93	4137.55	920.09	94.53	
10	4	43822.00	8820.63	5046.45	133.45	23	60920.52	9522.65	2004.51	251.36	
11	5	113180.00	28624.31	4278.91	306.20	21	84168.95	22725.62	1435.94	171.93	
12	2	42408.00	19316.00	4076.18	679.70	11	71742.91	17360.39	1391.27	320.14	
13						12	65361.67	9835.11	1157.69	322.40	
14						10	57067.20	9224.08	1289.85	295.06	
15						16	48319.50	6283.77	3284.94	184.52	
16						18	126940.00	35793.74	4846.67	189.47	
17						13	73472.31	20966.81	1994.84	217.85	
18						7	38556.57	11868.80	2727.80	231.89	
19						7	53124.57	20262.96	2426.77	163.70	
20						7	71191.43	29948.41	1693.71	310.11	
21						5	44608.80	7729.51	2580.33	621.81	
22						4	33335.00	9991.44	3135.53	352.71	
23						2	44246.00	15386.00	4220.30	409.42	

Table 5

Table 6. Coorelation of Cluster PSD Category Proportions with PSD to Mitochondria Distance

	Ast	rocyte 1		Astrocyte 2			
	Coorelation Coeff.	Significance	p value	Coorelation Coeff.	Significance	p value	
Synapse Location							
Spine	0.0705	ns	0.819	0.432	*	0.0351	
Shaft	-0.381	ns	0.199	-0.432	*	0.0351	
Cell Body	0.203	ns	0.506				
Synapse Type							
Asym	-0.0575	ns	0.852	0.269	ns	0.205	
Sym	0.0575	ns	0.852	-0.269	ns	0.205	
Spine Apparatus (SA)							
Absent	0.169	ns	0.581	0.379	ns	0.0676	
Present	-0.169	ns	0.581	0.0132	ns	0.951	
Perforation							
Macular	-0.394	ns	0.182	-0.199	ns	0.352	
Perforated	0.394	ns	0.182	0.199	ns	0.352	

Pearson product moment correlation was used to test correlations.

Table 6

Table 7. Pairwise comparisons for Astrocyte 1 clusters

			,
Cluster Comparison	Diff. of Means (nm)	p value	Signficance
11 vs. 5	4447.631	<0.001	
11 vs. 1	3711.885	<0.001	***
11 vs. 7	3456.393	< 0.001	***
11 vs. 6 11 vs. 2	3336.156 3313.243	<0.001 <0.001	***
11 vs. 2 11 vs. 4	2897.825	< 0.001	***
11 vs. 10	2405.326	0.09	ns
11 vs. 3	2356.292		
11 vs. 8	1699.096	0.351	Do Not Test Do Not Test
11 vs. 9	1064.909	0.883	Do Not Test
11 vs. 13	970.266	0.995	Do Not Test
11 vs. 12 12 vs. 5	767.54 3680.09	0.994 <0.001	Do Not Test
12 vs. 5	2944.345	< 0.001	***
12 vs. 7	2688.853	< 0.001	***
12 vs. 6	2568.616	0.001	***
12 vs. 2	2545.702	<0.001	***
12 vs. 4	2130.285	0.008	***
12 vs. 10	1637.786		Do Not Test
12 vs. 3 12 vs. 8	1588.751 931.555		Do Not Test Do Not Test
12 vs. o 12 vs. 9	297.368	0.936	Do Not Test
12 vs. 3	202.726	1	Do Not Test
13 vs. 5	3477.365	0.002	**
13 vs. 1	2741.619	0.024	*
13 vs. 7	2486.127	0.072	No
13 vs. 6	2365.89		Do Not Test
13 vs. 2	2342.977	0.096	Do Not Test
13 vs. 4 13 vs. 10	1927.559 1435.06		Do Not Test Do Not Test
13 VS. 10 13 VS. 3	1386.026	0.93	Do Not Test
13 vs. 8	728.83	1	Do Not Test
13 vs. 9	94.643	1	Do Not Test
9 vs. 5	3382.722	<0.001	***
9 vs. 1	2646.976	<0.001	***
9 vs. 7	2391.484		Do Not Test
9 vs. 6 9 vs. 2	2271.247 2248.334	0.002	Do Not Test Do Not Test
9 vs. 4	1832.916		Do Not Test
9 vs. 10	1340.417	0.755	Do Not Test
9 vs. 3	1291.383		Do Not Test
9 vs. 8	634.187	0.997	
8 vs. 5	2748.535	<0.001	***
8 vs. 1	2012.79	0.012	* D- N-4 T4
8 vs. 7 8 vs. 6	1757.298 1637.06		Do Not Test
8 vs. 2	1614.147		Do Not Test Do Not Test
8 vs. 4	1198.73		Do Not Test
8 vs. 10	706.23	0.999	Do Not Test
8 vs. 3	657.196	0.986	Do Not Test
3 vs. 5	2091.339	<0.001	***
3 vs. 1	1355.593	0.027	Do Not Tool
3 vs. 7 3 vs. 6	1100.101 979.864	0.221 0.551	Do Not Test Do Not Test
3 vs. 2	956.951	0.331	Do Not Test
3 vs. 4	541.533	0.975	Do Not Test
3 vs. 10	49.034	1	Do Not Test
10 vs. 5	2042.305	0.126	No
10 vs. 1	1306.559		Do Not Test
10 vs. 7	1051.067		Do Not Test
10 vs. 6 10 vs. 2	930.83 907.917		Do Not Test Do Not Test
10 vs. 2 10 vs. 4	492.499		Do Not Test
4 vs. 5	1549.805		Do Not Test
4 vs. 1	814.06		Do Not Test
4 vs. 7	558.568	0.982	Do Not Test
4 vs. 6	438.331	0.999	Do Not Test
4 vs. 2	415.418	0.997	Do Not Test
2 vs. 5	1134.388	0.299	Do Not Test
2 vs. 1 2 vs. 7	398.642 143.15	0.997	Do Not Test Do Not Test
2 vs. 7 2 vs. 6	22.913	1	Do Not Test
6 vs. 5	1111.475	0.562	Do Not Test

This is an abridged list of comparisons that shows all testable differences.

Table 7

Table 8. Pairwise comparisons for Astrocyte 2 clusters

Cluster Comparison	Diff. of Means (nm)	p value	Signficance
16 vs. 0	4846.67	<0.001	***
16 vs. 1	4057.27	<0.001	***
16 vs. 9	3926.578	<0.001	***
16 vs. 3	3707.591	<0.001	***
16 vs. 13	3688.985	<0.001	***
16 vs. 14	3556.824	<0.001	***
16 vs. 5 16 vs. 6	3475.348	<0.001	***
16 vs. 12	3468.168 3455.397	<0.001	***
16 vs. 12 16 vs. 11	3410.733	<0.001 <0.001	***
16 vs. 2	3393.44	<0.001	***
16 vs. 20	3152.959	<0.001	***
16 vs. `7	2851.828	< 0.001	***
16 vs. 10	2842.164	< 0.001	***
16 vs. 8	2653.009	<0.001	***
16 vs. 4	2469.462	<0.001	***
16 vs. 19	2419.897	<0.001	***
16 vs. 21	2266.345	<0.001	***
16 vs. 7	2134.841	<0.001	***
16 vs. 18 16 vs. 22	2118.871 1711.141	<0.001 0.058	ns
16 vs. 22	1561.729	<0.001	Do Not Test
16 vs. 13	626.37	1	Do Not Test
23 vs. 0	4220.3	0.014	*
23 vs. 1	3430.9	<0.001	***
23 vs. 9	3300.208	< 0.001	***
23 vs. 3	3081.221	<0.001	***
23 vs. 13	3062.615	<0.001	***
23 vs. 14	2930.454	0.003	**
23 vs. 5	2848.978	0.002	**
23 vs. 6	2841.798	0.002	**
23 vs. 12 23 vs. 11	2829.027 2784.363	0.004 0.003	**
23 vs. 2	2767.07	0.003	**
23 vs. 20	2526.589	0.047	*
23 vs. `7	2225.458	0.105	ns
23 vs. 10	2215.794	0.08	Do Not Test
23 vs. 8	2026.639	0.189	Do Not Test
23 vs. 4	1843.092	0.397	Do Not Test
23 vs. 19	1793.527	0.599	Do Not Test
23 vs. 21	1639.975	0.83	Do Not Test
23 vs. 7 23 vs. 18	1508.471 1492.501	0.773 0.889	Do Not Test
23 vs. 10 23 vs. 22	1084.771	0.009	Do Not Test Do Not Test
23 vs. 22 23 vs. 15	935.359	0.999	Do Not Test
15 vs. 0	3284.941	0.04	*
15 vs. 1	2495.541	<0.001	***
15 vs. 9	2364.85	< 0.001	***
15 vs. 3	2145.863	<0.001	***
15 vs. 13	2127.256	<0.001	***
15 vs. 14	1995.095	<0.001	***
15 vs. 5	1913.62	<0.001	***
15 vs. 6 15 vs. 12	1906.439 1893.668	<0.001	***
15 vs. 12 15 vs. 11	1849.004	<0.001 <0.001	***
15 vs. 11	1831.712	<0.001	***
15 vs. 20	1591.231	0.01	**
15 vs. `7	1290.099	0.013	Do Not Test
15 vs. 10	1280.435	0.001	Do Not Test
15 vs. 8	1091.281	0.023	Do Not Test
15 vs. 4	907.733	0.306	Do Not Test
15 vs. 19	858.168	0.872	Do Not Test
15 vs. 21	704.617	0.997	Do Not Test
15 vs. 7	573.112	0.946	Do Not Test
15 vs. 18 15 vs. 22	557.143 149.412	0.999 1	Do Not Test Do Not Test
22 vs. 0	3135.529	0.158	ns not rest
22 13. 0	0100.020	0.100	110

This is an abridged list of comparisons that shows all testable differences.

Table 8

3.9 Figure Legends

Figure 1. FIBSEM of astrocytic and synaptic ultrastructure. A) Block renders of the volumes from which Astrocyte 1 (top) and Astrocyte 2 (bottom) were segmented (width = 8.5μm; length = 12.7μm). B) Unsegmented ultrastructure (i), with a zoom on the boxed area in Bi showing an portion of astrocyte unsegmented (ii) and segmented (iii) (yellow) with astrocyte mitochondria (lilac) and PSDs that it contacts (seafoam green). Scale = 1μm (i) and 0.5μm (ii). C) Segmentation of all astrocytic compartments that belong to a continuous piece of traced astrocyte and PSDs that it contacts. D,E) Unsegmented (D) and segmented (E) zooms of boxed regions in C showing asymmetric, perforated spine PSD with spine apparatuses (i,ii); a macular spine PSD; and symmetric synapses on dendritic shafts (white arrow heads; iv, v). Scale = 0.2μm. F,G) Three dimensional rendering of continuous portions of Astrocyte 1 (F) and Astrocyte 2 (G). H-I) PAPs associated with PSDs.

Figure 2. Categories of synapses contacted by segmented astrocytic processes distribute as expected. A) Proportions of synapses contacted by Astrocyte 1 and 2 (indicated on horizontal-axes) that fall into the categories that were assessed (indicated in legends above graphs). See Table 1 for raw counts. **B)** Comparison of the volumes of PSDs that did not and did contain spine apparatuses (SA). (Astrocyte 1 SA Absent, $0.33 \times 10^5 \pm 0.08 \times 10^5$ nm³, Astrocyte 1 SA present, $1.22 \times 10^5 \pm 0.10 \times 10^5$ nm³, p < 0.001; Astrocyte 2 SA absent, $0.37 \times 10^5 \pm 0.06 \times 10^5$ nm³, Astrocyte 1 SA present, $1.07 \times 10^5 \pm 0.06 \times 10^5$ nm³, p < 0.001; 2-Way ANOVA (p < 0.001 within SA) with Tukey pairwise comparisons. No difference between Astrocytes p=0.47, no interaction p=0.223). **C)** Comparison of volumes of macular and perforated PSDs. (Astrocyte 1 macular, $0.50 \times 10^5 \pm 0.06 \times 10^5$ nm³, Astrocyte 1 perforated, $1.73 \times 10^5 \pm 0.12 \times 10^5$ nm³, p < 0.001; Astrocyte 2 macular, $0.46 \times 10^5 \pm 0.06 \times 10^5$ nm³, Astrocyte 1 perforated, $1.39 \times 10^5 \pm 0.07 \times 10^5$ nm³, p < 0.001; 2-Way ANOVA (p < 0.001 within perforation, p = 0.019 within Astrocytes) with Tukey pairwise comparisons. No interaction p=0.068. Astrocyte 2 perforated

PSDs were significantly larger than Astrocyte 1, p = 0.021.) **D,E)** Frequency density histograms a PSD volumes for Astrocytes 1 and 2, respectively.

Figure 3. Using wave-front propagation to determine shortest paths A) Sequence depicting how the wave-front evolved from the mitochondria in the traces portion of Astrocyte 2. B) Sequence depicting wave-front evolution from the surface of the astrocyte. C) Schematic depicting the tripartite synapse. A dendritic spine is shown in green with it's PSD shaded darker. An *en passant* axonal bouton is shown in magenta with its active zone and vesicles shaded darker. An astrocyte is depicted in yellow, containing a mitochondrion in purple. Examples of PSD to astrocyte distance and astrocyte to mitochondrion distance are show with red circles and dotted lines. PSD-Astro-Mito distance is the sum of these two distances. D) A zoom of the centre of the tripartite synapse schematized in C to better illustrate PDS to astrocyte distance. E) Results of distance measurements from the wave-front propagation approach. Ei) The mitocondria from which the wave-front was evolved shown surrounded by transparent astrocytic membrane. Eii) PSDs colored to indicate their distance to the nearest mitochondrion. Eiii) Overlay of i and ii. Eiv) PSDs from iii overlaid onto the astrocyte membrane, which is also heat mapped to indicate the astrocyte to mitochondria distance for each point on the astrocyte membrane. Heat map scale corresponds to both the relative PSD to mitochondria distances mapped onto PSDs and relative mitochondria to astrocytic surface distances mapped onto all points on the astrocytic surface.

Figure 4. Mitochondria are not localized more closely to individual PSDs of particular categories. A,B) Summary plots for Astrocyte 1 and 2, respectively, showing that there were no significant differences between the proximity of PSDs of certain classes to the nearest astrocytic mitochondrion. See Table 2 for values and statistics. (Dendritic mitochondria- and MAM- distances were also tested and are included in Table 2, however, sample sizes were low.) C,D) Correlation of PSD to mitochondria distance with PSD volume for Astrocyte 1 and 2, respectively, with frequency histograms describing variable distributions (Volume top,

Distance right). (Astrocyte 1, r = -0.045, p = 0.55; Astrocyte 2 excluding outliers, r = 0.050, p = 0.36; Astrocyte 2 including outliers, r = 0.13, p = 0.014. Pearson Product Moment Correlation).

Figure 5. Mitochondria are not localized more closely to clusters of PSDs displaying higher proportions of synapses of particular categories. A,B) Correlation matrices of distances between all pairs of PSD landing points along the surface of the astrocyte for Astrocyte 1 and 2, respectively. PSDs are grouped into clusters identified through dominant set clustering, and color coded by cluster on the left axes. The heat maps on the top axes are based on the distances between clusters. C,D) Mean volumes of PSDs in each cluster, ordered from largest to smallest, for Astrocytes 1 and 2 respectively. E,F) Mean distance of PSDs in each cluster ordered from largest to smallest, for Astrocytes 1 and 2 respectively. Stars denote p<0.001 for ANOVA. Pairwise comparisons are summarized in Tables 7 and 8. G,H) Correlation of cluster mean distance with cluster mean volume, for Astrocytes 1 and 2 respectively. (Pearson Product Moment Correlation.)

Chapter 4 TetOn Inducible Gene Expression in the Mouse Brain Across the Lifespan

4.1 Preamble

In Chapter 2, I presented work performed *in vitro* suggesting that depolarizing GABA_A transmission restrains glutamatergic synapse formation. The main benefit of the slice culture approach I took in that study was the ability to probe hippocampal circuitry during precise windows of development. We wanted to test if those findings translated to *in vivo* synaptic development, however research into developmental processes in the CNS *in vivo* is complicated by problems of access to the brain and temporal and spatial precision of manipulations. To circumvent these limitations, we devised a combination of techniques that would allow for temporal control over expression of genes of interest that could be targeted to discrete neuronal populations including the hippocampus. The following study presents the fruits of that effort. Importantly, while developing this system, I also engineered a number of DNA constructs that, when used in conjunction with the system described below, would allow for cell autonomous disruption of GABAergic signalling *in vivo*, with the aim of investigating the role of immature GABA_A transmission in the developing mouse brain. These constructs are currently being tested and I discuss them more extensively in Chapter 5.

While testing the inducible gene expression technique presented in the current chapter, we recognized its potential utility in other projects in the lab. As a result, we applied the methodology to the question of how neurons can diversify astrocytic molecular phenotype, demonstrating the utility of the approach for investigating neuron-astrocyte interactions. This work is also included below.

TetOn Inducible Gene Expression in the Mouse Brain Across the Lifespan

Christopher K. Salmon¹, Gael Quesseveur¹, J. Benjamin Kacerovsky¹, Gee Hung Leo Cheong¹, Michael P. Rosen¹, Miranda Green¹, Andy Y.L. Gao², and Keith K. Murai^{1*}

¹Centre for Research in Neuroscience, Department of Neurology and Neurosurgery, Brain Repair and Integrative Neuroscience Program, The Research Institute of the McGill University Health Centre, Montreal General Hospital, Montreal, Quebec, H3G 1A4, Canada.

²Department of Pharmacology and Therapeutics, McGill University, Montreal, QC, Canada.

The authors declare no financial interests or conflicts of interest.

*Correspondence should be addressed to:

Dr. Keith K. Murai Centre for Research in Neuroscience Montreal General Hospital 1650 Cedar Avenue L7-212 Montreal, QC, H3G 1A4 Canada Telephone: (514) 934-1934 x43477

Fax: (514) 934-8216 keith.murai@mcgill.ca

Number of Figures: 12 Number of words: 10,023

Key Words: TetOn, conditional, Shh, in utero electroporation, DOX, piggyBAC

Acknowledgements: The authors would like to acknowledge technical assistance from Dr. Emma Joes, Michael Pratte, Nensi Alivodej, and Amy Zhou. We would like to thank Dr. Min Fu and Shi-Bo Feng at the Molecular Imaging Platform of the Research Institute of the McGill University Health Centre for services provided. The pCAG-Cre-myc vector was kindly provided by Dr. Artur Kania, and in utero electroporation training was provided by Julie Cardin of the Kania Lab. The hSynapsin promoter was extracted from a pSKN-hSynapsin backbone kindly provided by Dr. Ellis Cooper. The Gli-Luciferase reporter cell line was kindly provided by Dr. Jorge Filmus by way of Dr. Frédéric Charron. Human γ 2 subunit cDNAs were kindly provided by Dr.'s Horia Pribiag and David Stellwagen. This work was supported by the Canadian Institutes of Health Research (MOP111152, MOP123390, and PJT156247) to K.K.M.

4.2 Abstract

The ability to experimentally express genes of interest with precise temporal control is essential for genetic and molecular biological interrogation of neural development and function. Although a number of tools exist for conditional gene expression, techniques for fast, temporally precise expression are still needed. The doxycycline-inducible TetOn expression system has been used successfully for conditional gene expression in the nervous system, however results have been variable and it has been found that the system tends to be silenced in adulthood. We tested the ability of the TetOn system to provide inducible gene expression after being introduced to neurons via in utero electroporation and found that delivery of episomal TetOn plasmids allowed for robust expression a ZsGreen reporter gene when mice were induced at one week of age, but little to no induction at 3 or 5 weeks. However, when introduced in transposable elements that integrate into the genome, the TetOn system allowed for robust induction of expression across the lifespan of the mouse. Induction was observed in neurons of sensorimotor and retrospleninal cortex, hippocampus and the olfactory bulb. To test the experimental utility of this system, we induced ectopic expression of the potent morphogen, Sonic hedgehog, in layer 2/3 cortical neurons, demonstrating that its expression can diversify astrocytic expression of Kir4.1. in surrounding astrocytes. Together, these data demonstrates that in utero electroporation of transposable TetOn inducible plasmids is a powerful system for inducible gene expression in multiple brain areas across the lifespan.

4.3 Introduction

Obtaining control over the timing of expression and silencing of genes of interest is a central challenge in molecular biology. While transgenic approaches have proven tremendously useful in determining gene function though expression of exogenous molecules or disrupting endogenous gene function, this classical methodology is hampered by the fact that genes play multiple different roles across cell types and at different stages of the life cycle of cells and organisms (Luo et al., 2018). For this reason, identification and validation of molecular and genetic switches for controlling gene expression in vivo have long been pursued (Lewandoski, 2002). Development of fast-acting and robust inducible gene expression systems is of particular importance for studies of the central nervous system (CNS), as development of neural circuits involves many steps that occur in rapid succession and continues after birth. While mouse lines expressing the CreER/CreERT2-LoxP and FLPeR/FlpERT2-FRT recombinase systems are routinely used for spatial and temporal control of gene expression in vivo, there remain substantial limitations in these approaches for understanding the function of molecules and pathways in neurons and glial cells of the CNS. High recombination efficiency through tamoxifen-based induction can be challenging especially in adult mice where recombination efficiency can be low (Slezak et al., 2007; Farmer et al., 2016). Cre- and Flp-based techniques also lack the ability to titrate gene expression levels as the transcription of the gene-of-interest relies on promoter activity and not dosage of a drug or transcription factor. Finally, these approaches lead to permanent changes in gene expression. Thus, additional in vivo approaches are needed to overcome these limitations and to complement the powerful toolkit currently provided by conditional CreERT2 and FlpERT2 systems.

The TetOn and TetOff tetracycline transactivation systems have been successfully employed to control the timing of gene expression in numerous organ systems (Baron and Bujard, 2000). The TetOff expression system employs the tetracycline transactivator (tTA),

which binds to the tet operator (tetO) in the absence of substrate (tetracycline or doxycycline), thereby driving expression. TetOn employs the reverse tTA (rtTA), which drives expression in the presence of substrate. Both TetOn and TetOff expression systems have been employed in multiple cell types and regions in the nervous system (Mayford et al., 1996; Agulhon et al., 2010), and importantly, expression has been successfully turned on and then off again in neurons in vivo using the TetOn system (Mansuy et al., 1998). However, while the TetOff system has been used frequently for inducible gene expression in the CNS (Luo et al., 2018), it has been found that the TetOn system is progressively silenced in the adult mouse CNS, and as a result it has been seldom used (Zhu et al., 2007).

Since its initial publication, in utero electroporation (IUE) has proven to be a cost effective and flexible tool for gene expression in neurons in vivo (Fukuchi-Shimogori and Grove, 2001; Saito and Nakatsuji, 2001; Tabata and Nakajima, 2001). The introduction of oriented bipolar electric fields and triple-electrode approaches has since made it possible to specifically target numerous brain areas using IUE (Carlson et al., 2011; dal Maschio et al., 2012; Baumgart and Baumgart, 2016). Given the flexibility of IUE for targeting distinct neuronal populations in the CNS and the possibility of achieving fast induction and on-off control of gene expression using the Tet expression systems, we sought to combine these techniques. The TetOff system requires that mice be reared on DOX diets to supress gene expression until it is desired. DOX is lipophilic and long-term administration leads to its deposition in muscle and bone, meaning that induction upon removal of the DOX diet can take up to 20 days (Mansuy and Bujard, 2000). On the other hand, TetOn-mediated gene expression has been observed as few as 4 hours after DOX administration begins in most organ systems (Kistner et al., 1996; Watanabe et al., 2007). To harness these fast induction kinetics, which are critical for attaining the high temporal precision needed to manipulate experimental gene expression during development, we assessed the ability of electroporated TetOn inducible constructs to provide precise, fast, and robust induction of gene expression. We

found that although an episomal TetOn system allowed for induction of expression in electroporated mouse pups at one week of age, as suggested by previous work (Zhu et al., 2007), induction was not consistently attainable at three weeks, and not at all at five weeks. The fact that some TetOn transgenic lines do not experience such silencing (Mansuy and Bujard, 2000) indicates that TRE silencing does not occur in certain genomic loci. We therefore hypothesized that stably integrating electroporated plasmids into random loci in the genome would circumvent the silencing we and others have observed. To test this, we employed the piggyBAC transposase system. In the presence of piggyBac transposase derived from the moth, Trichoplusia ni, inverted terminal repeats that flank the transposable element (ie the gene of interest) allow for homologous recombination of the construct into the genome at TTAA tetranucleotide sequences (Fraser et al., 1995, 1996; Toshiki et al., 2000). This system has been used previously in conjunction with IUE to allow for gene expression in astrocytes which, due to the postnatal proliferation of their progenitors, are difficult to target with IUE of episomal plasmids (García-Marqués and López-Mascaraque, 2012; Figueres-Oñate et al., 2016). When we incorporated the electroporated TetOn constructs into the genome using this approach, we observed robust induction in neurons across the lifespan of the mouse. Furthermore, induction was achieved in multiple cortical areas, as well as in the hippocampus and olfactory bulbs. As a proof-of-concept for the utility of this approach, we demonstrated that the potent developmental morphogen, Sonic Hedgehog (Shh), can be conditionally expressed in neurons to non-cell autonomously alter the molecular properties of neighboring astrocytes in the mature mouse brain. Thus, our results suggest that IUE of transposable TetOn inducible plasmids is a viable tool for conditional expression of genes of interest across the lifespan in the mouse brain.

4.4 Materials and Methods

DNA Plasmids and Molecular Biology

Plasmids were cloned as indicated in Supplementary Table 1. pTetO-ZsGreen (pTetO-ZsG) was obtained from Clontech (pmRi-ZsGreen; Cat. No. 631121) and all other pTetO promoters were derived from the PTet-14 promoter (Urlinger et al., 2000) from this backbone. The rtTA-expressing plasmids used in this study were constructed from the rtTA2S-M2 (Urlinger et al., 2000) present in pTetOn-Advanced (Clontech, Cat. No. 631124). All plasmids engineered for this study were verified by Sanger sequencing provided at the McGill and Genome Quebec Innovation Centre. Sequencing was performed with primers designed to attain full coverage on both strands of the coding regions of the genes of interest to ensure the absence of mutations. Novel plasmids engineered for this study will be made available through Addgene.

Animals and Animal Care

Experiments were approved by the Montreal General Hospital Facility Animal Care Committee and followed guidelines of the Canadian Council on Animal Care. The R26R Confetti Brainbow knock-in mouse was obtained from The Jackson Laboratory (R26R Confetti, Stock Gt(ROSA)26Sortm1(CAG-Brainbow2.1)Cle/J, Stock No. 013731).

In utero Electroporation (IUE)

IUE was performed on C57BL/6 mice (Supp. Fig. 2,3 only) produced from an in-house colony, or timed-pregnant ICR/CD1 mice ordered from Charles River Laboratories (Senneville, Québec). ICR/CD1 mice were housed on-site for a minimum of 2 days before surgery. Mice were kept on a 12/12 light/dark cycle and allowed access to food and water ad libitum.

Pregnant mice were anaesthetized with 5% isoflurane and maintained with 2% isofluorane on a homeothermic warming pad for the duration of the IUE surgery. Opthalamic ointment was used to prevent drying of the eyes. Breathing, temperature and color of mucosal membranes were monitored throughout the surgery. If any aberrations were observed, isoflurane flow was temporarily decreased until symptoms were resolved. The abdomen was shaved and cleaned with providone and isopropanol wipes. A 1.5cm vertical incision was then made at the midline of the abdomen with scissors. Sterile gauze (soaked with sterile, 39°C phosphate buffered saline (PBS)) was positioned around the incision to provide a clean, well hydrated surface on which to place the uterine horns. The uterine horns were extracted from the peritoneal cavity by massaging the abdomen with PBS-wetted gloves, and laid on the moist gauze. Uterine horns were kept moist and warm by frequent application of warm PBS throughout the surgery. A pulled glass micropipette attached to a foot pedal-controlled microinjector (Harvard Apparatus, MA) was used to deliver 2μL (E13-E14) or 3μL (E15-E16) of 2-3.5µg/µL solution of DNA to the lateral ventricle of the embryo's brain. Micropipettes were bevelled at a 35-45° angle using diamond lapping film attached to a repurposed computer hard drive. The bevelled, sharpened pipet tip helped to minimize damage to the CNS. DNA was dissolved in endotoxin free water or TE buffer and brought to the final concentration in PBS and 0.03% Fast Green dye. Five to seven 36-42V pulses of approximately 50ms were applied horizontally across embryo's cranium using an BTX ECM 830 square pulse generator and 3mm platinum-coated tweezer electrodes (BTX, MA). The embryos on either side of the uterine corpus were left untouched, and otherwise all embryos were electroporated unless excessive manipulation was required to expose the top of the cranium. The incision was then flushed with warm PBS, the abdomen was closed with 6-0 nylon running sutures, and the skin with 5-0 nylon running sutures. The mother was then returned to its home cage and allowed to recover until mobile and grooming resumed in a 28°C recovery chamber. Wet food and analgesia were provided following the surgery.

Doxycycline Administration

100μg/g DOX per day was administered in PBS solution via IP injection by two doses of 50μg/g (5 mg/mL). Induction of hippocampal expression was performed with one 50μg/g dose per day. For 3-week induction of Shh-myc expression from PB-pTetO-Shh-myc, electroporated mice were given a maltodextrine based DOX diet containing 3mg/g DOX (Custom Diet #TD.170534, Envigo) ad libitum. Fresh DOX diet was provided every 3 days.

Tissue and Cell Culture

Primary hippocampal neuronal cultures were prepared as described previously in detail (Jones et al., 2012). Briefly, hippocampi were extracted from postnatal day 0 C57BL/6 mice, incubated in 0.1% papain, 0.02% BSA in Neurobasal-A medium (NBA) (Invitrogen) at 37°C for 15 minutes with periodic agitation. Hippocampal tissue was then transferred to warm NBA containing 1% egg white trypsin inhibitor and 1% BSA and triturated 8 to 10 times with fire polished Pasteur pipettes of decreasing pore diameter, discarding undissociated debris after each trituration. Neurons were then plated on coverslips coated with poly-L-lysine (0.1mg/mL) at 40,000 cells/well in 500μL of neuronal culture medium in 24 well plates. Neuronal culture medium contained NBA supplemented with 2% B27 (Invitrogen), 1mM GlutaMax (Invitrogen) and 1% penicillin/streptomycin, and one third of medium was changed every 2 to 3 days by removing 200µL and adding 300µL. Cytarabine (ara-C) was added to a final concentration of 3µM after 3 days in vitro to prevent glial overgrowth. Neuronal transfections were performed with lipofectaine at 6 to 8 days in vitro. For each well, 75μL of unsupplemented NBA containing 1 to 2μg DNA was combined with 75μL unsupplemented NBA containing 3µL of lipofectamine. While this mixture was allowed to stand for 20 to 40 minutes, neurons were transferred into 400µL of equilibrated unsupplemented NBA in 24 well plates. Transfection mixtures were then added to neurons dropwise and incubated for 2 to 3 hours before being transferred back to their conditioned

neuronal culture medium. Expression of transfected plasmids proceeded overnight, followed by DOX-induction for 24 to 48h.

HEK293T and 8XGli-Luciferase C3H 10T1/2 (Gli-Luc reporter) cells were cultured in medium containing 10% FBS/ 1% Penicillin-Streptomycin/DMEM and passaged at a ratio of 1:10 when 70-90% confluent.

Immunofluorescence

Mice were transcardially perfused with PBS wash followed by 4% paraformaldehyde/0.1M phosphate buffer (PB), pH 7.4 (P8: 2mL wash, 15mL paraformaldehyde at a rate of 2mL per minute; P23: 3mL wash, 20mL paraformaldehyde, 3 mL/min; P35: 5mL wash, 35-40mL paraformaldehyde, 5mL/min; 20months; 5 mL wash, 50 mL paraformaldehyde, 5mL/min). Brains were post-fixed submerged in 4% paraformaldehyde/0.1M PB overnight, cryoprotected in 30% sucrose/PBS, and embedded in OCT embedding medium. Freefloating coronal sections (40µm) of the entire cerebrum were cut, collected in PBS, and screened for the region of the sensorimotor cortex containing the electroporation epicentre. Sections were permeabilized for 15 min in 1%Triton X-100 (TX-100)/PBS, blocked in 10% normal donkey serum (NDS) (Jackson Laboratories)/0.2% TrX-100/PBS for 1.5-2h and stained with primary antibodies in 1% NDS/ 0.2% TX-100/PBS for 16 to 72 hours. Sections were then washed 3 times in 1%NDS/ 0.2% TX-100/PBS, incubated with fluorescent secondary antibodies (Alexa Fluors, Invitrogen) for 2 hours, washed 3 times in PBS and mounted in Slowfade Gold mounting medium (Invitrogen). Primary antibodies used were mouse anti-mCherry (Clontech, Cat. No. 632543), chicken anti-GFP (Abcam, ab13970), and mouse anti-myc (Santa Cruz, 9E10). TO-PRO-3 Iodide (TOPRO) (Thermo-Fisher) was used to stain nuclei to demonstrate the location of imaging in the neuropil.

Primary neuronal cultures were washed briefly with 4°C PBS and then fixed with a solution of 4% formaldehyde/4% sucrose/0.1M PB cooled to 4°C, left for 15 min at room temperature,

washed three times with PBS, permeabilized in 0.2% TX-100/PBS for 15 minutes, and blocked in 10% NDS/PBS for 1.5 to 2h. Coverslips were incubated in primary antibodies with 1% NDS/PBS overnight at 4°C, washed 3 times in 1%NDS/PBS, incubated with secondary antibodies (Alexa Fluors) for 2 hours in 1%NDS/PBS, washed 3 times in PBS and mounted in Slowfade Gold. Antibodies used were rabbit anti-γ2 (Alomone Labs, AGA-005) and chicken anti-GFP (Abcam).

Microscopy and Image Analysis

All single frame example images presented in figures were acquired on an FV-1000 laser scanning confocal microscope (Olympus). Images of primary neuronal cultures were acquired using an Ultraview spinning disc confocal system (Perkin Elmer) attached to a Nikon TE-2000 microscope. Mosaics presented in Figures 2, 4 and 5 were acquire on an LSM780-NLO laser scanning confocal (Zeiss) and an Axio Observer Z1 spinning disk microscopes (Zeiss). For analysis of DOX-mediated ZsGreen (ZsG) induction, we used an XLUMPlanFL N, 1.00 NA 20X objective mounted on an FV1200MPE laser scanning system equipped with a variable bandpass filter (Olympus). To optimally separate tdTomato (tdTom) and ZsG signals, we acquired fluorescent bands of 500–540 nm (ZsG) and 565–665 nm (tdTom). Fluorescence intensity in all cases was measured with corrected total cell fluorescence (CTCF = Sum of pixel values in ROI – [mean background pixel value * area of ROI]).

Western Blot Analysis

Following 24h of induction with 1 μ M DOX, HEK293T cells were briefly washed with ice cold PBS and then lifted from wells with cell scraper in Triton Lysis Buffer (TLB) containing 20mM Tris ph7.4, 137mM NaCl, 2mM EDTA, 1% TX-100, 0.1% SDS, 10% glycerol, and supplemented with protease inhibitors and sodium orthovanadate. Cells were lysed on ice for 10 minutes with periodic agitation, and lysates were centrifuged at 16,000 rpm for 10 min. Supernatants were stored at -80°C in sample buffer containing 6% SDS and 16% β -

mercaptoethanol. To assess NShh-myc expression in cell culture medium, medium was collected, supplemented with protease inhibitors, spun down at 16,000 rpm to remove any cells in suspension, and stored at -80°C in sample buffer. Standard SDS-PAGE Western blotting procedures were used. Immunoblotting was performed with anti-myc (Cell Signalling, 9B11, 1:10,000 in 5% non-fat milk), anti-GFP (Clontech, JL-8, 1:10,000 in 5% non-fat milk) and anti-GAPDH (Millipore, MAB374, 1:300,000 in 3%BSA).

Luciferase Assay

C3H10T1/2 cells stably transfected with a construct containing 8 repeats of a minimal Gli promoter driving expression of firefly luciferase (8XGli-luc reporter) were plated at a density of 75,000 cells per well in 24 well plates at time (t) = 0 hours. HEK293T cells were plated at the same time at 100,000 cells per well (t = 0h). Cells were allowed to grow overnight. HEK293T cells were transfected with molar equivalents (1.5x1026 mol/well) of Shh constructs for 4 hours (start at t=16h) with Lipofectamine2000 (Invitrogen) as per manufacturer instructions, and expression was allowed to proceed overnight in 0.5mL of medium to concentrate secreted Shh peptide. Gli-luc C3H 10T1/2 cells were starved overnight in 0.5%FBS/DMEM (starting at t = 20h). At t = 36h, conditioned medium form HEK293T cells was centrifuged at 5000 rmp to remove any Shh plasmid-expressing cells from suspension, and conditioned supernatant was added to starved Gli-luc C3H 10T1/2 cells. After 24 hours (t = 60h), Gli-luc C3H 10T1/2 reporter cells were rinsed with cold PBS, lysed on ice in Luciferase Cell Culture Lysis Reagent (Promega) by scraping with the back of 200µL pipette tips (using a different tip for each well). Luciferase expression was assessed using a beetle luciferin-based assay system (Promega, Cat. No. PR-E1500), and luciferase activity was quantified with an LMax Luminometer (Molecular Devices). Briefly, one well at a time, 100μL of Luciferase Assay Substrate solution was added to 20μL of lysates in a 96 well plate, followed by a 3s pause and a 10s read.

Statistical Analysis

Data are presented as mean ± SEM. Statistical analysis was performed with SigmaPlot software and specific tests used are indicated in the text. For mean comparisons, *p<0.05, **p<0.01, ***p<0.001. Student t-test and One and Two-way ANOVAs with Tukey HSD pariwise comparisons were used unless otherwise noted. For IUE, statistics were performed on datasets comprising cells analyzed from 3 to 6 animals, and 2 -3 coronal sections per animal, with the exception of Figure 6 F and G where the Ctrl and DOX 2d conditions comprised 2 animals each.

4.5 Results

A TetOn System for Robust Induction of Gene Expression in Cultured Hippocampal Neurons.

To assess the potential utility of the TetOn system in for the IUE context, we tested plasmids coding for an enhanced reverse tetracycline transactivator (rtTA2^S-M2, referred to here as rtTA) and a TetOn-inducible ZsGreen1 (ZsG). ZsG is a codon optimized green fluorescent protein cloned from *Zonanthus sp.* reef coral (Matz et al., 1999). In the presence of doxycycline (DOX), rtTA binds to the tet-operator (*tetO*) upstream of pTetO-ZsG, thereby inducing expression of ZsG, ZsG is useful for sensitive detection of expression as it displays a quantum yield much higher than that of EGFP (Kaishima et al., 2016) and forms aggregates that are more clearly visible than diffuse fluorescent proteins at low expression levels.

We first assessed the induction potential of this system by coexpressing pCMV-rtTA and pTetO-ZsG in HEK293T cells and found that both 0.1µg/mL and 1µg/mL DOX mediated an increase in ZsG expression of approximately two orders of magnitude over control levels (Fig. 1A-C). The number of cells displaying leaky expression was low but apparent, however this may have been caused in part by amplification of the pTetO-ZsG plasmid (which contains the SV40 origin of replication) by the large T antigen expressed in

HEK293T cells. We next tested induction of the TetOn system in primary cultures of hippocampal neurons. To restrict expression of rtTA to neurons, mitigate leaky induction and transcriptional squelching by high levels of rtTA (Baron and Bujard, 2000), and finally to avoid the regulation of the CMV promoter by neuronal depolarization (Wheeler and Cooper, 2001), we replaced the CMV promoter with a human Synapsin1 promoter fragment (hSyn) to produce pSyn-rtTA, which has been used extensively for targeting viral transduction specifically to neurons (Kügler et al., 2003; Rincon et al., 2018). We co-transfected this neuron-specific transactivator plasmid with pTetO-ZsG and a plasmid coding for constitutively expressed tdTomato (pCA-tdTom) as a positive transfection marker. Induction with 0.1 and 1 μg/mL DOX resulted in robust ZsG expression (Fig. 1D,E). Control conditions showed very low levels of background green fluorescence. We also replicated this robust DOX-mediated induction of expression in dissociated neurons transfected with pSyn-rtTA and DOX-inducible GABA receptor subunits (Fig. S1).

Episomal TetOn system can induce expression in neurons *in vivo* during early development but not at more mature time points.

We next tested DOX-mediated expression of ZsG in neurons *in vivo*. To do so, we introduced pCAG-rtTA and pTetO-Zsg to layer 2/3 sensorimotor cortical neurons at equal concentrations of 1 μ g/mL via IUE. We included pCA-tdTom (0.5 μ g/mL) in the DNA solution as a positive control for electroporation. DOX-mediated expression from TetOn systems delivered by IUE has been previously demonstrated to function in young mice when DOX is delivered directly to pups (Sato et al., 2015). We therefore tested if a less invasive approach of delivering DOX to the mother would allow for induction through the milk. We administered DOX to the mother in food (3 mg/g body weight) and via daily IP injections (50 μ g/g per day), and found that this caused robust ZsG expression in somatosensory cortex of P8 following 48 hours of administration, demonstrating that DOX-mediated induction can be attained without physical interventions on electroporated pups.

We next investigated the potential for DOX-mediated induction in P21 and P35 mice that had been electroporated with pSyn-rtTA, pTetO-ZsG and pCA-tdTom. However, virtually no expression was observed following 3 days of DOX administration (two IP injections of 50µg/g, daily) (Fig. 1 H and S2). Sparse expression of ZsG was observed in one experiment in C57B/6 mice induced at P21, however ZsG⁺ cells were only found in a rostrocaudal band of approximately 200µm around the epicenter of the electroporated field (Fig. S3). Multiple IUEs with different inducible plasmids (pTetO-ZsG, pTetO-EGFPf-2A-NShh-myc) failed to show any induction when DOX was administered at P35. Thus, while IUE of episomal TetOn plasmids allows for induction at one week of age, this system is not reliable for expression in older animals.

Robust DOX-Mediated Induction of Transposable pTetO-ZsGreen

Previous work suggests that the *tetO*-based promoters are silenced in neurons when they are present, either in the genome or episomally, during development (Zhu et al., 2007). This likely explains the lack of induction we observed in adolescent and adult mice electroporated with the TetOn system. It was also demonstrated that enhanced delivery of DOX across the blood brain barrier did not improve induction (Zhu et al., 2007), suggesting that optimization of DOX administration would not greatly improve induction in electroporated neurons. Interestingly, some transgenic mice that harbor neuron specific *tetOs* that allow for induction (Mansuy et al., 1998; Yamamoto et al., 2003), while others have little or no penetrance (Beard et al., 2006; Eckenstein et al., 2006; Uchida et al., 2006; Zhu et al., 2007). This suggests that the integration site of *tetO*-controlled constructs may play an important role in the extent of inducible expression of the gene of interest. We therefore hypothesized that integrating the TetOn system into numerous locations in the genome of a population of electroporated neurons would overcome the silencing observed in other studies. To test this, we cloned the promoters and coding sequences of pTetO-ZsG and pSyn-rtTA into piggyBac (PB) transposable elements (Ding et al., 2005).

We targeted the transposable TetOn system to layer 2/3 cortical neurons by IUE (Fig. 2A), electroporating 1μg/μL PB-pSyn-rtTA with 1 or 0.1 μg/μL PB-pTetO-ZsG. We induced expression at P35 for 2 days (two IP injections of 50μg/g DOX per day). In both cases, we observed robust induction of ZsG that spanned the entire field of electroporated cells marked by constitutive tdTom expression (Fig. 2B,C). Furthermore ZsG⁺ cells overlapped closely with the field of tdTom⁺ cells (Fig. 2C,E and S5 F,G).

When quantifying ZsG intensity, we accounted for varying efficiency of electroporation from animal to animal by normalizing ZsG intensity to constitutively expressed tdTom. Furthermore, for both concentrations of PB-pTetO-ZsG, we observed a ZsG* and ZsG* population of tdTom* cells. To better assess the magnitude of induction of the system, we focussed on the ZsG* cells, filtering out non-expressing cells using bleed-through of tdTom into the green channel to set a threshold of inclusion equal to the mean plus three times the standard deviation (12.24 a.u.) of green fluorescence from tdTom. This resulted in the exclusion of $0.7 \pm .04\%$ and $0.1 \pm 0.02\%$ of the cells from the 1 and $0.1 \,\mu$ g/uL conditions (Fig. S5 A, B, and D). Quantification of ZsG:tdTom fluorescence ratios demonstrated that DOX induced highly significant expression of ZsG for both concentrations of PB-pTetO-ZsG delivered. There was a significant statistical interaction between the effect of DOX and that of DNA dosage (2-way ANOVA, P<0.001), wherein normalized ZsG expression was significantly higher for 1μ g/µL (High) PB-pTetO-ZsG than for 0.1μ g/µL (Low) ZsG IUE (Fig 2. F,G). Both conditions allowed for roughly two orders of magnitude of increase in ZsG signal.

As expected with TetOn/Off systems, we observed a low level of basal leaky expression in control conditions, which is visible under epifluorescence and when confocal images are highly thresholded (white arrow heads; Fig. 1H, 2D, E). This leak was also demonstrated when we electroporated either a constituitively expressed Cre-recombinase (pCAG-Cre) (Fig. S4 A) or Cre under the control of the *tetO* (pTetO-Cre) (Fig S4 B) in confetti transgenic mice

harboring a Cre-dependent brainbow cassette. Both electroporations caused recombination and expression of fluorescent proteins in the cortex (Fig. S4C), demonstrating at least low levels of Cre produced pTetO-Cre in the absence of rtTA. Due to several technical sources error, such as variations in fixation introduced during intracardial perfusion and changes in laser power, fluorescence microscopy is not an optimal technique for assessing small changes in leaky expression from the TRE. For this reason, bulk tissue luciferase assays are preferable for determining leak from TetOn systems (Furth et al., 1994). Nonetheless, our data suggest that ZsG leak could be mitigated by lowering the concentration of PB-pTetO-ZsG plasmid in the electroporated DNA mixture. We compared uninduced high and low concentration PB-pTetO-ZsG electroporations to animals electroporated with tdTom alone, and found that mean green levels in low PB-pTetO-ZsG IUEs did not differ significantly from those of tdTom alone animals. High PB-pTet-ZsG on the other hand did show significantly higher leaky green fluorescence than low PB-pTet-ZsG and tdTom alone (Fig. 2H). However, for the low concentration, some proportion of tdTom+ cells may not have received any PB-TetO-ZsG, and thus to provide a more conservative estimate of tetO leak, we excluded cells that fell below one of two thresholds based on green fluorescence of tdTom alone; the mean pixel value + 3 standard deviations (12.24 a.u.), or the maximal green pixel value of 29.9 observed in tdTom +ve cells. Applying these thresholds did not change the observation that 0.1μg/μL PB-pmRi-ZsG provided significantly lower leak than 1μg/μL PB-pmRi-ZsG, however in both cases 0.1μg/μL PB-pmRi-ZsG differ significantly from background tdTom green fluorescence (Fig. 2I and S5H). Interestingly, even the less stringent of these thresholds resulted in the exclusion of high proportions of tdTom⁺ cells (90 ± 0.07% for low PB-pTetO-ZsG and $64 \pm 0.14\%$ for high; Fig. S5 A,B,D). This is much higher than the above-mentioned proportions excluded from the induced animals, suggesting that most cells containing PBpTetO-ZsG and PB-pSyn-rtTA in uninduced animals show negligible or no leaky expression. Taken together, these data demonstrate that incorporating the TetOn system into

transposable elements circumvents silencing of the *tetO* during development in the IUE context, and that lowering the concentration of the inducible plasmid mitigates leaky expression in the absence of DOX.

Transposable TetOn system confers DOX-mediated gene expression across the lifespan and in other cortical areas.

We next tested whether the transposable TetOn system would overcome the silencing observed for episomal plasmids at P21. After inducing for 2 days at P21, we observed robust induction of ZsG in layer 2/3 cortical neurons (Fig. 3A). Given that we and others have observed episomal TetOn constructs to be active during development (i.e. postnatal day 6) but silent in more mature neurons, we tested if our approach of using transposable constructs only delays silencing of the system. We therefore allowed animals to mature to an age of 20 months and administered DOX in the food (3mg/g) and once daily IP injections (50μg/μL) for 5 days. Although by this point the co-electroporated episomal tdTom expression conferred by pCA-tdTom had waned, we observed strong expression of ZsG with no apparent leak (Fig. 3B). We also wondered whether we could attain induction in the hippocampus and retrosplenial cortex following IUE of the transposable TetOn system to these areas with tripolar electrodes (dal Maschio et al., 2012; Szczurkowska et al., 2015). Clear DOX-mediated induction was observed after induction at P35, but was only apparent in a subset of electroporated CA1 and subiculum neurons (Fig. 4Ai, ii). It may be possible to improve upon this with alternative DOX administration strategies. In contrast, strong induction of the retrosplenial cortex was detected (Fig. 4B).

Olfactory granule cells can be targeted with the transposable TetOn system

Progenitors of the subventricular zone (SVZ) give rise to cortical neurons during development, as well as neural precursors that migrate through the rostral migratory stream to the olfactory bulbs throughout life. To investigate the possibility that the PB expression

system integrates into the neurogenic niche of the SVZ that produces olfactory neurons, we examined the olfactory bulbs of animals electroporated with 1µg/µL PB-pTetO-ZsG, induced at P21 and 20 months. We found that at both time points ZsG expression was strongly induced (Fig. 5). Only a very small level of leak, similar to that seen in layer 2/3 neurons in control animals, was observed in animals induced at P21 (white arrow heads, Fig. 5B). This leak was not visible in the olfactory bulbs examined from animals induced at 20 months (Fig. 5C). As was the case for induction in layer 2/3 neurons, it is reasonable to expect a lower dose of PB-pTetO-ZsG should mitigate this leak while preserving appreciable induction of the gene of interest. DOX-mediated expression in the olfactory bulb was a post hoc observation, and unfortunately olfactory bulbs from the 5-6 week-old animals were discarded, however given the successful inductions observed at P21 and 20 months, induction would likely be successful throughout the lifespan. Furthermore, we did find what appeared to be migrating precursors expressing ZsG at the centre of the caudal extreme of the olfactory bulb (Fig. S6).

DOX-mediated expression of Sonic Hedgehog in neurons drives astrocytic Kir4.1 expression in cortex.

Our group has previously shown that the morphogen, Sonic hedgehog (Shh), is expressed by mature neurons, and that the Shh signalling pathway is involved in diversifying astrocytic molecular phenotypes (Farmer et al., 2016). However, it has yet to be shown that Shh peptide expressed by neurons is sufficient to change expression profiles of astrocytes *in vivo*. We therefore asked whether the transposable TetOn system could provide inducible expression with low enough leak to cause a Shh gain of function effect by promoting astrocytic expression of Kir4.1, a potassium channel whose expression was shown to be regulated by Shh pathway signalling (Farmer et al., 2016). We first verified that the TetOn system was capable of producing secreted Shh signalling peptide following DOX induction (Fig S7A-F). We then designed a construct (Shh-myc) coding for a full length Shh protein that, after undergoing auto-catalytic cleavage, leaves an epitope tagged autocatalytic domain

as a reporter (Shh-C-myc), and a fully mature wild type signalling peptide (Shh-Np) (Fig 6A) (Beug et al., 2011). We tested the ability of Shh-myc to drive Shh signalling in a luciferase reporter cell line (Gli-Luc C3H 10T1/2 cells) and found that it performed as well as other constructs expressing wild type full length Shh and the N-terminal peptide alone (Fig. S7G,H). We then co-electroporated a transposable, DOX-inducible Shh-myc construct (PBpTetO-Shh-myc) with PB-pSyn-rtTA and constitutively expressed EGFP (Fig. 6B). We induced expression of Shh-myc with one DOX injection per day for 2 days (50 μg/g) or with DOX in the food (3mg/g) for 3 weeks. We found that although 2 days of intraperitoneal DOX administration did induce Shh-myc expression, it did not change Kir4.1 expression levels (Fig. 6F). However, the 3-week induction with dietary DOX induced both Shh-myc expression and an increase in Kir4.1 expression in surrounding astrocytes (Fig. 6C). Interestingly, Kir4.1 expression levels can vary from brain region to brain region, as well as differ among neighboring astrocytes within a given brain region (Tang et al., 2009; Farmer and Murai, 2017). To take this into account in our analysis, we measured Kir4.1 immunofluorescence in the centre of the electroporated field, medial to the electroporated field, and lateral to the electroporated field (Fig 6D), and found that Kir4.1 was significantly upregulated in the central field of induced animals, but not in uninduced animals or those induced for 2 days (Fig. 6D-G). Furthermore, Kir4.1 upregulation did not extend laterally or medially out of the electroporated field. The specificity of the effect was further confirmed by quantifying Kir4.1 expression in the contralateral hemisphere, which showed no change. (Fig. 6E,G). Thus, Shh can be ectopically expressed by cortical neurons to modulate Kir4.1 expression in neighboring astrocytes in a non-cell autonomous manner.

4.6 Discussion

Fine scale dissection of gene function, particularly during development and learning, requires fast and strong experimental induction of gene expression in the mouse brain. Here we examined the ability of IUE of TetOn inducible plasmids to allow for fast DOX-mediated expression of a gene of interest. We found that although episomal TetOn plasmids provided adequate DOX-mediated induction in dissociated neurons and cortical neurons of young pups *in vivo*, these constructs were not capable of providing reliable induction in more mature animals. However, when TetO and rtTA constructs were incorporated into transposable elements and co-electroporated with piggyBac transposase, robust DOX-mediated induction of gene expression was observed across all time points examined and in multiple brain regions.

Currently, the method of choice for conditional gene expression is Cre-mediated recombination. Specific promoters driving Cre expression have been employed to control the timing of recombination. For more precise temporal control, CreER and FLPeR approaches are often used (Matsuda and Cepko, 2007). However, CreER/FLPeR-based strategies normally require longer dosing periods with tamoxifen and provide variable degrees of recombination (Slezak et al., 2007; Farmer et al., 2016). Tamoxifen, an estrogen analog, is known to alter dendritic spine numbers and morphology in both male and female rodents (González-Burgos et al., 2012). This, combined with variable latency to induction, limits the usability of CreER/FLPeR strategies for probing neural development. Here we have demonstrated that IUE of the TetOn system can be used to induce high levels of expression of a gene of interest in a variety of brain regions with short latency, providing a new tool for conditional expression studies.

One concern when using binary conditional expression strategies that rely on TetOn/Off, as opposed to recombination techniques, is leaky expression from the *tetO*. TetOn systems have produced mixed results in terms of leaky expression in the absence of DOX. In early testing using transient transfection, rtTA was observed to drive low level but consistent

basal expression from the *tet*O (Gossen and Bujard, 1992). However, stable cell lines had markedly lower leaky expression from the *tet*O (Gossen et al., 1995). Indeed, TetOn mouse lines have not been observed to have significant problems with leak (Baron and Bujard, 2000). Our results indicate that very low levels of leaky expression from the *tetO* does occur when IUE is used to introduce TetOn inducible transposable plasmids, but only in small subsets of electroporated neurons (Fig 2 and S5). Furthermore, by lowering the dose of PB-pTetO-ZsG delivered during IUE, the extent of leak can be mitigated and an optimal balance between leak and induction level can be readily achieved (Fig. 2L).

Proper titration of transactivator levels also need to be considered. As can occur with Cre (Forni, 2006; Schmidt-Supprian and Rajewsky, 2007), excessive expression of rtTA can cause transcriptional squelching whereby exogenous transcription factors sequester endogenous transcription machinery to such an extent that cellular health is compromised (Baron and Bujard, 2000). IUE results in varying levels of expression throughout the field of electroporated neurons. While the variable efficiency of IUE on a cell by cell basis may be relied on to dilute out effects of squelching when considering a population of neurons, these effects can be controlled for by including a rtTA-lacking condition. However, it may be optimal to use rtTA-transgenic mice with moderate and consistent rtTA levels (eg, Mansuy et al., 1998), electroporating only the inducible plasmid expressing the gene of interest. This would simultaneously open the possibility of using genomic loci to attain cell-type specific expression of rtTA.

It has been suggested that tTA-mediated transactivation is superior to rtTA-mediated transactivation due to its low levels of basal leak (Baron and Bujard, 2000). However, others highlight downsides of the tTA system – namely that tTA requires long-term, and in most cases *in utero* administration of DOX. Furthermore, even in cell culture the TetOff system displays slow kinetics for optimal induction (up to 216h) (A-Mohammadi et al., 1997), and in mice, the build-up of the lipophilic DOX in bone and muscle results in a 15 to 20 day lag in

induction once DOX administration is terminated (Furth et al., 1994; Kistner et al., 1996; Mayford et al., 1996; Mansuy et al., 1998; Mansuy and Bujard, 2000). Given these points and our desire for high temporal precision, we opted to risk the potential leakiness of rtTA in favor of its more optimal induction kinetics. Indeed, herein lies a major benefit of IUE – riskier approaches that would otherwise be avoided when designing a transgenic animal can be employed more confidently when start-up only involves the minimal time and financial costs of basic cloning and as little as a single surgery, as opposed to creating a transgenic mouse model. Nonetheless, we found that IUE of the TetOn system demonstrated very low levels of leaky expression, and that this can be mitigated by lowering the amount of inducible DNA electroporated. Varying the dose of electroporated rtTA may also help to address this.

The use of piggyBAC transposase expression systems is also not without drawbacks. Notably, integrating transposable elements into the genome at TTAA sequences likely disrupts coding and non-coding sequences, and it should be noted the piggyBAC system displays a preference for targeting transcription units (Ding et al., 2005). While disruption of gene function by piggyBAC-mediated transposition cannot be neglected, the relatively random nature of the integration at the common TTAA nucleotide consensus sequence likely results in widely varying mutations in the population of electroporated cells. Thus, assessing phenotypes associated with the electroporated gene of interest across a large population of cells should control for deficits induced in individual cells, or small groups of cells. Confounds associated with piggyBAC-associated mutagenesis can also be avoided with carefully designed negative controls. Furthermore, as opposed to other transposases, piggyBAC does not cause large-scale genomic instability, and also displays a very low likelihood of leaving footprint mutations following excision due to persistent transposase activity (Yusa et al., 2011).

Shh overexpression alters astrocyte molecular phenotype.

Previous work from our group demonstrated that the Shh is expressed in neurons and that the Shh signalling pathway is involved in diversifying the molecular profile of neighboring astrocytes (Farmer et al., 2016). Driving this pathway via a constitutively active Shh receptor in astrocytes caused changes to the expression profile of hundreds of genes in cerebellar and cortical astrocytes. The current results provide the first direct evidence that the Shh peptide itself is capable of changing the expression profile of astrocytes in the adult mouse *in vivo*. Importantly, Shh binds its receptor, Patched, with high affinity (Stone et al., 1996), suggesting that appreciable leak from PB-pTetO-Shh would be detected. However, control animals did not show an elevation in Kir4.1 expression relative to adjacent or contralateral brain areas, suggesting that the transposable TetOn system does not display problematic levels of leaky expression in the absence of DOX.

Future Directions

While we found that a dose of 50ug/g DOX provided good induction of gene expression (Fig. 6F) it should be noted that this is a high systemic dosage of DOX. This likely leads to changes in the microbiome due to the antibiotic actions of DOX, and may also cause other adverse effects as DOX cytotoxicity has been reported in the context of Tet-regulated gene expression (Ermak et al., 2003). These issues may lead to altered behaviour, and indeed changes in the microbiome may alter brain function directly (Foster and Neufeld, 2013). It is therefore essential that rigorous controls are incorporated into the experimental design when applying IUE of TetOn.

Potential off-target effects of DOX can also be mitigated by more advanced dosing strategies. Intravenous injections of DOX may allow for smaller and/or more concentrated doses. Furthermore, DOX has poor kinetics in crossing the blood brain barrier (Beard et al., 2006), with a cerebrospinal fluid availability only 15% of that in serum reported in humans

(Dotevall and Hagberg, 1989). To circumvent this, higher doses could be administered, however as stated above this comes with its own concerns. It has been found that the tetracycline derivative, metacycline, is capable of driving expression of TetOn systems, and is less toxic at high doses (Krueger et al., 2004). Metacycline may therefore be useful in cases where greater and longer induction is necessary. Importantly, metacycline's serum half-life is shorter than DOX, which may be either detrimental or beneficial if a faster run down of induction is required. Alternatively, a more lipid-soluble derivative of DOX called 9-tertbutyl-DOX (9TB-DOX), which has been reported to have a 10-fold higher binding affinity for the wild type Tetracycline Repressor (Zhu et al., 2007). Inducing with 9TB-DOX may allow for improved hippocampal induction as well. While these strategies will likely improve both adult inductions and inductions of pups through the mother's milk, further improvements can also likely be achieved in pups via more sophisticated experimental design. DOX is known to build up in muscle and bone (Mansuy and Bujard, 2000). Taking this into account, foster mothers could be pre-loaded with DOX prior to birth of pups, and pups could be transferred to the foster mother at the time when induction is desired, insuring a maximal dose of DOX in the milk as soon as fostering occurs. Finally, combinations of DOX delivery by injection, in the diet, and in the drinking water with appropriate supplements (Cawthorne et al., 2007), should be systematically tested to find the optimal dosing regimen for a variety of different induction needs.

We have presented a novel combination of tools that allow for fast, robust expression of genes across the lifespan of the mouse in a variety of neuronal subtypes. Our work shows that IUE of transposable TetOn plasmids allows for graded induction levels based the amount of plasmid electroporated, and likely also by varying DOX dosage. Furthermore, previous work performed with the TetOn system in neurons *in vivo* suggests that induced gene expression can be ended when DOX is withdrawn (Mansuy et al., 1998). Combined with the

possibilities for honing this approach detailed above, IUE of transposable TetOn plasmids represents a powerful new tool for conditional gene expression in neurons.

4.7 References

A-Mohammadi S, Alvarez-Vallina L, Ashworth LJ, Hawkins RE (1997) Delay in resumption of the activity of tetracycline-regulatable promoter following removal of tetracycline analogues. Gene Ther 4:993–997.

Agulhon C, Fiacco TA, McCarthy KD (2010) Hippocampal short- and long-term plasticity are not modulated by astrocyte Ca2+ signaling. Science 327:1250–1254.

Baron U, Bujard H (2000) Tet repressor-based system for regulated gene expression in eukaryotic cells: principles and advances. Methods Enzymol 327:401–421.

Baumgart J, Baumgart N (2016) Cortex-, Hippocampus-, Thalamus-, Hypothalamus-, Lateral Septal Nucleus- and Striatum-specific In Utero Electroporation in the C57BL/6 Mouse. J Vis Exp:1–11.

Beard C, Hochedlinger K, Plath K, Wutz A, Jaenisch R (2006) Efficient method to generate single-copy transgenic mice by site-specific integration in embryonic stem cells. Genesis 44:23–28.

Beug ST, Parks RJ, McBride HM, Wallace VA (2011) Processing-dependent trafficking of Sonic hedgehog to the regulated secretory pathway in neurons. Mol Cell Neurosci 46:583–596.

Carlson BR, Lloyd KE, Kruszewski A, Kim I-H, Rodriguiz RM, Heindel C, Faytell M, Dudek SM, Wetsel WC, Soderling SH (2011) WRP/srGAP3 facilitates the initiation of spine development by an inverse F-BAR domain, and its loss impairs long-term memory. J Neurosci 31:2447–2460.

Cawthorne C, Swindell R, Stratford IJ, Dive C, Welman A (2007) Comparison of doxycycline delivery methods for Tet-Inducible gene expression in a subcutaneous xenograft model. J Biomol Tech 18:120–123.

dal Maschio M, Ghezzi D, Bony G, Alabastri A, Deidda G, Brondi M, Sato SS, Zaccaria RP, Di Fabrizio E, Ratto GM, Cancedda L (2012) High-performance and site-directed in utero electroporation by a triple-electrode probe. Nat Commun 3:960.

Ding S, Wu X, Li G, Han M, Zhuang Y, Xu T (2005) Efficient transposition of the piggyBac (PB) transposon in mammalian cells and mice. Cell 122:473–483.

Dotevall L, Hagberg L (1989) Penetration of doxycycline into cerebrospinal fluid in patients treated for suspected Lyme neuroborreliosis. Antimicrob Agents Chemother 33:1078–1080.

Eckenstein FP, McGovern T, Kern D, Deignan J (2006) Neuronal vulnerability in transgenic mice expressing an inducible dominant-negative FGF receptor. Exp Neurol 198:338–349.

Ermak G, Cancasci VJ, Davies KJA (2003) Cytotoxic effect of doxycycline and its implications for tet-on gene expression systems. Anal Biochem 318:152–154.

Farmer WT, Abrahamsson T, Chierzi S, Lui C, Zaelzer C, Jones E V., Bally BP, Chen GG, Théroux J-F, Peng J, Bourque CW, Charron F, Ernst C, Sjöström PJ, Murai KK (2016) Neurons diversify astrocytes in the adult brain through sonic hedgehog signaling. Science (80-) 351:849–854.

Farmer WT, Murai K (2017) Resolving Astrocyte Heterogeneity in the CNS. Front Cell Neurosci 11:1–7.

Figueres-Oñate M, García-Marqués J, López-Mascaraque L (2016) UbC- StarTrack, a clonal method to target the entire progeny of individual progenitors. Sci Rep 6:1–13.

Forni PE (2006) High Levels of Cre Expression in Neuronal Progenitors Cause Defects in Brain Development Leading to Microencephaly and Hydrocephaly. J Neurosci 26:9593–9602.

Foster JA, Neufeld K-AM (2013) Gut brain axis how the microbiome influences anxiety - allpdfblog. Thrends Neurosci 36:305–312.

Fraser MJ, Cary L, Boonvisudhi K, Wang H-GH (1995) Assay for Movement of Lepidopteran Transposon IFP2 in Insect Cells Using a Baculovirus Genome as a Target DNA. Virology:397–407.

Fraser MJ, Ciszczon T, Elick T, Bauser C (1996) Precise excision of TTAA-specific lepidopteran transposons piggyBac (IFP2) and tagalong (TFP3) from the baculovirus genome in cell lines from two species of Lepidoptera. Insect Mol Biol 5:141–151.

Fukuchi-Shimogori T, Grove E a (2001) Neocortex patterning by the secreted signaling molecule FGF8. Science 294:1071–1074.

Furth PA, St OL, Boger H, Gruss P, Gossen M, Kistner A, Bujard H, Hennighausen L (1994) Temporal control of gene expression in transgenic mice by a tetracycline-responsive promoter. Pnas 91:9302–9306.

García-Marqués J, López-Mascaraque L (2012) Clonal Identity Determines Astrocyte Cortical Heterogeneity. Cereb Cortex.

González-Burgos I, Rivera-Cervantes MC, Velázquez-Zamora DA, Feria-Velasco A, Garcia-Segura LM (2012) Selective estrogen receptor modulators regulate dendritic spine plasticity in the hippocampus of male rats. Neural Plast 2012:309494.

Gossen M, Bujard H (1992) Tight control of gene expression in mammalian cells by tetracycline-responsive promoters. Proc Natl Acad Sci U S A 89:5547–5551.

Gossen M, Freundlieb S, Bender G, Müller G, Hillen W, Bujard H (1995) Transcriptional activation by tetracyclines in mammalian cells. Science 268:1766–1769.

Jones E V, Cook D, Murai KK (2012) A Neuron-Astrocyte Co-Culture System to Investigate Astrocyte-Secreted Factors in Mouse Neuronal Development. 814:341–352.

Kaishima M, Ishii J, Matsuno T, Fukuda N, Kondo A (2016) Expression of varied GFPs in Saccharomyces cerevisiae: codon optimization yields stronger than expected expression and fluorescence intensity. Sci Repors2:3675–3680.

Kistner A, Gossen M, Zimmermann F, Jerecic J, Ullmer C, Lubbert H, Bujard H (1996) Doxycycline-mediated quantitative and tissue-specific control of gene expression in transgenic mice. Proc Natl Acad Sci 93:10933–10938.

Krueger C, Pfleiderer K, Hillen W, Berens C (2004) Tetracycline derivatives: Alternative effectors for Tet transregulators. Biotechniques 37:546–550.

Kügler S, Kilic E, Bähr M (2003) Human synapsin 1 gene promoter confers highly neuron-specific long-term transgene expression from an adenoviral vector in the adult rat brain depending on the transduced area. Gene Ther 10:337–347.

Lewandoski M (2002) Conditional control of gene expression in the mouse. Nat Rev Genet 2:743–755.

Luo L, Callaway EM, Svoboda K (2018) Genetic Dissection of Neural Circuits: A Decade of Progress. Neuron 98:256–281.

Mansuy IM, Bujard H (2000) Tetracycline-regulated gene expression in the brain. Curr Opin Neurobiol 10:593–596.

Mansuy IM, Winder DG, Moallem TM, Osman M, Mayford M, Hawkins RD, Kandel ER (1998) Inducible and reversible gene expression with the rtTA system for the study of memory. Neuron 21:257–265.

Matsuda T, Cepko CL (2007) Controlled expression of transgenes introduced by in vivo electroporation. Proc Natl Acad Sci 104:1027–1032.

Matz M V, Fradkov AF, Labas YA, Savitsky AP, Zaraisky AG, Markelov ML, Lukyanov SA (1999) Fluorescent proteins from nonbioluminescent Anthozoa species [see comments] [published erratum appears in Nat Biotechnol 1999 Dec;17(12):1227]. Nat Biotechnol 17:969–973.

Mayford M, Bach ME, Huang YY, Wang L, Hawkins RD, Kandel ER (1996) Control of memory formation through regulated expression of a CaMKII transgene. Science 274:1678–1683.

Rincon MY, De Vin F, Duqué SI, Fripont S, Castaldo SA, Bouhuijzen-Wenger J, Holt MG (2018) Widespread transduction of astrocytes and neurons in the mouse central nervous system after systemic delivery of a self-complementary AAV-PHP.B vector. Gene Ther 25:83–92.

Saito T, Nakatsuji N (2001) Efficient gene transfer into the embryonic mouse brain using in vivo electroporation. Dev Biol 240:237–246.

Sato T, Muroyama Y, Saito T (2015) Inducible gene expression in postmitotic neurons by an in vivo electroporation-based tetracycline system. Electroporation Methods Neurosci 214:187–195.

Schmidt-Supprian M, Rajewsky K (2007) Vagaries of conditional gene targeting. Nat Immunol 8:665–668.

Slezak M, Goritz C, Niemic A, Frisen J, Chambon P, Metzger D, Pfrieger FW (2007) Transgenic Mice for Conditional Gene Manipulation in Astroglial Cells. Glia 55:1565–1576.

Stone DM, Hynes M, Armanini M, Swanson TA, Gu Q, Johnson RL, Scott MP, Pennica D, Goddard A, Phillips H, Noll M, Hooper JE, Sauvage F de, Rosenthal A (1996) The tumor-supressor gene patched encodes a candidate receptor for Sonic hedgegoh=g. Nature 384:129–123.

Szczurkowska J, Cwetsch AW, Maschio M, Ghezzi D, Ratto GM, Cancedda L (2015) Targeted in vivo genetic manipulation of the mouse or rat brain by in utero electroporation with a triple-electrode probe. Nat Protoc 11:399–412.

Tabata H, Nakajima K (2001) Efficient in utero gene transfer system to the developing mouse brain using electroporation: visualization of neuronal migration in the developing cortex. Neuroscience 103:865–872.

Tang X, Taniguchi K, Kofuji P (2009) Heterogeneity of Kir4.1 channel expression in glia revealed by mouse transgenesis. Glia 57:1706–1715.

Toshiki T, Chantal T, Corinne R, Toshio K, Eappen A, Mari K, Natuo K, Jean-Luc T, Bernard M, Gérard C, Paul S, Malcolm F, Jean-Claude P, Pierre C (2000) Germline transformation of the silkworm Bombyx mori L. using a piggyBac transposon-derived vector. Nat Biotechnol 18:81–84.

Uchida S, Sakai S, Furuichi T, Hosoda H, Toyota K, Ishii T, Kitamoto A, Sekine M, Koike K, Masushige S, Murphy G, Silva AJ, Kida S (2006) Tight regulation of transgene expression by tetracycline-dependent activator and repressor in brain. Genes, Brain Behav 5:96–106.

Urlinger S, Baron U, Thellmann M, Hasan MT, Bujard H, Hillen W (2000) Exploring the sequence space for tetracycline-dependent transcriptional activators: novel mutations yield expanded range and sensitivity. Proc Natl Acad Sci U S A 97:7963–7968.

Watanabe T, Saito D, Tanabe K, Suetsugu R, Nakaya Y, Nakagawa S, Takahashi Y (2007) Tet-on inducible system combined with in ovo electroporation dissects multiple roles of genes in somitogenesis of chicken embryos. Dev Biol 305:625–636.

Wheeler DG, Cooper E (2001) Depolarization strongly induces human cytomegalovirus major immediate-early promoter/enhancer activity in neurons. J Biol Chem 276:31978–31985.

Yamamoto M, Wada N, Kitabatake Y, Watanabe D, Anzai M, Yokoyama M, Teranishi Y, Nakanishi S (2003) Reversible Suppression of Glutamatergic Neurotransmission of Cerebellar Granule Cells. J Neurosci 23:6759–6767.

Yusa K, Zhou L, Li MA, Bradley A, Craig NL (2011) A hyperactive piggyBac transposase for mammalian applications. Proc Natl Acad Sci 108:1531–1536.

Zhu P, Aller MI, Baron U, Cambridge S, Bausen M, Herb J, Sawinski J, Cetin A, Osten P, Nelson ML, Kügler S, Seeburg PH, Sprengel R, Hasan MT (2007) Silencing and un-silencing of tetracycline-controlled genes in neurons. PLoS One 2:e533.

4.8 Figures and Tables

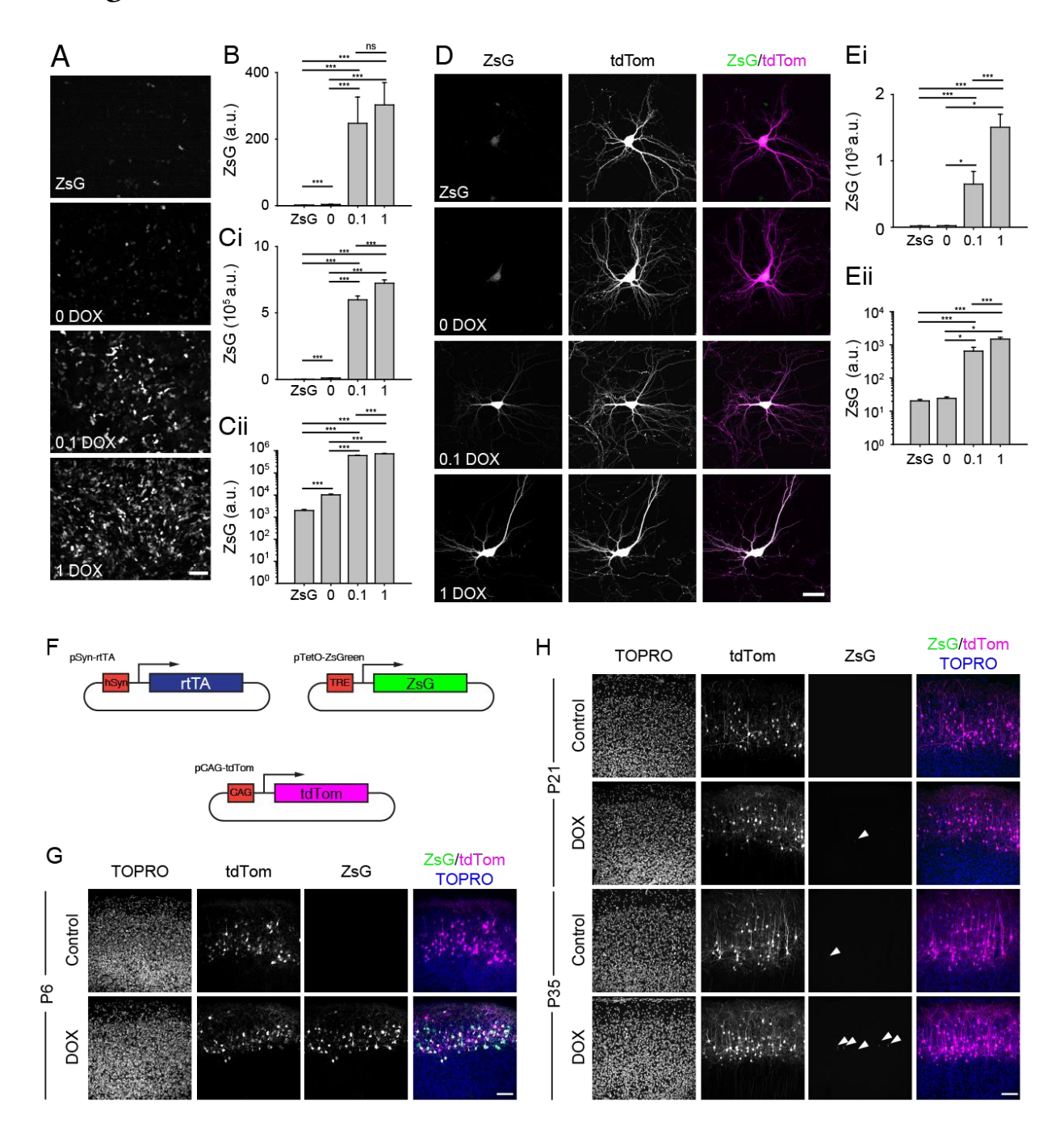


Figure 1

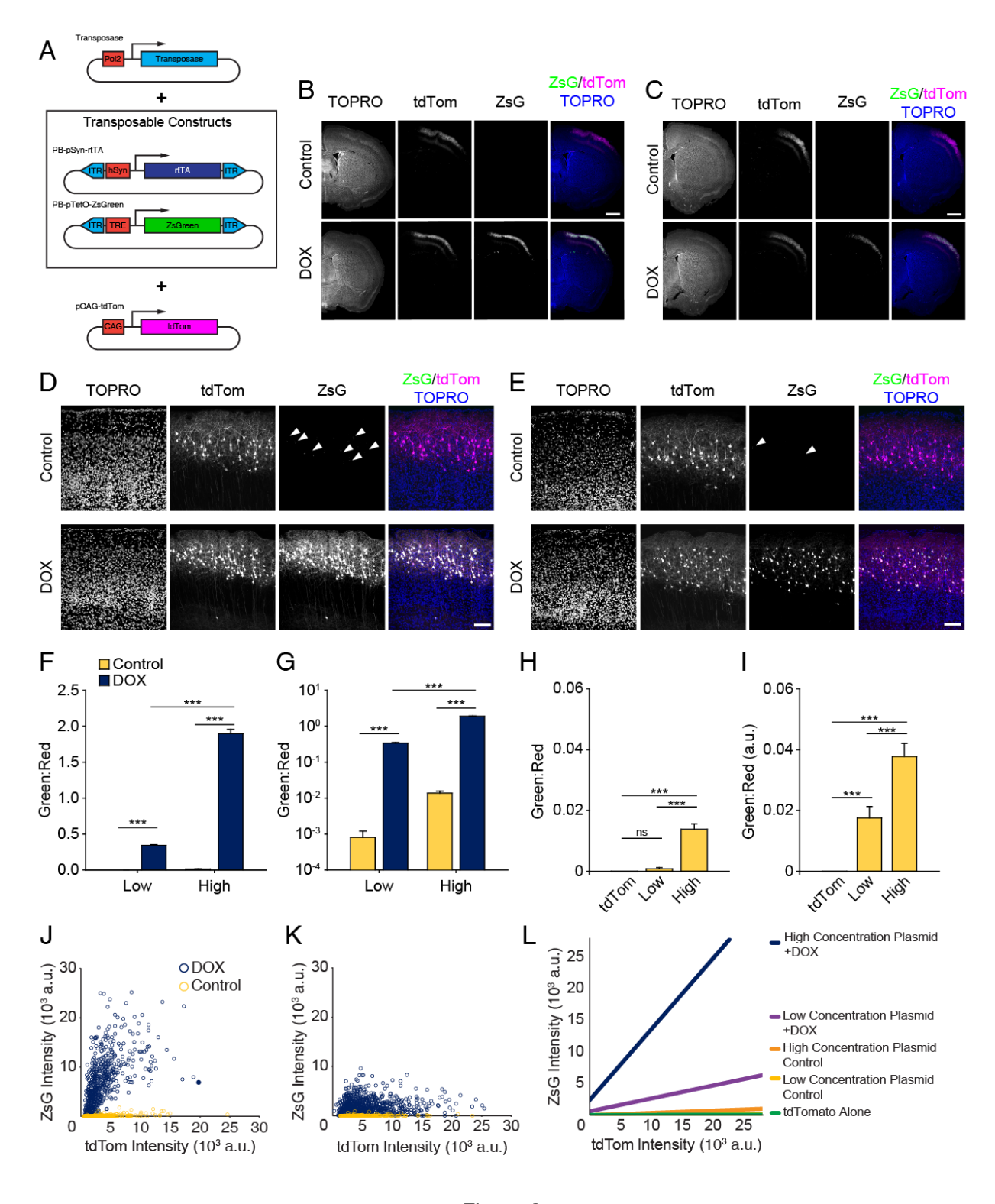


Figure 2

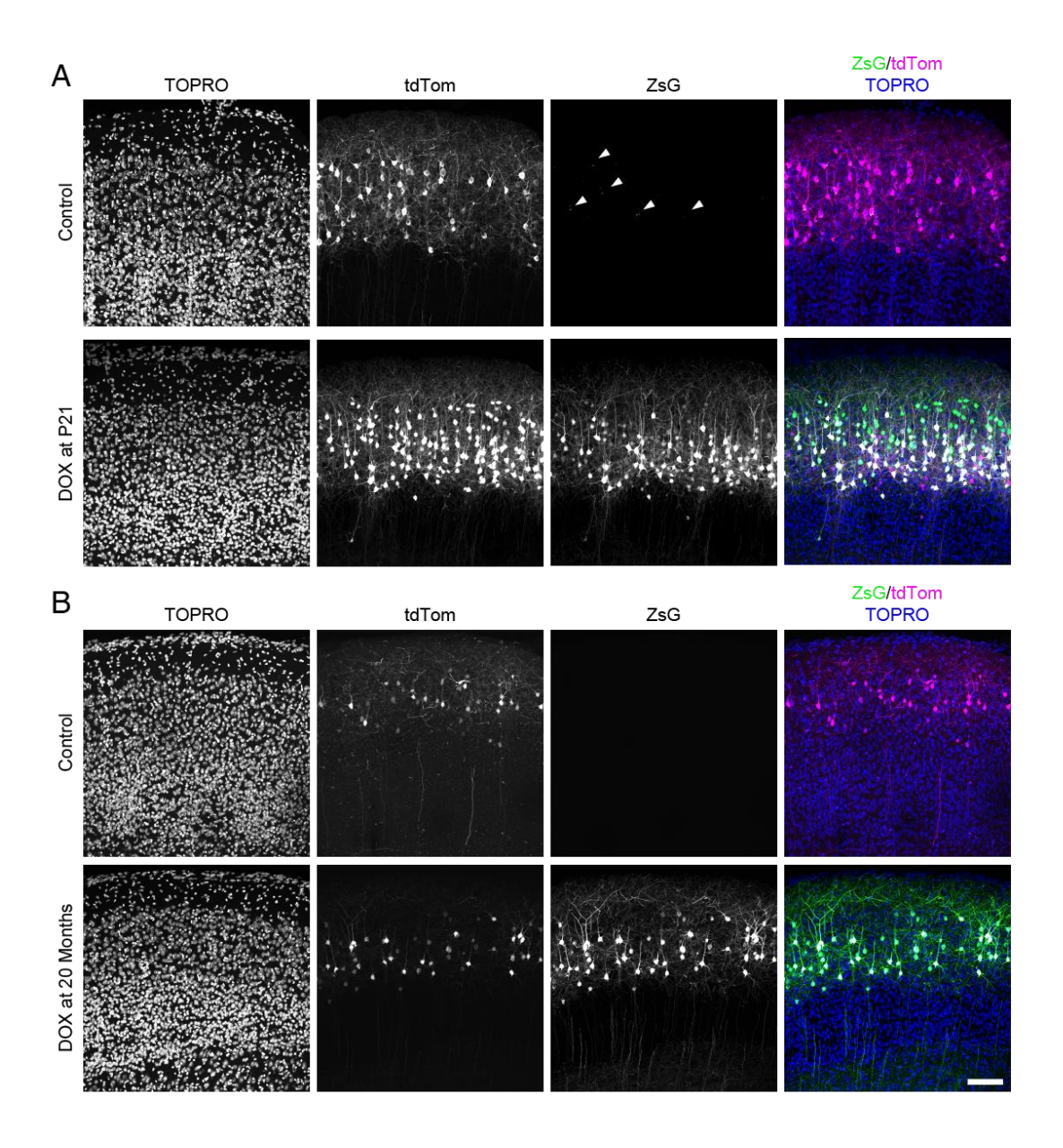


Figure 3

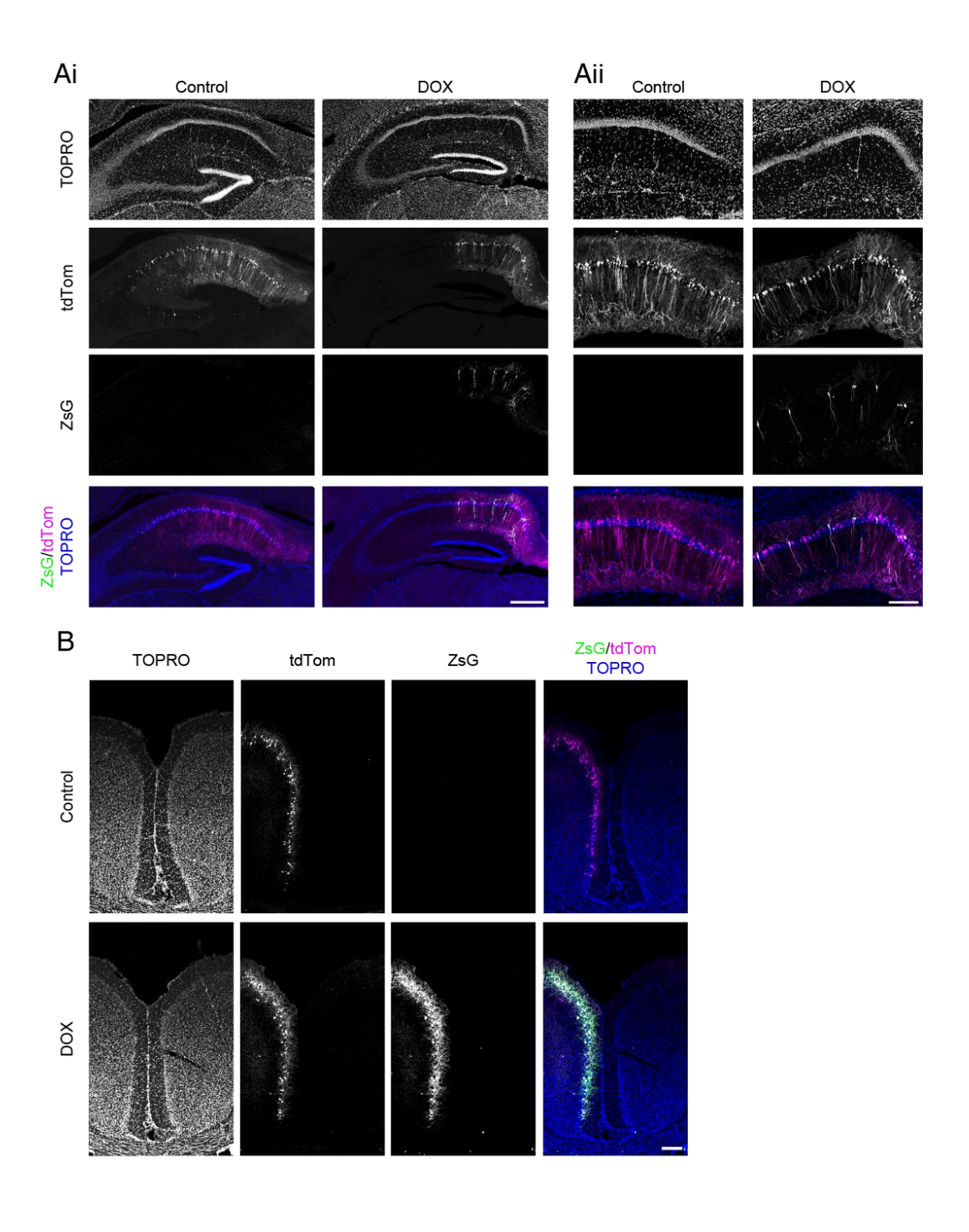


Figure 4

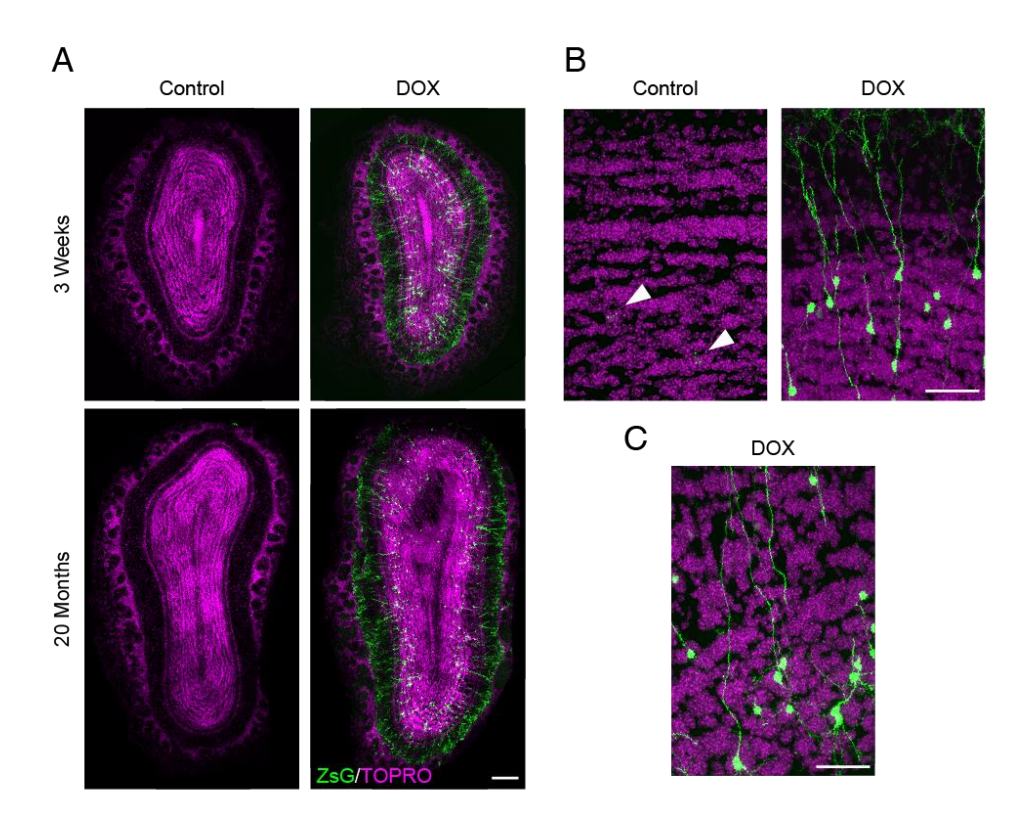


Figure 5

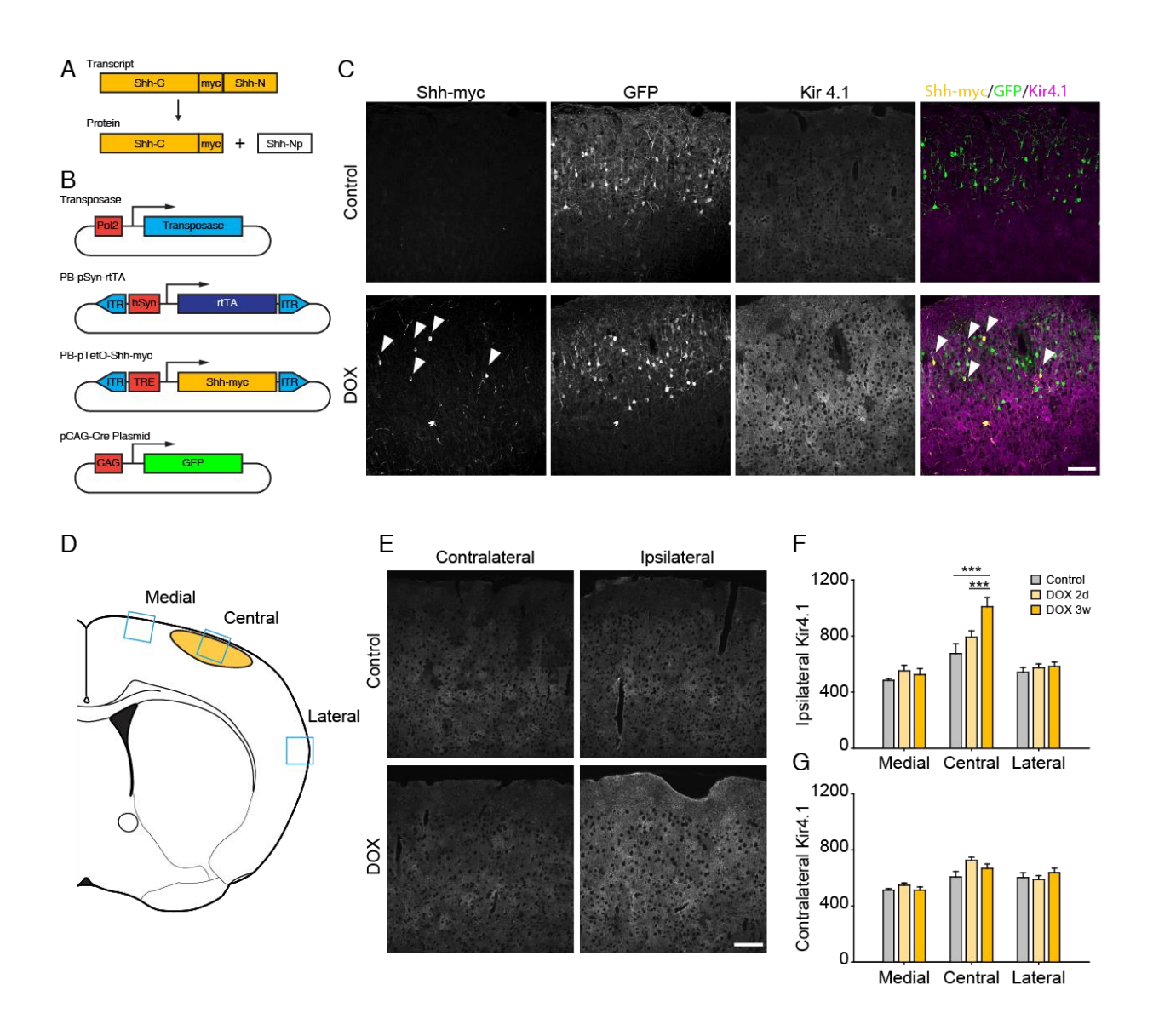
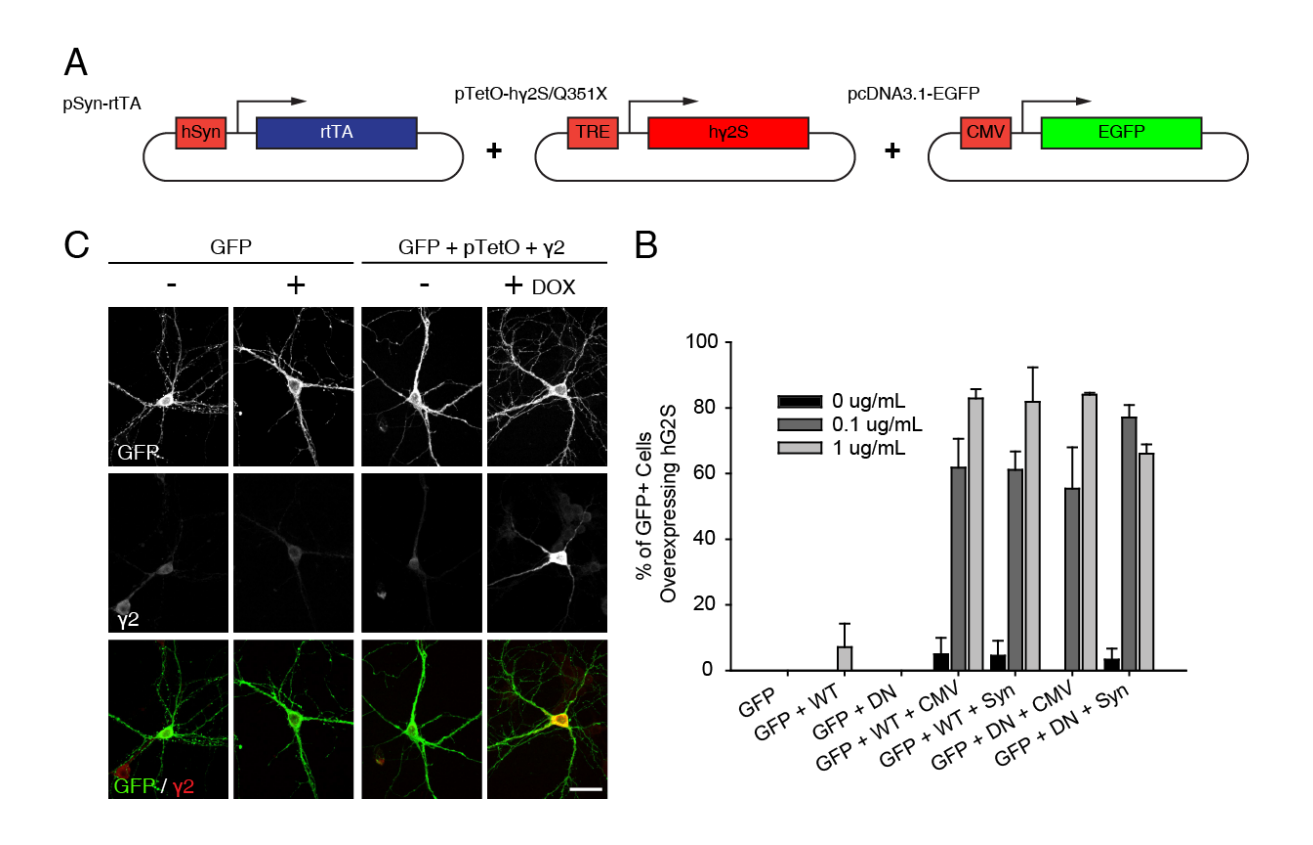
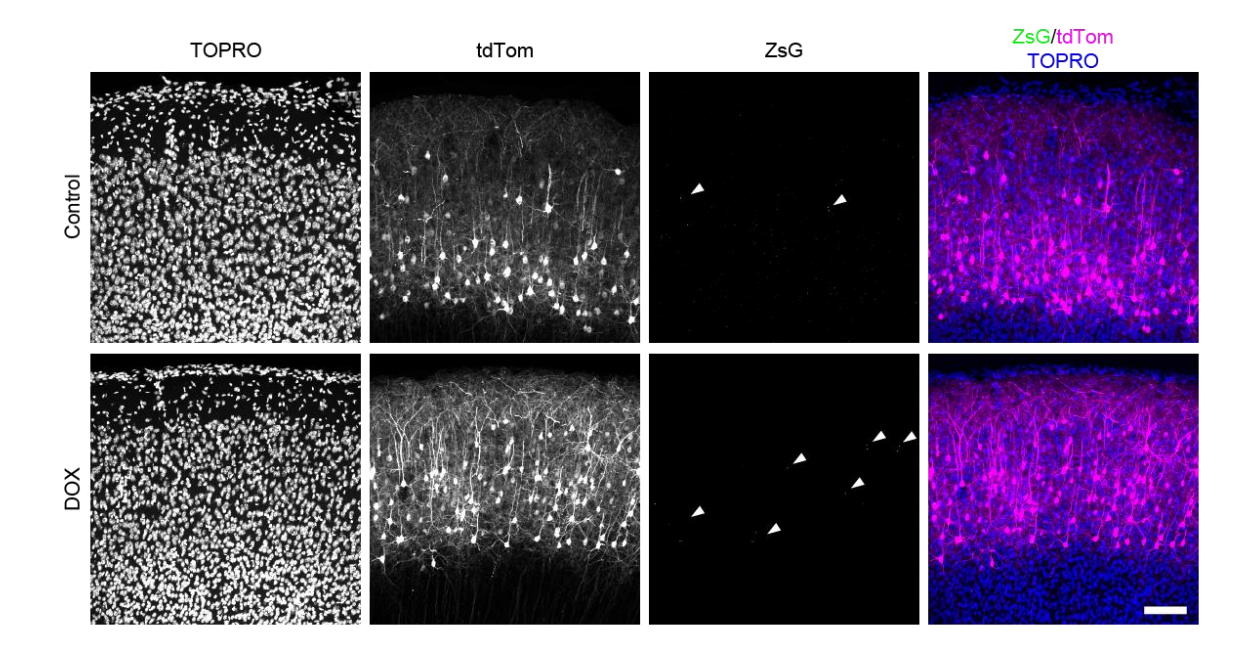


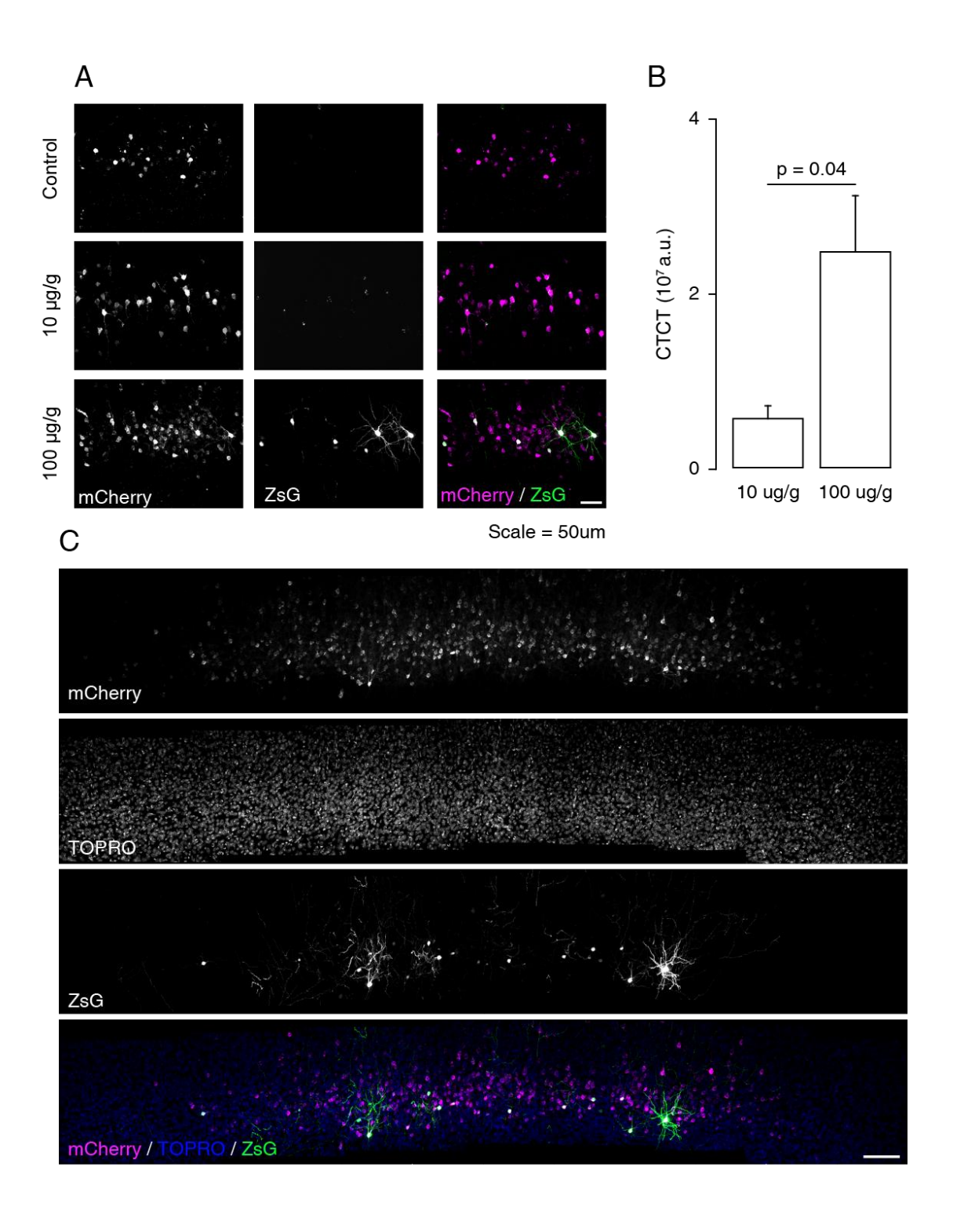
Figure 6



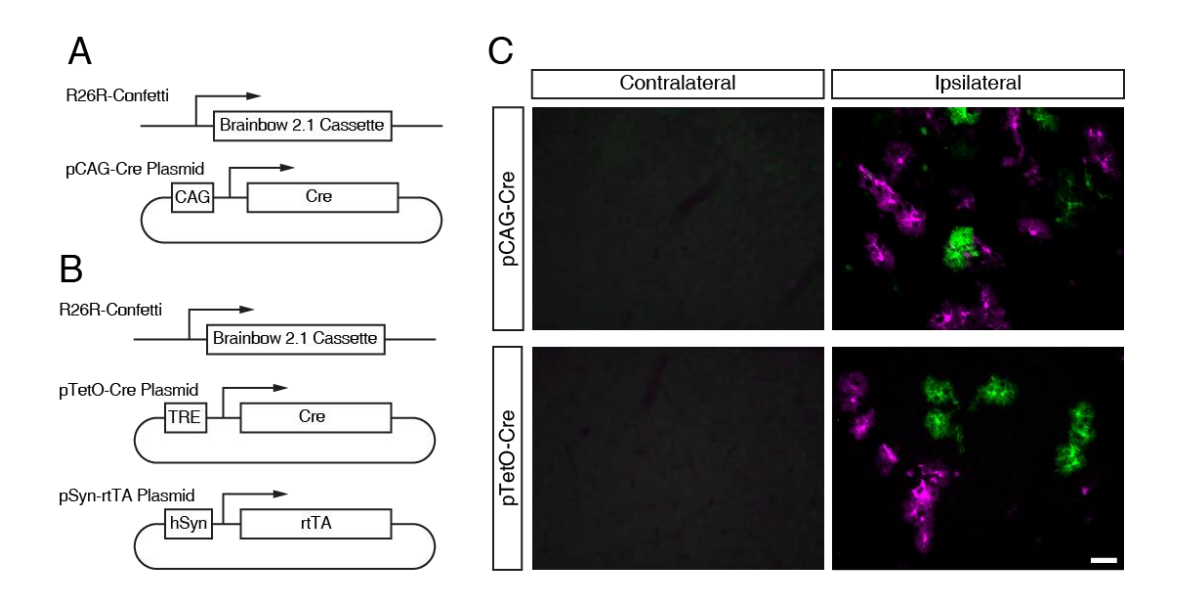
Supp. Figure 1



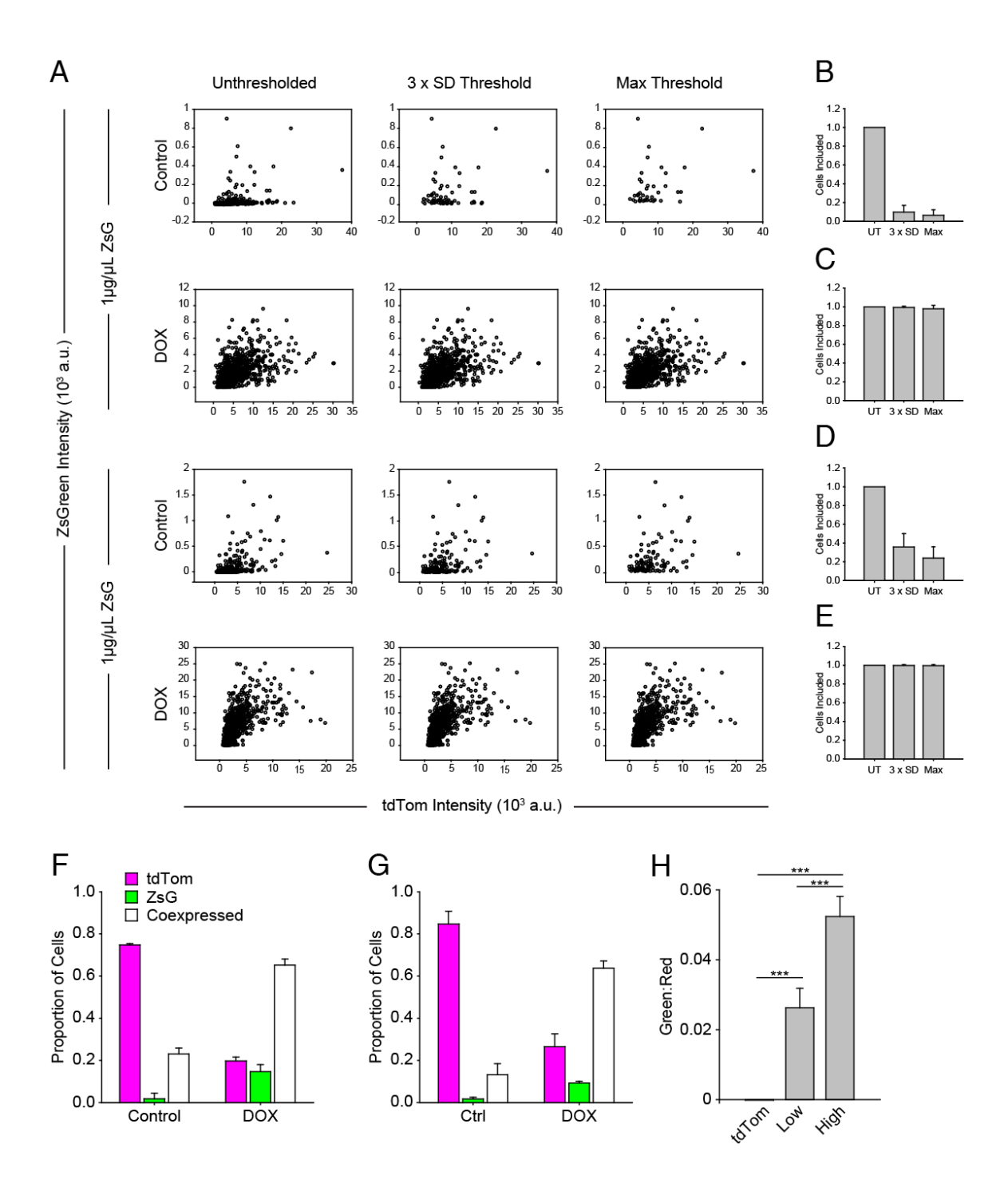
Supp. Figure 2



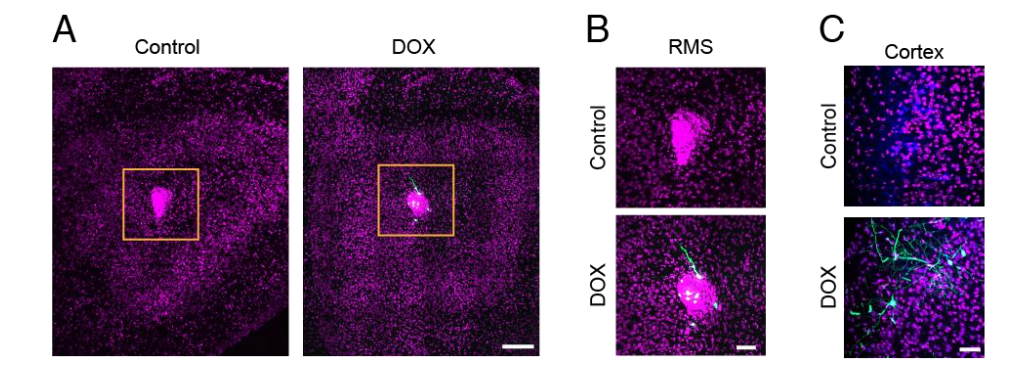
Supp. Figure 3



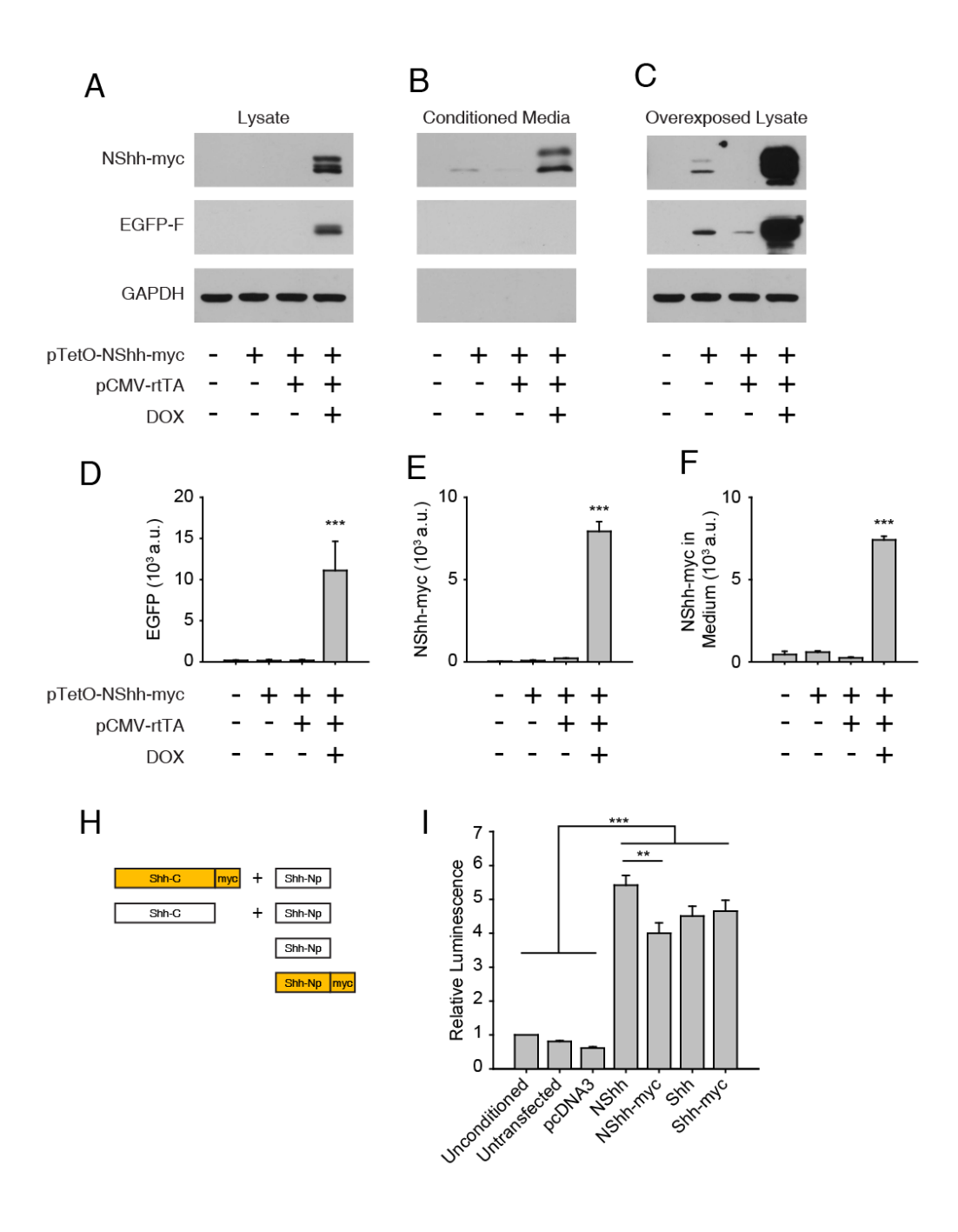
Supp. Figure 4



Supp. Figure 5



Supp. Figure 6



Supp. Figure 7

Table 1. Plasmids

Plasmid Name	Plasmid Origin	Backbone Origin	Insert Origin	Methods
pTetO-ZsGreen	Clontech (pmRi-ZsGreen)	-		
pSyn-rtTA	Novel	pTetOn Advanced	pSKN-Syn (Dr. Ellis Cooper)	Restriction Cloning
pCA-tdTom	Addgene (pCA-tdT3Myc) (Tasic et al. 2012) Addgene		(SI. Ziio Gooper)	
pCAG-Cre-myc	(Mastsuda and Cepko 2007)			
pTetO-Cre-myc	Novel	pmRi-ZsGreen	pCAG-Cre-myc	
PB-pTetO-ZsG	Novel	PB-CMV-MCS-EF1α-RedPuro (System Biosciences, Cat. No. PB514B-1)	pmRi-ZsGreen	Restriction Cloning
PB-pSyn-rtTA	Novel Systems Biosciences (Super PiggyBac	, , , , , , , , , , , , , , , , , , , ,	pSyn-rtTA	Restriction Cloning
pPol2-Transposase	Transposase Expression Vector, Cat. No. PB200A-1)			
pTetO-hY2S	Novel	pmRi-ZsGreen	Dr.s Pribiag and Stellwagen	
pTetO-Q351X	Novel	pmRi-ZsGreen	Dr.s Pribiag and Stellwagen	
pCMV-rtTA	Clontech (pTetOn Avdanced) (Urlinger et al. 2000)			
PB-TetO-Shh-myc	Novel	PB-pTetO-ZsGreen	pCAG-Shh-myc	Restriction Cloning
pCAG-NShh-myc-2A-EGFPF	Novel	pCAG-Cre-myc	Synthesized	Gibson Assembly, Restriction Cloning
pCAG-Shh-myc	Novel	pCAG-Cre-myc	Synthesized	Gibson Assembly, Restriction Cloning
pCAG-Shh	Novel	pCAG-Cre-myc	Synthesized	Gibson Assembly, Restriction Cloning
pCAG-NShh-myc	Novel	pCAG-Cre-myc	Synthesized	Gibson Assembly, Restriction Cloning
pCAG-NShh	Novel	pCAG-Cre-myc	Synthesized	Gibson Assembly, Restriction Cloning
pCAG-EGFP	Novel	pCAG-mCherry (Dr. Gael Quesseveur)	pcDNA3-EGFP-C3 (Clontech)	Restriction Cloning
pTetO-EGFPf-2A-NShh-myc	Novel	pTetOn Advanced		Gibson Assembly, Restriction Cloning

4.9 Figure Legends

Figure 1. Episomal TetOn allows for induction in cultured neurons and postnatal neurons in vivo. A) DOX-induced ZsG in HEK293T cells, showing expression of ZsG when pTetO-ZsG was transfected alone (ZsG) or with pCMV-rtTA (with 0, 0.1 or 1 μg/μL DOX). B) Summary data of full frame ZsG fluorescence of near confluent cells (mean pixel value in a.u.: ZsG Alone 1.36±0.075;0μg/μL DOX 3.46±0.87; 0.1μg/μL DOX 247.38±79.06; 1μg/μL DOX 302.75±67.16). C) Summary data of ZsG fluorescence in individual cells on a linear (Ci) and logarithmic scale (Cii). (CTCF in 10³a.u.: ZsG Alone 2.00±0.19;0μg/μL DOX 10.19±0.78; 0.1μg/μL DOX 598.33±28.73; 1μg/μL DOX 722.81±26.12; ANOVA p=0.002.) D) Dissociated hippocampal neurons cotransfected with pCAG-tdTom and pTetO-ZsG alone (ZsG) or ZsG plus pSyn-rtTA (with 0, 0.1 or 1 μg/μL DOX). E) Summary data of ZsG fluorescence in individual neurons on a linear (Ei) and logarithmic scale (Eii). (In 10³a.u.: ZsG Alone 0.02±0.002 ;0μg/μL DOX .025±0.003; 0.1μg/μL DOX 0.65±0.19; 1μg/μL DOX 1.50±0.20; ANOVA p<0.001) F) Schematic of plasmids for testing DOX-inducible expression of ZsG in the mouse brain following IUE. G) Induction of ZsG following two days of DOX administration via the mother starting at P6. H) Absence of induction of ZsG expression after two days of IP DOX at P21 and P35. White arrow heads denote cells displaying low levels of leaky expression.

Scale 50μm (A,D); 100μm (G,H).

Figure. 2 IUE of transposable TetOn system allows for robust induction in adult neurons with low leak. A) Schematic of plasmids used for testing DOX-inducible expression of ZsG from transposable TetOn system. B,C) Coronal sections demonstrating DOX induction of ZsG in animals electroporated with 1 (B, High) or 0.1 μg/μL (C, Low) PB-pTetO-ZsG, respectively. D,E) Higher magnification images of epicentre of electroporated cortical field from animals electroporated with 1 (D, High) or 0.1 (C, Low) μg/μL PB-pTetO-ZsG, respectively. White arrow heads denote cells displaying low levels of

leaky expression. F,G) Summary plots of single cell measurements of green fluorescence normalized to red fluorescence to take into account variable efficiency of electroporation from cell to cell, on a linear (F) and logarithmic (G) scale. (Low Ctrl 8.06x10⁻⁴±0.03; Low DOX 0.34±0.02; High Ctrl 0.014±0.04; High DOX 1.90±0.03; 2-way ANOVA p<0.001 for Treatment, Condition and Interaction.) H,I) Comparison of green fluorescence from uninduced Control animals electroporated with tdTom alone, 0.1 (Low) or 1 (High) μg/μL PB-pTetO-ZsG. Data presented comprise all cells analysed (H) or cells kept after threshold of mean+3 standard deviations applied (I). (H as 10⁻⁴: tdTom -1.7±1.7; Low Ctrl 8.1±4.0; High Ctrl 140±20; I as 10⁻⁴: tdTom -1.7±1.7; Low Ctrl 180±40; High Ctrl 380±40; both ANOVAs p<0.001) J,K) Scatter plots of ZsG intensity measured in all cells analysed from 1 (J, High) or 0.1 (K, Low) μg/μL PB-pTetO-ZsG electroporations, respectively. L) Lines of best fit for all conditions tested, based on scatter plots in I and K and for tdTom expressed alone. This demonstrates the robust induction and low leak of DOX inducible expression from high and low concentrations of electroporated PB-pTetO-ZsG/PB-pSyn-rtTA. (Line of best fit statistics present as slope, Spearman Correlation Coefficient: tdTom 0.0013, 0.45; Ctrl Low 0.0057, 0.30; Ctrl High 0.037, 0.52; DOX Low 0.20, 0.53; DOX High 1.11, 0.60; p<0.0001 for all Spearman Correlation tests). Scale 1mm (B,C); 100 μm (D,E).

Figure 3. DOX-induced ZsG expression from transposable TetOn system at P21 and 20 months. A) Expression of ZsG at P21 after 2 days of IP DOX administration. White arrow heads denote cells displaying low levels of leaky expression. B) Expression of ZsG at 20 months of age after 5 days of IP DOX administration. Weak tdTom expression was observed here compared to at P21 and P35. IUE of 1 μg/μL PB-pTetO-ZsG Scale 100μm.

Figure 4. DOX-inducible expression in hippocampus and retrosplenial cortex. A) DOX-inducible ZsG from transposable TetOn system targeted to the hippocampus by tripolar IUE configuration at low (i) and higher (ii) magnification. B) DOX induced ZsG

expression in incidental electroporation of the retrosplenial cortex. IUE of 1 μ g/ μ L PB-pTetO-ZsG in both A and B. Scale 0.5mm (Ai); 0.2mm (Aii); 100 μ m (B).

Figure 5. DOX-inducible expression in the olfactory bulbs. A) DOX-induced expression of ZsG from transposable TetOn system in olfactory granule cells following induction at P21 or 20 months of age using the same induction protocols as mentioned in Figure 3. B,C) Higher magnification images showing ZsG in granule cells following induction at P21 (B) and 20 months (C). White arrow heads denote cells displaying low levels of leaky expression. No tdTom was observed and this only the leak was able to indicate the presence of electroporated cells. At 20 months, no leak was visible and thus electroporated cells could not be identified. Scale 200μm (A); 50μm (B)

Figure 6. DOX induced expression of Shh drives astrocytic Kir4.1 expression. A) Schematic of autocleavage of the Shh-myc protein produced by PB-pTetO-Shh-myc. The mature signalling peptide is released, while the myc-tagged C-terminal autocatalytic domain is revealed by myc immunofluorescence. B) Suite of plasmids, including transposable PBpSyn-rtTA and PB-pTetO-Shh-myc, which were electroporated to test whether Shh-myc overexpression in neurons can alter phenotypes of surrounding astrocytes. C) Exemplary demonstrating that DOX-induced Shh-myc expression elevates Kir4.1 immunoflurescence in astrocytes in the electroporated field. D) Schematic of regions of coronal sections imaged to assess upregulation of Kir4.1 expression. Yellow denotes field of electroporated neurons. E) Comparison of Kir4.1 immunofluorescence in the centre of the electroporated fields (ipsilateral) and the same area in the contralateral hemisphere (contralateral). F) Quantification of Kir4.1 immunofluorence in the regions shown in D in the ipsilateral (ie electroporated) hemisphere. (Centre, in a.u.: Ctrl, 675.56±69.0; DOX 2d, 790.77±45.9; DOX 3w, 1009.28±65.0; ANOVA p=0.005) G) Quantification of Kir4.1 immunofluorescence in the regions shown in D in the contralateral (ie non-electroporated) hemisphere. Scale 100μm.

Supplementaty Figure 1. Expression of γ2 GABA_A receptor subunits under control of episomal TetOn system in dissociated hippocampal neurons. A) Schematic of TetOn system for expressing γ2 GABA_AR subunits. B) Summary plots of DOX mediated induction of WT and dominant negative (DN) subunits, driven by rtTA under control of either the hSyn or CMV promoter. C) Example images demonstrating induction. Scale 50μm

Supplementary Figure 2. DOX fails to induce expression of ZsG from low concentration of electroporate episomal TetOn system. White arrow heads denote cells displaying low levels of ZsG expression. Scale 100µm.

Supplementary Figure 3. Example of sparse induction of episomal ZsG at P21.

A) Example images demonstrating sparse expression and graded induction with increasing DOX concentration. B) Summary plot of the corrected total cell fluorescence intensity of ZsG in neurons that visibly expressed ZsG (0.1ug/g DOX 0.58±0.15 a.u.; 0.1ug/g DOX 2.48±0.64 a.u., p=0.044). C) Mosaic of a coronal section showing the most dense induction of ZsG at the rostrocaudal epicentre of the electroporated field. Scale 50μm (A); 100μm (B).

Supplementary Figure 4. Leaky expression of Cre from episomal pTetO-Cre A,B) Schematic of genomic Brainbow allele and electroporated plasmids for constitutively expressed Cre (A) and DOX-inducible Cre (B). C) Example image demonstrating that both sets of electrorporated plasmids expressed sufficient levels of Cre to cause recombination. Note that this mouse line is known to have much higher expression in astrocytes. Scale 50μm.

Supplementary Figure 5. Proportions of thresholded neurons and neurons coexpressing tdTom and ZsG. A) Scatter plots of unthresholded data and with the two thresholds applied. B-E) Summary plots of the proportions of cells kept after thresholds were applied averaged across sections. UT=unthresholed, 3xSD = 3 x standard deviation, max = 29.9 a.u. (Ctrl Low: UT 1, 3xSD 0.097±0.023, Max 0.063±0.02; DOX Low: UT 1, 3xSD

0.99±0.004; Max 0.98±0.01; Ctrl High: UT 1, 0.36±0.04, Max 0.24±0.03; DOX High UT 1; 3xSD 0.998±0.002; Max 0.995±0.003) **F,G)** Proportions of cells expression tdTom, ZsG or both in induced and uninduced animals that had been electroporated with 0.1 (F) or 1 μg/g (G) PB-pTetO-ZsG. (F, Ctrl 0.85±0.06 tdTom⁺, 0.02±0.008 ZsG⁺, 0.13±0.05 Coexpressed; F, DOX 0.27±0.006 tdTom⁺, 0.09±0.008 ZsG⁺, 0.64±0.03 Coexpressed; G, Ctrl 0.75±0.006 tdTom⁺, 0.019±0.03 ZsG⁺, 0.23±0.02 Coexpressed; G, DOX 0.20±0.02 tdTom⁺, 0.14±0.03 ZsG⁺, 0.65±0.03 Coexpressed.) **H)** Comparison of green fluorescence from animals electroporated with tdTom alone, 0.1 (Low) or 1 (High) μg/μL PB-pTetO-ZsG. Data presented comprise cells kept after application of Max threshold of 29.9 a.u. (tdTom Alone -1.7x10⁻⁴±1.7x10⁻⁴; Ctrl Low 0.026±0.006; Ctrl High 0.052±0.006, ANOVA p<0.001).

Supplementary Figure 6. Induction of ZsG at P35 at caudal pole of olfactory bulb. A) Images of the caudal poles of the olfactory bulbs showing DOX-mediated ZsG expression in migrating precursors. B) Zooms of boxed regions in A. C) Images of prefrontral cortex above the olfactory bulbs pictured in A. Scale 150μm (A); 50μm (B,C)

Supplementary Figure 7. DOX inducible expression of functional Shh peptides. A) Western blot (WB) of DOX induced NShh-myc expressed in HEK293T cells. UT=untransfected. B) WB of Shh in the medium. GAPDH from cell lysates of the same wells that the medium was collected from was used as a loading control. Total protein from supernatant was used to adjust loading volumes. UT=untransfected. C) Blot in (A) overexposed to show low level leak in uninduced conditions. UT=untransfected. D,E,F) Summary plots corresponding to A, B and C respectively. (D in a.u.: UT 27.8±18.9, -rtTA 72.4±40.8, -DOX 207.1±17.8, +DOX 7924.5±600.5, ANOVA p<0.001; E in a.u.: UT 159.5.8±66.9, -rtTA 141.7±133.5, -DOX 159.4±105.7, +DOX 11093.3±3556.2, ANOVA p=0.002; F in a.u.: UT 444.7±199.6, -rtTA 590.6±72.9, -DOX 236.9±59.0, +DOX 7405.4±220.7, ANOVA p=0.001) H) Schematic of protein products of panel of Shh expressing plasmids, pCAG-Shh-my, pCAG-Shh (WT), pCAG-NShh (signalling peptide only) and

pCAG-NShh-myc. **I)** Summary plot of Shh signalling driven by expression of Shh peptides in (H) based on luminescence produced by C3H 10T1/2 cells stimulated with medium conditioned by HEK293T cells expressing Shh peptides (Unconditioned 1; Untransfected 0.81±0.02; pcDNA3.1, 0.61±0.36; NShh 5.42±0.29; NShh-myc 4.00±0.31; Shh 4.51±0.28; ±18.9; Shh-myc 4.65±0.32; ANOVA p<0.001).

Chapter 5 Discussion and Future Directions

5.1 Discussion and Future Directions

Synapse formation and regulation of synapse function by astrocytes at the tripartite synapse are two classical areas of neurobiological study that continue to be exciting and challenging (Bazargani and Attwell, 2016; Sudhof, 2018). In this dissertation I have presented two main studies, one detailing new insights into the mechanisms that establish the proper number of synapses during development, and another looking into the structural arrangement of the tripartite synapse in the adult. Both studies present fertile ground for further work that will shed more light on the complexities of building the nervous system and keeping it running. Moving forward, both avenues of research will continue to be enriched through technical advances, and I would submit that IUE of transposable TetOn plasmids will aid in furthering our understanding of both areas of neurobiological research presented in this dissertation.

5.2 Further Inquiry into Activity-Dependent Processes Driven by Inhibiting Depolarizing but Shunting GABA_A Transmission

In Chapter 1, I demonstrated that the transcription of two classical activity-regulated genes, BDNF and cFos, are upregulated following blockade of depolarizing but shunting GABA_A transmission (Chapter 2). However, the experiments identifying that the expression of these genes was upregulated yielded no direct insight as to the molecular mechanisms downstream of activity-dependent transcription that resulted in enhanced glutamatergic synapse number and strength following GABA_A-blockade. It will therefore be interesting to investigate other activity regulated genes and processes that control synapse formation at this period of development to determine how new synapses are built when depolarizing but inhibitory GABA_A transmission is blocked. Although a variety of candidates could be chosen for further study (Flavell et al., 2008; Kim et al., 2010; Malik et al., 2014; Mardinly et al., 2016), a broader screen may be more efficient to identify key molecular players and pathways

involved. My observations suggest the existence of a sensitive period in which GABAergic activity is essential for restraining synapse formation during circuit development. Thus, it may be worthwhile to investigate how the transcriptome changes when synapse formation is accelerated by inhibiting depolarizing but inhibitory GABA transmission. This may uncover a unique transcriptional program that is impinged upon by depolarization and/or GABAAR opening and may also unveil novel factors involved in activity-dependent synapse development. One particular candidate gene that may warrant further study is diazepam binding inhibitor (DBI). DBI is an endogenous GABAAR agonist (Alfonso et al., 2012; Christian et al., 2013) whose expression peaks during the first weeks of development (Lein et al., 2007). Interestingly, DBI is expressed by astrocytes during this period, thus presenting the intriguing possibility that astrocytes can control synapse formation through modulating immature GABA_A transmission. Another family of molecules that may be of interesting are the myocyte enhancer factor 2 (MEF2) transcription factors. MEF2C is activated by calcium and activity-dependent calcineurin activity, and has been demonstrated to negatively regulate glutamatergic synapse formation by driving expression of synGAP, Arc and Homer1a (Flavell et al., 2006; Greer and Greenberg, 2008). Thus, depolarizing but inhibitory GABA_A transmission, which has been shown to mediate calcium influx while also providing shunting inhibition (Kirmse et al., 2015b), seems well-equipped to promote MEF2 signalling. Although MEF2 signalling has been suggested to play a role in pruning once excitatory synapses have formed, it may play a similar role to restrain synapse formation in the hippocampus during the peak of synapse formation (Greer and Greenberg, 2008).

5.3 Depolarizing GABA_A Transmission in Neurodevelopmental Disorders

Polymorphisms disrupting GABA_AR function during development are associated with ASD. In particular, mutation of the $\beta 3$ GABA_A receptor subunit, the expression of which peaks during development when GABA is depolarizing, has been observed in ASD (Menold

et al., 2001; Buxbaum et al., 2002; Chen et al., 2014). This suggests that disrupting GABA_A transmission during development may play a role in the etiology of ASD. Furthermore, ASD is generally thought to be associated with increased levels of connectivity and increased numbers of dendritic spines in humans (Lacey and Terplan, 1987; Irwin et al., 2000, 2001; Kaufmann and Moser, 2000; Fiala et al., 2002; Hutsler and Zhang, 2010). Thus, observations in humans that malfunction of depolarizing GABA transmission may be involved in the pathogenesis of ASD, do not correspond well with work suggesting that experimental disruption of immature depolarizing GABA_A transmission decreases glutamatergic synapse formation and spines numbers (Ge et al., 2006; Wang and Kriegstein, 2008; Chen and Kriegstein, 2015a). However, my work, showing depolarizing GABA_A transmission can limit synapse formation, supported by the observation that enhancing depolarizing GABAA transmission in development can decrease spine numbers (Puskarjov et al., 2017), suggests that a decrease in immature, depolarizing but inhibitory GABA_A transmission during human development could result in increased synapse formation similar to that seen in ASD. Thus, work presented in this thesis may provide insight into how disrupted GABAA transmission may contribute to development of neuronal and synaptic phenotypes associated with ASD. Moreover, the work opens the possibility of using pharmaceuticals that act on GABA_ARs to prophylactically treat deficits in circuit development associated with neurodevelopmental disability.

Evidence from *Xenopus* also suggests that interfering with depolarizing GABA_A transmission during development disrupts excitatory/inhibitory (E/I) balance by causing changes in synaptic physiology, consistent with decreased excitatory synapse number and increased inhibitory synapses (Akerman and Cline, 2006), or by simply augmenting the strength of GABAergic synapses (Shen et al., 2009). We observed the opposite effect of GABA-blockade on excitatory synapses, however we did not investigate the repercussions of this on the GABAergic system itself. It will be important to further investigate whether

disrupting depolarizing but inhibitory GABA_A transmission during the period of interest that we identified causes changes in GABAergic synapse formation or maturation concomitant to those in glutamatergic synapses observed in my studies. To investigate this in the organotypic hippocampal slice, we have engineered and tested a construct for Semliki Forest Virusmediated simultaneous expression of membrane targeted red fluorescent protein and EGFP-tagged Gephyrin to label inhibitory synapses (EGFP-Gephyrin-IRES-RFPf). Gephyrin is a critical scaffolding molecule at inhibitory synapses that has been used extensively as a GABAergic synapse marker (Chen et al., 2012). In concordance with other work using similar constructs, following introduction of this virus to organotypic hippocampal slices, EGFP-Gephyrin is present as punctate green labelling in CA1 pyramidal cell dendrites consistent with the distribution of inhibitory synapses (Villa et al., 2016; Boivin and Nedivi, 2018). As neurodevelopmental disorders like ASD and schizophrenia are believed to be associated with changes in E/I balance (Rubenstein and Merzenich, 2003; Gao and Penzes, 2015), investigating whether depolarizing but inhibitory GABA_A transmission plays a role in establishing this balance may enhance our understanding of these disorders.

5.4 New Tools for Blocking GABA_A Transmission

We initially conceived of introducing TetOn inducible plasmids to the CNS with IUE to attempt to disrupt depolarizing GABA_A transmission *in vivo* with high temporal precision. We proposed to accomplish this by expressing one of a number of peptides that would interfere with GABA_A transmission. We reasoned that targeting the γ2 subunit of the GABA_AR that is responsible for synaptic clustering of GABA_ARs would allow us to disrupt GABAergic synaptic function (Schweizer et al., 2003). We are currently testing the ability of: (1) a dominant negative γ2 GABA_AR associated with human epilepsy (Kang et al., 2009); (2) a small peptide that blocks GABA_AR clustering at synapses (Shen et al., 2009); and (3) a series miRNAs against the γ2 GABA_AR, for their ability to disrupt GABA_A synaptic transmission. Indeed, knocking down γ2 expression has been shown to disrupt GABA_A transmission (Li et

al., 2005). However, one complication is that GABA_AR subunits display a high degree of redundancy (Martenson and Tomita, 2015). A reasonable alternative may be to use an approach from a recent study that engineered an E3-ubiquitin ligase to selectively target Gephyrin for reversible degradation, thereby ablating GABAergic synapses (Gross et al., 2016). Using one or multiple of these tools in conjunction with the IUE and TetOn methodology presented in Chapter 4 may prove to be effective in assessing the role of depolarizing GABA_A transmission in synapse and circuit development *in vivo*. The fast induction provided by IUE of TetOn plasmids will allow for a high degree of temporal precision for disrupting GABA_ARs, and thus will enable a dissection of GABA_A function at multiple developmental stages.

5.5 Next Steps in Examining Astrocytic Ultrastructure

A number of large, open source SSEM datasets have been made available, providing a potentially rich resource for extending our investigation of the ultrastructure of astrocytes and the tripartite synapse (Harris et al., 2015; Kasthuri et al., 2015; Zheng et al., 2018). However, very few studies in general have investigated ultrastructure at high spatial resolution like what can be accomplished with FIB-SEM (i.e. ~4x4x8nm voxels in our study) (Korogod et al., 2015). Two studies of large serial section TEM datasets have performed extensive segmentation of astrocytes. However, a thorough analysis of astrocytic volumes generally has not been performed beyond reporting the proportion of the volume occupied by astrocytic compartments (Mishchenko et al., 2010; Kasthuri et al., 2015). Thus, the extent of continuity of the segmented astrocytic volumes in these large TEM datasets is unclear. An important aspect of experimental design that needs to be better understood is what is the optimal sampling frequency for obtaining sufficient sample size (i.e. largest possible volumes) without losing the ability to follow continuous astrocytic volumes. Due to the very thin diameter of protoplasmic astrocytic filaments, the optimal z-resolution may be lower than that used in traditional serial TEM (30-100μm). This can be answered by subsampling our datasets to

determine at what z-resolution the continuous astrocytic volumes we produced start to fragment. This will be an valuable piece of information as we expand our analyses to other freely available large open-source SSEM datasets (Harris et al., 2015; Kasthuri et al., 2015; Zheng et al., 2018). Overcoming these challenges, along with other technical hurdles such as the current need to manually segment astrocytes in serial sections, will allow more detailed quantitative assessment of astrocytic morphology and the tripartite synapse.

5.6 The Possibility of Astrocytic Loops

Given the nanoscale complexity of astrocytes, it is unclear whether astrocytic branching networks are dendritic, with every branch eventually leading to a branch tip, or if they are capable of forming loops, in which branches reconnect back to the network of branches. However, astrocytic loops have been reported (Rusakov, 2015). Our preliminary observations suggest that loops do exist in astrocytic branches, however when obvious, they are generally made by very thin processes and thus it is difficult to tell if there is a break in the membrane at some point using the resolution of our data sets. Larger loops are also possible, but much harder to identify by eye. Thus, a mathematically driven approach should to be taken to verify the distribution of these loops. Although this is simply a descriptive question, it raises interesting biological questions. If loops form in astrocytic branches, it may be through an active process by which branches touch and fuse, or by which perforations are created in lamellar structures to allow other, extracellular structures, such as spines, dendrites, or portions of cell bodies, to pass through. What are the factors allowing for this to occur? How is it regulated? Furthermore, aside from being connected into an astrocytic reticulum by gap junctions (Giaume et al. 2010), a number of reports suggest that branches of single astrocytes are reciprocally (or "reflexively") coupled by gap junctions (Nagy et al. 1997; Wolff et al. 1998). Why might there be some full cytoplasmic fusions and some fusions through gap junctions? A systematic quantitative approach to understanding loop architecture will help to

verify the prevalence and distribution of these structures and understand their potential roles in controlling the ability of astrocytes to respond to and regulate surrounding neural circuitry.

5.7 Investigating Neuron-Astrocyte Shh Signalling with IUE of TetOn

In Chapter 4, I demonstrated the utility of IUE of transposable TetOn plasmids for driving fast, inducible expression of genes of interest in the adult mouse brain. Indeed, fast induction of conditional gene expression is perhaps one of the main benefits of IUE of TetOn plasmids. Many virally-mediated gene-expression strategies require weeks after virus injection before performing experiments that rely on the gene of interest (Kügler et al., 2003; Aschauer et al., 2013; Rincon et al., 2018). Even studies during development require up to seven days for robust virally mediated expression (Chen and Kriegstein, 2015b). With IUE of TetOn plasmids, we obtained robust expression within 2 days. Furthermore, based on other studies, the lag to appreciable expression is likely less than a day (Kistner et al., 1996; Sato et al., 2015). These fast induction kinetics allowed us to demonstrate in the adult mouse that short-term expression (2.5 days) of Shh by cortical neurons was not sufficient to alter astrocyte Kir4.1 expression, but long-term expression over a 3 week period was. An additional question we wished to address by overexpressing Shh in cortical neurons was that of the location of Shh release. From our results, it is clear that Shh can be released in the vicinity of the cell bodies and dendritic trees of neurons that overexpress it. However, we also wondered if Shh can be released from axon terminals as a way for neurons making longer range inputs to regulate the microenvironment in which they make connections. IUE targets neurons unilaterally, and layer 2/3 neurons that are targeted by electroporation at embryonic day 15 or 16 make callosal projections to the contralateral hemisphere (Wang et al., 2007). Furthermore, the projections from electroporated neurons to their contralateral counterparts can often be discerned by expression of fluorescent proteins. We thus wondered if Shh overexpression would result in changes in astrocytic Kir 4.1 expression in the contralateral field innervated by the electroporated neurons, however this appeared not to be the case (Chapter 4, Fig. 6). I am

currently testing this hypothesis in the hippocampus as well, where CA1 neurons, which can be targeted with IUE (Chapter 4, Fig. 4), send extensive projections to the contralateral hippocampus via the anterior commissure.

5.8 Conclusion and Contribution to Knowledge

The three studies composing this thesis represent important steps forward that open new avenues of research in exciting areas of neurobiology. I have demonstrated, in contrast to predominating theories in the field, that depolarizing GABA_A transmission can restrain glutamatergic synapse formation during development. I have also presented data that suggest there is no immediately apparent overarching rule relating astrocytic mitochondrial distribution to basic parameters of the surrounding synapses. However, the results indicate that mitochondria are not distributed randomly relative to clusters of synapses. This observation is an invitation to examine astrocytic ultrastructure in larger, richer data sets. Finally, I have presented a novel combination of techniques that allow for fast, inducible gene expression in the mouse brain across the lifespan. This technology allowed me to show for the first time that neuronal expression of the Shh signalling peptide is capable of driving Kir4.1 expression in surrounding neurons. Furthermore, IUE of transposable TetOn plasmids not only provides an opportunity to rigorously examine the precise roles of GABA_A transmission in synapse and circuit formation *in vivo*, but also expands the toolkit that will continue to enhance our understanding of the development and function of the central nervous system.

Bibliography

- Adamsky A, Kol A, Kreisel T, Doron A, Ozeri-Engelhard N, Melcer T, Refaeli R, Horn H, Regev L, Groysman M, London M, Goshen I (2018) Astrocytic Activation Generates De Novo Neuronal Potentiation and Memory Enhancement. Cell 174:59–71.e14.
- Agarwal A, Wu P, Hughes EG, Fukaya M, Tischfield MA, Langseth AJ, Wirtz D, Bergles DE (2017a) Transient Opening of the Mitochondrial Permeability Transition Pore Induces Microdomain Calcium Transients in Astrocyte Processes. Neuron 93:587–605.e7.
- Agulhon C, Fiacco TA, McCarthy KD (2010) Hippocampal short- and long-term plasticity are not modulated by astrocyte Ca2+ signaling. Science 327:1250–1254.
- Akerman CJ, Cline HT (2006) Depolarizing GABAergic conductances regulate the balance of excitation to inhibition in the developing retinotectal circuit in vivo. J Neurosci 26:5117–5130.
- Akerman CJ, Cline HT (2007) Refining the roles of GABAergic signaling during neural circuit formation. Trends Neurosci 30:382–389.
- Alfonso J, Le Magueresse C, Zuccotti A, Khodosevich K, Monyer H (2012) Diazepam binding inhibitor promotes progenitor proliferation in the postnatal SVZ by reducing GABA signaling. Cell Stem Cell 10:76–87.
- Allen NJ, Bennett ML, Foo LC, Wang GX, Chakraborty C, Smith SJ, Barres BA (2012) Astrocyte glypicans 4 and 6 promote formation of excitatory synapses via GluA1 AMPA receptors. Nature 486:410–414.
- Allen NJ, Eroglu C (2017) Cell Biology of Astrocyte-Synapse Interactions. Neuron 96:697–708.
- Araque A, Parpura V, Sanzgiri RP, Haydon PG (1999) Tripartite synapses: Glia, the unacknowledged partner. Trends Neurosci 22:207–208.
- Aschauer DF, Kreuz S, Rumpel S (2013) Analysis of Transduction Efficiency, Tropism and Axonal Transport of AAV Serotypes 1, 2, 5, 6, 8 and 9 in the Mouse Brain. PLoS One 8:1–16.
- Awapara J, Landua AlJ, Fuerst R, Seale B (1950) Free gamma-Aminobutyric Acid in Brain. J Biol Chem 187:35–39.
- Bak LK, Schousboe A, Waagepetersen HS (2006) The glutamate/GABA-glutamine cycle: Aspects of transport, neurotransmitter homeostasis and ammonia transfer. J Neurochem

- 98:641-653.
- Banker GA (1980) Trophic interactions between astroglial cells and hippocampal neurons in culture. Science (80-) 209:809–810.
- Barres BA (2008) The Mystery and Magic of Glia: A Perspective on Their Roles in Health and Disease. Neuron 60:430–440.
- Bazargani N, Attwell D (2016) Astrocyte calcium signaling: The third wave. Nat Neurosci 19:182–189.
- Bazemore A, Elliot KAC, Florey E (1956) Factor I and gamma-Aminobutyric Acid. Nature 178:1052–1053.
- Behar TN, Schaffner AE, Scott CA, Greene CL, Barker JL (2000) GABA receptor antagonists modulate postmitotic cell migration in slice cultures of embryonic rat cortex. Cereb Cortex 10:899–909.
- Bekri A, Drapeau P (2018) Glycine Promotes the Survival of a Subpopulation of Neural Stem Cells. Front Cell Dev Biol 6:1–11.
- Ben-Ari Y (2002) Excitatory actions of GABA during development: the nature of the nurture. Nat Rev Neurosci 3:728–739.
- Ben-Ari Y, Cherubini E, Corradetti R, Gaiarsa J (1989) Giant synaptic potentials in immature rat CA3 hippocampal neurones. J Physiol 416:303–325.
- Ben-Ari Y, Gaiarsa J-L, Tyzio R, Khazipov R (2007) GABA: a pioneer transmitter that excites immature neurons and generates primitive oscillations. Physiol Rev 87:1215–1284.
- Ben-ari Y, Khazipov R, Leinekugel X, Caillard O, Gaiarsa J (1997) GABAA, NMDA and AMPA receptors: a developmentally regulated 'ménage à trois.' Trends Neurosci 20:523–529.
- Ben-Ari Y, Woodin MA, Sernagor E, Cancedda L, Vinay L, Rivera C, Legendre P, Luhmann HJ, Bordey A, Wenner P, Fukuda A, van den Pol AN, Gaiarsa J-L, Cherubini E (2012) Refuting the challenges of the developmental shift of polarity of GABA actions: GABA more exciting than ever! Front Cell Neurosci 6:35.
- Bernardinelli Y, Randall J, Janett E, Nikonenko I, König S, Jones EV, Flores CE, Murai KK, Bochet CG, Holtmaat A, Muller D (2014) Activity-dependent structural plasticity of perisynaptic astrocytic domains promotes excitatory synapse stability. Curr Biol 24:1679–1688.
- Berns DS, DeNardo LA, Pederick DT, Luo L (2018) Teneurin-3 controls topographic

- circuit assembly in the hippocampus. Nature.
- Blanco-Suarez E, Liu TF, Kopelevich A, Allen NJ (2018) Astrocyte-Secreted Chordin-like 1 Drives Synapse Maturation and Limits Plasticity by Increasing Synaptic GluA2 AMPA Receptors. Neuron:1116–1132.
- Boivin JR, Nedivi E (2018) Functional implications of inhibitory synapse placement on signal processing in pyramidal neuron dendrites. Curr Opin Neurobiol 51:16–22.
- Brickley SG, Cull-candy SG, Farrant M (1996) Development of a tonic form of synaptic inhibition in rat cerebellar granule cells resulting from persistent activation of GABAA receptors. J Physiol 497:753–759.
- Buxbaum JD, Silverman JM, Smith CJ, Greenberg D a, Kilifarski M, Reichert J, Cook EH, Fang Y, Song C-Y, Vitale R (2002) Association between a GABRB3 polymorphism and autism. Mol Psychiatry 7:311–316.
- Cancedda L, Fiumelli H, Chen K, Poo M (2007) Excitatory GABA action is essential for morphological maturation of cortical neurons in vivo. J Neurosci 27:5224–5235.
- Cellot G, Cherubini E (2014) GABAergic signaling as therapeutic target for autism spectrum disorders. Front Pediatr 2:70.
- Chancey JH, Adlaf EW, Sapp MC, Pugh PC, Wadiche JI, Overstreet-Wadiche LS (2013) GABA depolarization is required for experience-dependent synapse unsilencing in adult-born neurons. J Neurosci 33:6614–6622.
- Che A, Babij R, Iannone AF, Liston C, Fishell G, De Marco Garcia N V (2018) Layer I Interneurons Sharpen Sensory Maps during Neonatal Development. Neuron 99:98–116.
- Chen C-H, Huang C-C, Cheng M-C, Chiu Y-N, Tsai W-C, Wu Y-Y, Liu S-K, Gau SS-F (2014) Genetic analysis of GABRB3 as a candidate gene of autism spectrum disorders. Mol Autism 5:36.
- Chen G, Trombley PQ, Anthony N, Neurosurgery S, Street C (1996) Excitatory actions of GABA in developing rat hypothalamic neurones. J Physiol 494:451–464.
- Chen J, Kriegstein AR (2015a) A GABAergic projection from the zona incerta to cortex promotes cortical neuron development. Science (80-) 350:554–558.
- Chen J, Kriegstein AR (2015b) A GABAergic projection from the zona incerta to cortex promotes cortical neuron development. Science (80-) 1:1–8.
- Chen JL, Villa KL, Cha JW, So PTC, Kubota Y, Nedivi E (2012) Clustered Dynamics of Inhibitory Synapses and Dendritic Spines in the Adult Neocortex. Neuron 74:361–373.

- Chia PH, Li P, Shen K (2013) Cellular and molecular mechanisms underlying presynapse formation. J Cell Biol 203:11–22.
- Christian C a, Herbert AG, Holt RL, Peng K, Sherwood KD, Pangratz-Fuehrer S, Rudolph U, Huguenard JR (2013) Endogenous Positive Allosteric Modulation of GABAA Receptors by Diazepam binding inhibitor. Neuron:1–12.
- Christopherson KS, Ullian EM, Stokes CC, Mullowney CE, Hell JW, Agah A, Lawler J, Mosher DF, Bornstein P, Barres BA (2005) Thrombospondis Are Astrocyte-Secreted Proteins that Promote CNS Synaptogenesis. Cell 120:421–433.
- Clayton GH, Owens GC, Wolff JS, Smith RL (1998) Ontogeny of cation-Cl- cotransporter expression in rat neocortex. Dev Brain Res 109:281–292.
- Cornell-Bell AH, Finkbeiner SM, Cooper MS, Smith SJ (1990) Glutamate Induces Calcium Waves in Cultured Astrocytes: Long-Range Glial Signalling. Science (80-) 247:2-5.
- Corradini I, Focchi E, Rasile M, Morini R, Desiato G, Tomasoni R, Lizier M, Ghirardini E, Fesce R, Morone D, Barajon I, Antonucci F, Pozzi D, Matteoli M (2017) Maternal Immune Activation Delays Excitatory-to-Inhibitory Gamma-Aminobutyric Acid Switch in Offspring. BiolPsychiatry:1–12.
- Dammerman RS, Flint AC, Noctor S, Kriegstein AR (2000) An Excitatory GABAergic Plexus in Developing Neocortical Layer 1. J Neurophysiol 84:428–434.
- Dani JW, Chernjavsky A, Smith SJ (1992) Neuronal activity triggers calcium waves in hippocampal astrocyte networks. Neuron 8:429–440.
- Daw JR, Mintzes B, Law MR, Hanley GE, Morgan SG (2012) Prescription drug use in pregnancy: a retrospective, population-based study in British Columbia, Canada (2001–2006). Clin Ther 34:239–249.e2.
- Dean J, Hailey H, Moore S, Lloyd D, Turnpenny P, Little J (2002) Long term health and neurodevelopment in children exposed to antiepileptic drugs before birth. J Med Genet 39:251–259.
- Deidda G, Allegra M, Cerri C, Naskar S, Bony G, Zunino G, Bozzi Y, Caleo M, Cancedda L (2014) Early depolarizing GABA controls critical-period plasticity in the rat visual cortex. Nat Neurosci 18:87–96.
- Demarque M, Represa A, Becq H, Khalilov I, Ben-Ari Y, Aniksztejn L (2002) Paracrine intercellular communication by a Ca2+- and SNARE-independent release of GABA and glutamate prior to synapse formation. Neuron 36:1051–1061.
- Diniz LP, Almeida JC, Tortelli V, Lopes CV, Setti-Perdigão P, Stipursky J, Kahn SA,

- Romão LF, De Miranda J, Alves-Leon SV, De Souza JM, Castro NG, Panizzutti R, Gomes FCA (2012) Astrocyte-induced synaptogenesis is mediated by transforming growth factor β signaling through modulation of d-serine levels in cerebral cortex neurons. J Biol Chem 287:41432–41445.
- Diniz LP, Tortelli V, Garcia MN, Araújo APB, Melo HM, Seixas da Silva GS, De Felice FG, Alves-Leon SV, de Souza JM, Romão LF, Castro NG, Gomes FCA (2014) Astrocyte transforming growth factor beta 1 promotes inhibitory synapse formation via CaM kinase II signaling. Glia 62:1917–1931.
- Douglas RJ, Martin KAC (2009) Inhibition in cortical circuits. Curr Biol 19:398–402.
- El Marroun H, White T, Verhulst FC, Tiemeier H (2014) Maternal use of antidepressant or anxiolytic medication during pregnancy and childhood neurodevelopmental outcomes: a systematic review. Eur Child Adolesc Psychiatry 23:973–992.
- Fiacco T a, Agulhon C, Taves SR, Petravicz J, Casper KB, Dong X, Chen J, McCarthy KD (2007) Selective stimulation of astrocyte calcium in situ does not affect neuronal excitatory synaptic activity. Neuron 54:611–626.
- Fiala JC, Spacek J, Harris KM (2002) Dendritic Spine Pathology: Cause or Consequence of Neurological Disorders? Brain Res Rev 39:29–54.
- Fine A, Amos WB, Durbin RM, McNaughton PA (1988) Confocal microscopy: applications in neurobiology. Trends Neurosci 11:346–351.
- Fiumelli H, Briner A, Puskarjov M, Blaesse P, Belem BJ, Dayer AG, Kaila K, Martin J-L, Vutskits L (2012) An Ion Transport-Independent Role for the Cation-Chloride Cotransporter KCC2 in Dendritic Spinogenesis In Vivo. Cereb Cortex.
- Flavell SW, Cowan CW, Kim T-K, Greer PL, Lin Y, Paradis S, Griffith EC, Hu LS, Chen C, Greenberg ME (2006) Activity-dependent regulation of MEF2 transcription factors suppresses excitatory synapse number. Science 311:1008–1012.
- Flavell SW, Kim TK, Gray JM, Harmin DA, Hemberg M, Hong EJ, Markenscoft-Papadimitriou E, Bear DM, Greenberg ME (2008) Genome-Wide Analysis of MEF2 Transcriptional Program Reveals Synaptic Target Genes and Neuronal Activity-Dependent Polyadenylation Site Selection. Neuron 60:1022–1038.
- Freund TF, Buzsáki G (1998) Interneurons of the hippocampus. Hippocampus 6:347-470.
- Fukuda A, Muramatsu K, Okabe A, Shimano Y, Hida H, Nishino H (1998) Changes in Intracellular Ca2 + Induced by GABAA Receptor Activation and Reduction in Cl-Gradient in Neonatal Rat Neocortex. J Neurophysiol 79:439–446.

- Furukawa T, Yamada J, Akita T, Matsushima Y, Yanagawa Y, Fukuda A (2014) Roles of taurine-mediated tonic GABAA receptor activation in the radial migration of neurons in the fetal mouse cerebral cortex. Front Cell Neurosci 8:1–18.
- Gamlin CR, Yu WQ, Wong ROL, Hoon M (2018) Assembly and maintenance of GABAergic and Glycinergic circuits in the mammalian nervous system. Neural Dev 13:1–17.
- Gao R, Penzes P (2015) Common Mechanisms of Excitatory and Inhibitory Imbalance in Schizophrenia and Autism Spectrum Disorders. Curr Mol Med 15:146–167.
- Gao X, Pol AN Van Den (2001) GABA, Not Glutamate, a Primary Transmitter Driving Action Potentials in Developing Hypothalamic Neurons GABA, Not Glutamate, a Primary Transmitter Driving Action Potentials in Developing Hypothalamic Neurons. J Neurophysiol 85:425–434.
- Gavrilov N, Golyagina I, Brazhe A, Scimemi A, Turlapov V, Semyanov A (2018) Astrocytic Coverage of Dendritic Spines, Dendritic Shafts, and Axonal Boutons in Hippocampal Neuropil. Front Cell Neurosci 12:1–16.
- Ge S, Goh ELK, Sailor K a, Kitabatake Y, Ming G, Song H (2006) GABA regulates synaptic integration of newly generated neurons in the adult brain. Nature 439:589–593.
- Gordon GRJ, Baimoukhametova D V., Hewitt SA, Rajapaksha WRAKJS, Fisher TE, Bains JS (2005) Norepinephrine triggers release of glial ATP to increase postsynaptic efficacy. Nat Neurosci 8:1078–1086.
- Greer PL, Greenberg ME (2008) From synapse to nucleus: calcium-dependent gene transcription in the control of synapse development and function. Neuron 59:846–860.
- Grosche J, Matyash V, Möller T, Verkhratsky A, Reichenbach A, Kettenmann H (1999) Microdomains for neuron-glia interaction: Parallel fiber signaling to Bergmann glial cells. Nat Neurosci 2:139–143.
- Gross GG, Straub C, Perez-Sanchez J, Dempsey WP, Junge JA, Roberts RW, Trinh LA, Fraser SE, De Koninck Y, De Koninck P, Sabatini BL, Arnold DB (2016) An E3-ligase-based method for ablating inhibitory synapses. Nat Methods 13:673–678.
- Gulledge AT, Stuart GJ (2003) Excitatory actions of GABA in the cortex. Neuron 37:299–309.
- Haber M, Zhou L, Murai KK (2006) Cooperative Astrocyte and Dendritic Spine Dynamics at Hippocampal Excitatory Synapses. 26:8881–8891.
- Hadjikhani N, Åsberg Johnels J, Lassalle A, Zürcher NR, Hippolyte L, Gillberg C,

- Lemonnier E, Ben-Ari Y (2018) Bumetanide for autism: more eye contact, less amygdala activation. Sci Rep 8:3602.
- Halestrap AP (2011) Monocarboxylic Acid Transport. Compr Physiol 3:1611–1643.
- Hanse E, Durand GM, Garaschuk O, Konnerth A (1997) Activity-dependent wiring of the developing hippocampal neuronal circuit. Semin Cell Dev Biol 8:35–42.
- Hanse E, Seth H, Riebe I (2013) AMPA-silent synapses in brain development and pathology. Nat Rev Neurosci 14:839–850.
- Harris KM, Spacek J, Bell ME, Parker PH, Lindsey LF, Baden AD, Vogelstein JT, Burns R (2015) A resource from 3D electron microscopy of hippocampal neuropil for user training and tool development. Sci data 2:150046.
- He Q, Arroyo ED, Smukowski SN, Xu J, Piochon C, Savas JN, Contractor CPA (2018) Critical period inhibition of NKCC1 recti fi es synapse plasticity in the somatosensory cortex and restores adult tactile response maps in fragile X mice.
- He Q, Nomura T, Xu J, Contractor A (2014) The Developmental Switch in GABA Polarity Is Delayed in Fragile X Mice. J Neurosci 34:446–450.
- Heck N, Kilb W, Reiprich P, Kubota H, Furukawa T, Fukuda A, Luhmann HJ (2007) GABA-A receptors regulate neocortical neuronal migration in vitro and in vivo. Cereb Cortex 17:138–148.
- Heller JP, Rusakov DA (2015) Morphological plasticity of astroglia: Understanding synaptic microenvironment. Glia 63:2133–2151.
- Helmchen F, Denk W (2005) Deep tissue two-photon microscopy. Nat Methods 2:932–940.
- Henneberger C, Bard L, Panatier A, Reynolds J, Medvidov NI, Minge D, Herde MK, Anders S, Kraev I, Zheng K, Jensen TP, Sanchez-Romero I, Janovjak H, Ottersen O-P, Nagelhus E-A, Oliet SHR, Stewart MG, Nagerl UV, Rusakov DA (2018) Astroglia withdraw from potentiated synapses boosting inter-synaptic cross-talk. bioRxiv:349233.
- Henneberger C, Papouin T, Oliet SHR, Rusakov DA (2010) Long-term potentiation depends on release of d-serine from astrocytes. Nature 463:232–236.
- Hensch TK (2005) Critical period plasticity in local cortical circuits. Nat Rev Neurosci 6:877–888.
- Holmseth S, Dehnes Y, Huang YH, Follin-Arbelet V V., Grutle NJ, Mylonakou MN, Plachez C, Zhou Y, Furness DN, Bergles DE, Lehre KP, Danbolt NC (2012) The

- Density of EAAC1 (EAAT3) Glutamate Transporters Expressed by Neurons in the Mammalian CNS. J Neurosci 32:6000–6013.
- Hutsler JJ, Zhang H (2010) Increased dendritic spine densities on cortical projection neurons in autism spectrum disorders. Brain Res 1309:83–94.
- Irwin SA, Galvez R, William T (2000) Dendritic Spine Structural Anomalies in Fragile-X Mental Retardation Syndrome. :1038–1044.
- Irwin SA, Patel B, Idupulapati M, Harris JB, Crisostomo RA, Larsen BP, Kooy F, Willems PJ, Cras P, Kozlowski PB, Swain RA, Weiler IJ, Greenough WT (2001) Abnormal dendritic spine characteristics in the temporal and visual cortices of patients with fragile-X syndrome: a quantitative examination. Am J Med Genet 98:161–167.
- Jasper HH (1984) The Saga of K.A.C. Elliott and Gaba. Neurochem Res 9:449–460.
- Jones E, Powell T (1970) An Electron Microscopic Study of the Laminar Pattern and Mode of Termination of Afferet Flbre Pathways in the Somatic Sensory Cortex of the Cat. Philos Trans R Soc B 257:45–62.
- Jones E V, Bernardinelli Y, Tse YC, Chierzi S, Wong TP, Murai KK (2011) Astrocytes control glutamate receptor levels at developing synapses through SPARC-beta-integrin interactions. J Neurosci 31:4154–4165.
- Kamijo S, Ishii Y, Horigane S, Suzuki K, Ohkura M, Nakai J, Fujii H, Takemoto-Kimura S, Bito H (2018) A critical neurodevelopmental role for L-type voltage-gated calcium channels in neurite extension and radial migration. J Neurosci 38:2357–17.
- Kaneko M, Stellwagen D, Malenka RC, Stryker MP (2008) Tumor Necrosis Factor-α Mediates One Component of Competitive, Experience-Dependent Plasticity in Developing Visual Cortex. Neuron 58:673–680.
- Kang J-Q, Shen W, Macdonald RL (2009) The GABRG2 mutation, Q351X, associated with generalized epilepsy with febrile seizures plus, has both loss of function and dominant-negative suppression. J Neurosci 29:2845–2856.
- Kang J, Jiang L, Goldman SA, Nedergaard M (1998) Astrocyte-mediated potentiation of inhibitory synaptic transmission. Nat Neurosci 1:683–692.
- Kano M, Hashimoto K (2009) Synapse elimination in the central nervous system. Curr Opin Neurobiol 19:154–161.
- Kasthuri N et al. (2015) Saturated Reconstruction of a Volume of Neocortex. Cell 162:648–661.
- Kaufmann WE, Moser HW (2000) Dendritic Anomalies in Disorders Associated with

- Mental Retardation. :981-991.
- Khalilov I, Minlebaev M, Mukhtarov M, Khazipov R (2015) Dynamic Changes from Depolarizing to Hyperpolarizing GABAergic Actions during Giant Depolarizing Potentials in the Neonatal Rat Hippocampus. 35:12635–12642.
- Khanna A, Walcott BP, Kahle KT (2013) Limitations of current GABA agonists in neonatal seizures: toward GABA modulation via the targeting of neuronal Cl transport. 4:1–8.
- Khazipov R, Esclapez M, Caillard O, Bernard C, Khalilov I, Tyzio R, Hirsch J, Dzhala V, Berger B, Ben-ari Y (2001) Early Development of Neuronal Activity in the Primate Hippocampus In Utero. J Neurosci 21:9770–9781.
- Kim CK, Adhikari A, Deisseroth K (2017) Integration of optogenetics with complementary methodologies in systems neuroscience. Nat Rev Neurosci 18:222–235.
- Kim T-K, Hemberg M, Gray JM, Costa AM, Bear DM, Wu J, Harmin D a, Laptewicz M, Barbara-Haley K, Kuersten S, Markenscoff-Papadimitriou E, Kuhl D, Bito H, Worley PF, Kreiman G, Greenberg ME (2010) Widespread transcription at neuronal activity-regulated enhancers. Nature 465:182–187.
- Kirmse K, Kummer M, Kovalchuk Y, Witte OW, Garaschuk O, Holthoff K (2015a) GABA depolarizes immature neurons and inhibits network activity in the neonatal neocortex in vivo. Nat Commun 6.
- Kirmse K, Kummer M, Kovalchuk Y, Witte OW, Garaschuk O, Holthoff K (2015b) GABA depolarizes immature neurons and inhibits network activity in the neonatal neocortex in vivo. Nat Commun 6:7750.
- Kistner A, Gossen M, Zimmermann F, Jerecic J, Ullmer C, Lubbert H, Bujard H (1996) Doxycycline-mediated quantitative and tissue-specific control of gene expression in transgenic mice. Proc Natl Acad Sci 93:10933–10938.
- Korogod N, Petersen CCH, Knott GW (2015) Ultrastructural analysis of adult mouse neocortex comparing aldehyde perfusion with cryo fixation. Elife 4:1–17.
- Kügler S, Kilic E, Bähr M (2003) Human synapsin 1 gene promoter confers highly neuron-specific long-term transgene expression from an adenoviral vector in the adult rat brain depending on the transduced area. Gene Ther 10:337–347.
- Lacey DJ, Terplan K (1987) Abnormal Cerebral Cortical Neurons in a Child With Maternal PKU Syndrome. J Child Neurol 2:201–204.
- Laurie DJ, Wisden W, Seeburg PH (1992) The distribution of thirteen GABAA receptor subunit mRNAs in the rat brain. III. Embryonic and postnatal development. J Neurosci

- 12:4151-4172.
- Le Magueresse C, Safiulina V, Changeux J-P, Cherubini E (2006) Nicotinic modulation of network and synaptic transmission in the immature hippocampus investigated with genetically modified mice. J Physiol 576:533–546.
- Lee E, Lee J, Kim E (2017) Excitation/Inhibition Imbalance in Animal Models of Autism Spectrum Disorders. Biol Psychiatry 81:838–847.
- Lehre KR, Rusakov DA (2002) Asymmetry of glia near central synapses favors presynaptically directed glutamate escape. Biophys J 83:125–134.
- Lein ES et al. (2007) Genome-wide atlas of gene expression in the adult mouse brain. Nature 445:168–176.
- Leinekugel X, Khazipov R, Cannon R, Hirase H, Ben-Ari Y, Buzsáki G (2002) Correlated bursts of activity in the neonatal hippocampus in vivo. Science 296:2049–2052.
- Leinekugel X, Tseeb V, Ben-ari Y, Bregestovski P (1995) Synaptic GABAA activation induces Ca2+ rise in pyramidal cells and interneurons from rat neonatal hippocampal slices. J Physiol 487:319–329.
- Lemonnier E, Villeneuve N, Sonie S, Serret S, Rosier A, Roue M, Brosset P, Viellard M, Ernoux DB, Rondeau S, Thummler S, Ravel D, Ben-Ari Y (2017) Effects of bumetanide on neurobehavioral function in children and adolescents with autism spectrum disorders. Transl Psychiatry 7:e1056-9.
- Levav T, Saar T, Berkovich L, Golan H (2004) Perinatal exposure to GABA-transaminase inhibitor impaired psychomotor function in the developing and adult mouse. Int J Dev Neurosci 22:137–147.
- Levav T, Wirthaim O, Weiss R, Grossman Y, Golan H (2008) Impaired synaptogenesis and long-term modulation of behavior following postnatal elevation of GABA levels in mice. Neuropharmacology 54:387–398.
- Li H, Tornberg J, Kaila K, Airaksinen MS, Rivera C (2002) Patterns of cation-chloride cotransporter expression during embryonic rodent CNS development. Eur J Neurosci 16:2358–2370.
- Li R-W, Yu W, Christie S, Miralles CP, Bai J, Loturco JJ, De Blas AL (2005) Disruption of postsynaptic GABA receptor clusters leads to decreased GABAergic innervation of pyramidal neurons. J Neurochem 95:756–770.
- Lin M, Takahashi MP, Takahashi Y, Tsumoto T (1994) Intracellular calcium increase induced by GABA in visual cortex of fetal and neonatal rats and its disappearance with

- development. Neurosci Res 20:85-94.
- Liu X, Wang Q, Haydar TF, Bordey A (2005) Nonsynaptic GABA signaling in postnatal subventricular zone controls proliferation of GFAP-expressing progenitors. Nat Neurosci 8:1179–1187.
- LoTurco JJ, Owens DF, Heath MJ, Davis MB, Kriegstein a R (1995a) GABA and glutamate depolarize cortical progenitor cells and inhibit DNA synthesis. Neuron 15:1287–1298.
- LoTurco JJ, Owens DF, Heath MJS, Davis MBE, Kriegstein AR (1995b) GABA and glutamate depolarize cortical progenitor cells and inhibit DNA synthesis. Neuron 15:1287–1298.
- Lu J, Karadsheh M, Delpire E (1999) Developmental Regulation of the Neuronal-Specific Isoform of K-Cl Cotransporter KCC2 in Postnatal Rat Brains. J Neurobiol 39:558–568.
- Lushnikova I, Skibo G, Muller D, Nikonenko I (2009) Synaptic potentiation induces increased glial coverage of excitatory synapses in CA1 hippocampus. Hippocampus 19:753–762.
- Magistretti PJ, Allaman I (2015) A Cellular Perspective on Brain Energy Metabolism and Functional Imaging. Neuron 86:883–901.
- Malik AN, Vierbuchen T, Hemberg M, Rubin AA, Ling E, Couch CH, Stroud H, Spiegel I, Farh KKH, Harmin DA, Greenberg ME (2014) Genome-wide identification and characterization of functional neuronal activity-dependent enhancers. Nat Neurosci 17:1330–1339.
- Mardinly AR, Spiegel I, Patrizi A, Centofante E, Bazinet JE, Tzeng CP, Mandel-Brehm C, Harmin DA, Adesnik H, Fagiolini M, Greenberg ME (2016) Sensory experience regulates cortical inhibition by inducing IGF1 in VIP neurons. Nature 531:371–375.
- Marques-Smith A, Lyngholm D, Kaufmann A-K, Stacey JA, Hoerder-Suabedissen A, Becker EB, Wilson M, Molnar Z, Butt SJB (2016) A Transient Translaminar GABAergic Interneuron Circuit Connects Thalamocortical Recipient Layers in Neonatal Somatosensory Cortex Article. Neuron 89:536–549.
- Martenson JS, Tomita S (2015) Synaptic localization of neurotransmitter receptors: comparing mechanisms for AMPA and GABAA receptors. Curr Opin Pharmacol 20:102–108.
- Medvedev N, Popov V, Henneberger C, Kraev I, Rusakov DA, Stewart MG (2014) Glia selectively approach synapses on thin dendritic spines. Philos Trans R Soc B Biol Sci 369:1–6.

- Meier E, Hertz L, Schousboe A (1991) Neurotransmitters as Developmental Signals. Neurochem Int 19:1–15.
- Menold MM, Shao Y, Wolpert CM, Donnelly SL, Raiford KL, Martin ER, Ravan S a, Abramson RK, Wright HH, Delong GR, Cuccaro ML, Pericak-Vance M a, Gilbert JR (2001) Association analysis of chromosome 15 gabaa receptor subunit genes in autistic disorder. J Neurogenet 15:245–259.
- Michaelsen K, Lohmann C (2010) Calcium dynamics at developing synapses: Mechanisms and functions. Eur J Neurosci 32:218–223.
- Michels G, Moss SJ (2007) GABAA receptors: properties and trafficking. Crit Rev Biochem Mol Biol 42:3–14.
- Mikawa S, Wang C, Shu F, Wang T, Fukuda A, Sato K (2002) Developmental changes in KCC1, KCC2 and NKCC1 mRNAs in the rat cerebellum. Dev Brain Res 136:93–100.
- Misgeld U, Deisz RA, Dodt HU, Lux HD (1986) The role of chloride transport in postsynaptic inhibition of hippocampal neurons. Science (80-) 232:1413–1415.
- Mishchenko Y, Hu T, Spacek J, Mendenhall J, Harris KM, Chklovskii DB (2010) Ultrastructural analysis of hippocampal neuropil from the connectomics perspective. Neuron 67:1009–1020.
- Murphy-Royal C, Dupuis JP, Varela JA, Panatier A, Pinson B, Baufreton J, Groc L, Oliet SHR (2015) Surface diffusion of astrocytic glutamate transporters shapes synaptic transmission. Nat Neurosci 18:219–226.
- Overstreet Wadiche L, Bromberg D a, Bensen AL, Westbrook GL (2005) GABAergic signaling to newborn neurons in dentate gyrus. J Neurophysiol 94:4528–4532.
- Owens DF, Boyce LH, Davis MBE, Kriegstein AR (1996) Excitatory GABA Responses in Embryonic and Neonatal Cortical Slices Demonstrated by Gramicidin Perforated-Patch Recordings and Calcium Imaging. J Neurosci 16:6414–6423.
- Owens DF, Kriegstein AR (2002) Is there more to GABA than synaptic inhibition? Nat Rev Neurosci 3:715–727.
- Owens DF, Liu X, Kriegstein AR (1999) Changing Properties of GABA A Receptor Mediated Signaling During Early Neocortical Development. J Neurophysiol 82:570–583.
- Palay BYSL, Palade GE (1955) The Fine Structures of Neurons. Public Health 1:69-87.
- Palay SL, Chan-Palay V (1974) Cerebellar Cortex: Cytology and Organization. Berlin, Heidelberg, New York: Springer-Verlag.

- Panatier A, Vallée J, Haber M, Murai KK, Lacaille JC, Robitaille R (2011) Astrocytes are endogenous regulators of basal transmission at central synapses. Cell 146:785–798.
- Papouin T, Ladépêche L, Ruel J, Sacchi S, Labasque M, Hanini M, Groc L, Pollegioni L, Mothet JP, Oliet SHR (2012) Synaptic and extrasynaptic NMDA receptors are gated by different endogenous coagonists. Cell 150:633–646.
- Patel AB, Lai JCK, Chowdhury GMI, Hyder F, Rothman DL, Shulman RG, Behar KL (2014) Direct evidence for activity-dependent glucose phosphorylation in neurons with implications for the astrocyte-to-neuron lactate shuttle. Proc Natl Acad Sci 111:5385–5390.
- Patrushev I, Gavrilov N, Turlapov V, Semyanov A (2013) Subcellular location of astrocytic calcium stores favors extrasynaptic neuron-astrocyte communication. Cell Calcium 54:343–349.
- Paul Weiss (1947) The Problem of Specificity in Growth and Development. Yale J Biol Med 19:235–278.
- Perea G, Navarrete M, Araque A (2009) Tripartite synapses: astrocytes process and control synaptic information. Trends Neurosci 32:421–431.
- Peters A, Palay S (1965) An Electron Microscope Study of Distribution and Patterns of Astroglial Processes in Central Nervous System. J Anatomy1.
- Peters A, Palay SL (1996) The morphology of synapses. J Neurocytol 25:687–700.
- Peters A, Palay SL, Webster H de F (1976) The Fine Structure of the Nervous System; the Neurons and Supporting Cells. Philadelphia, London, Toronto: W.B. Saunders Company.
- Pfrieger FW, Barres BA (1997) Synaptic Efficacy Enhanced by Glial Cells in Vitro showed low levels of synaptic activity with. Science (80-) 277:1684–1687.
- Plotkin MD, Snyder EY, Hebert SC, Delpire E (1997) Expression of the Na K 2Cl Cotransporter Is Developmentally Regulated in Postnatal Rat Brains: A Possible Mechanism Underlying GABA 's Excitatory Role in Immature Brain. J Neurobiol 33:781–795.
- Porter JT, McCarthy KD (1997) Astrocytic Neurotransmitter Receptors. Prog Neurobiol 51:439–455.
- Pribiag H, Stellwagen D (2013) TNF-α downregulates inhibitory neurotransmission through protein phosphatase 1-dependent trafficking of GABA(A) receptors. J Neurosci 33:15879–15893.

- Puskarjov M, Fiumelli H, Briner A, Bodogan T, Demeter K, Lacoh C, Mavrovic M, Blaesse P, Kaila K, Vutskits L (2017) K-Cl Cotransporter 2-mediated Cl- extrusion determine developmental stage-dependent impact of propofol mediated anesthesia on dendritic spines. Anesthesiology 126:1–13.
- Rincon MY, De Vin F, Duqué SI, Fripont S, Castaldo SA, Bouhuijzen-Wenger J, Holt MG (2018) Widespread transduction of astrocytes and neurons in the mouse central nervous system after systemic delivery of a self-complementary AAV-PHP.B vector. Gene Ther 25:83–92.
- Rivera C, Voipio J, Payne JA (1999) The K+/Cl- co-transporter KCC2 renders GABA hyperpolarizing during neuronal maturation. Nature 397:251–255.
- Roberts E, Frankel S (1950) Gamma-Aminobutyric Acid in Brain: Its Formation from Glutamic Acid. J Biol Chem 187:55–63.
- Rosenberg SS, Spitzer NC (2011) Calcium signaling in neuronal development. Cold Spring Harb Perspect Biol 3:1–13.
- Rubenstein J, Merzenich M (2003) Model of autism: increased ratio of excitation/ihibition in key neural systems. Genes, Brain Behav 2:255–267.
- Rusakov DA (2001) The role of perisynaptic glial sheaths in glutamate spillover and extracellular Ca2+depletion. Biophys J 81:1947–1959.
- Rusakov DA (2015) Disentangling calcium-driven astrocyte physiology. Nat Rev Neurosci 16:226–233.
- Rusakov DA, Kullmann DM (1998) Extrasynaptic Glutamate Diffusion in the Hippocampus: Ultrastructural Constraints, Uptake, and Receptor Activation. J Neurosci 18:3158–3170.
- Sato T, Muroyama Y, Saito T (2015) Control of Gene Expression in Neurons by the Use of In Vivo Electroporation and the Tetracycline System. In: Neuromethods, pp 187–195.
- Schousboe A, Bak LK, Waagepetersen HS (2013) Astrocytic control of biosynthesis and turnover of the neurotransmitters glutamate and GABA. Front Endocrinol (Lausanne) 4:1–11.
- Schulz K, Sydekum E, Krueppel R, Engelbrecht CJ, Schlegel F, Schröter A, Rudin M, Helmchen F (2012) Simultaneous BOLD fMRI and fiber-optic calcium recording in rat neocortex. Nat Methods 9:597–602.
- Schweizer C, Balsiger S, Bluethmann H, Mansury IM, Fritchy J-M, Mohler H, Luscher B (2003) The γ2 subunit of GABAA receptors is required for maintenance of receptors at

- mature synapses. Mol Cell Neurosci 24:442-450.
- Sedmak G, Jovanov-Milošević N, Puskarjov M, Ulamec M, Krušlin B, Kaila K, Judaš M (2015) Developmental Expression Patterns of KCC2 and Functionally Associated Molecules in the Human Brain. Cereb Cortex:1–16.
- Shen W, Da Silva JS, He H, Cline HT (2009) Type A GABA-receptor-dependent synaptic transmission sculpts dendritic arbor structure in Xenopus tadpoles in vivo. J Neurosci 29:5032–5043.
- Shigetomi E, Kracun S, Sofroniew M V., Khakh BS (2010) A genetically targeted optical sensor to monitor calcium signals in astrocyte processes. Nat Neurosci 13:759–766.
- Shigetomi E, Patel S, Khakh BS (2016) Probing the Complexities of Astrocyte Calcium Signaling. Trends Cell Biol 26:300–312.
- Spacek J (1985) Three-dimensional analysis of dendritic spines III. Glial sheath. Anat Embryol (Berl) 171:245–252.
- Sperry RW (1963) Chemoaffinity in the orderly growth of nerve fiber patterns and connections. Proc Natl Acad Sci 50:703–710.
- Spitzer NC, Rohrbough J (1996) Regulation of Intracellular Cotranspot-t Distinguishes Cl-Levels by Na + -Dependent Depolarizing from Hyperpolarizing Responses in Spinal Neurons. J Neurosci 16:82–91.
- Staley KJ, Mody I (1992) Shunting of excitatory input to dentate gyrus granule cells by a depolarizing GABAA receptor-mediated postsynaptic conductance. J Neurophysiol 68:197–212.
- Stellwagen D, Malenka RC (2006) Synaptic scaling mediated by glial TNF-α. Nature 440:1054–1059.
- Stogsdill JA, Ramirez J, Liu D, Kim YH, Baldwin KT, Enustun E, Ejikeme T, Ji RR, Eroglu C (2017) Astrocytic neuroligins control astrocyte morphogenesis and synaptogenesis. Nature 551:192–197.
- Sudhof T (2018) Towards an Understanding of Synapse Formation. Neuron:276–293.
- Sun W, McConnell E, Pare J-F, Xu Q, Chen M, Peng W, Lovatt D, Han X, Smith Y, Nedergaard M (2013) Glutamate-Dependent Neuroglial Calcium Signaling Differs Between Young and Adult Brains. Science (80-) 339:197–200.
- Toth AB, Shum AK, Prakriya M (2016) Regulation of neurogenesis by calcium signaling. Cell Calcium 59:124–134.

- Tozuka Y, Fukuda S, Namba T, Seki T, Hisatsune T (2005) GABAergic excitation promotes neuronal differentiation in adult hippocampal progenitor cells. Neuron 47:803–815.
- Tuncdemir SN, Wamsley B, Stam FJ, Osakada F, Goulding M, Callaway EM, Rudy B, Fishell G (2016) Early Somatostatin Interneuron Connectivity Mediates the Maturation of Deep Layer Cortical Circuits. Neuron 89:521–535.
- Tyzio R, Nardou R, Ferrari DC, Tsintsadze T, Shahrokhi A, Eftekhari S, Khalilov I, Tsintsadze V, Brouchoud C, Chazal G, Lemonnier E, Lozovaya N, Burnashev N, Ben-Ari Y (2014) Oxytocin-Mediated GABA Inhibition During Delivery Attenuates Autism Pathogenesis in Rodent Offspring. Science (80-) 343:675–680.
- Tyzio R, Represa A, Jorquera I, Ben-Ari Y, Gozlan H, Aniksztejn L (1999) The establishment of GABAergic and glutamatergic synapses on CA1 pyramidal neurons is sequential and correlates with the development of the apical dendrite. J Neurosci 19:10372–10382.
- Ullian EM, Sapperstein SK, Christopherson KS, Barres BA (2001) Control of synapse number by glia. Science (80-) 291:657–661.
- Valeeva G, Tressard T, Mukhtarov M, Baude A, Khazipov R (2016) An Optogenetic Approach for Investigation of Excitatory and Inhibitory Network GABA Actions in Mice Expressing Channelrhodopsin-2 in GABAergic Neurons. J Neurosci 36:5961–5973.
- Van Horn MR, Strasser A, Miraucourt LS, Pollegioni L, Ruthazer ES (2017) The Gliotransmitter d-Serine Promotes Synapse Maturation and Axonal Stabilization *In Vivo*. J Neurosci 37:6277–6288.
- Ventura R, Harris KM (1999) Three-dimensional relationships between hippocampal synapses and astrocytes. J Neurosci 19:6897–6906.
- Viggedal G, Hagberg BS, Laegreid L, Aronsson M (1993) Mental Development in Late Infancy after Prenatal Exposure to Benzodiazepines — a Prospective Study. J Child Psychol Psychiatry 1 34.
- Villa KL, Berry KP, Subramanian J, Cha JW, Oh WC, Kwon HB, Kubota Y, So PTC, Nedivi E (2016) Inhibitory Synapses Are Repeatedly Assembled and Removed at Persistent Sites In Vivo. Neuron 89:756–769.
- Vincent-Lamarre P, Lynn M, Beique J-C (2018) The Eloquent Silent Synapse. Trends Neurosci 41:557–559.
- Vu TQ, Payne JA, Copenhagen DR (2000) Localization and Developmental Expression

- Patterns of the Neuronal K Cl Cotransporter (KCC2) in the Rat Retina. J Neurosci 20:1414–1423.
- Wang C-L, Zhang L, Zhou Y, Zhou J, Yang X-J, Duan S -m., Xiong Z-Q, Ding Y-Q (2007) Activity-Dependent Development of Callosal Projections in the Somatosensory Cortex. J Neurosci 27:11334–11342.
- Wang DD, Kriegstein AR (2008) GABA regulates excitatory synapse formation in the neocortex via NMDA receptor activation. J Neurosci 28:5547–5558.
- Wang Y, Gao X, Pol AN Van Den, Pol ANVANDEN (2001) Membrane Properties Underlying Patterns of GABA-Dependent Action Potentials in Developing Mouse Hypothalamic Neurons Membrane Properties Underlying Patterns of GABA-Dependent Action Potentials in Developing Mouse Hypothalamic Neurons. J Neurophysiol 86:1252–1265.
- Waterhouse EG, An JJ, Orefice LL, Baydyuk M, Liao G-Y, Zheng K, Lu B, Xu B (2012) BDNF Promotes Differentiation and Maturation of Adult-born Neurons through GABAergic Transmission. J Neurosci 32:14318–14330.
- Weber B, Barros LF (2015) The astrocyte: Powerhouse and recycling center. Cold Spring Harb Perspect Biol 7:1–16.
- Witcher MR, Kirov SA, Harris KM (2007) Plasticity of Perisynaptic Astroglia During Synaptogenesis in the Mature Rat Hippocampus. Glia 55:13–23.
- Wolff JR, Joó F, Dames W (1978) Plasticity in dendrites shown by continuous GABA administration in superior cervical ganglion of adult rat. Nature 274:72–74.
- Wu YW, Tang X, Arizono M, Bannai H, Shih PY, Dembitskaya Y, Kazantsev V, Tanaka M, Itohara S, Mikoshiba K, Semyanov A (2014) Spatiotemporal calcium dynamics in single astrocytes and its modulation by neuronal activity. Cell Calcium 55:119–129.
- Yuste R, Katz LC (1991) Control of Postsynaptic Ca * + Influx in Developing Neocortex by Excitatory and Inhibitory Neurotransmitters. Neuron 6:333–344.
- Zhang RW, Wei HP, Xia YM, Du JL (2010) Development of light response and GABAergic excitation-to-inhibition switch in zebrafish retinal ganglion cells. J Physiol 588:2557–2569.
- Zheng Z et al. (2018) A Complete Electron Microscopy Volume of the Brain of Adult Drosophila melanogaster. Cell 174:730–743.e22.